

# Characterization of two hailstorms in Argentina

---

Author

Anthony Crespo

A thesis submitted in partial fulfillment of the requirements for the degree of

MASTER OF SCIENCE

(Atmospheric and Oceanic Sciences)

at the

UNIVERSITY OF WISCONSIN-MADISON

2020

## **Acknowledgments**

As a young scientist, I would never have reached my current level of experience and inspiration without the mentors that helped get to where I am at today. First, I would like to thank Prof. Jay Thomas, who since my second year of undergraduate education was able to see my potential and gave me the tools that enabled me to work on the initial stages of this project, which started as an undergraduate senior thesis proposal. Secondly, I would like to thank my research advisor, Prof. Ankur Desai, who was able to see my motivation and gave me a chance to pursue my graduate studies at UW-Madison, and has supported me since without hesitation. Like many students starting a research project, I didn't know where to get data sets, to start observations or start up a program correctly without that technician that helped go through all those coding lines. I would like to give special thanks to Pete Pokrandt for sitting down with me to look at how a simple comma or period in python prevented me from processing satellite images properly. I would also like to thank Dr. Angela Rowe, who, at the final stages of this project, was able to guide me and helped me wrap up my ideas wonderfully.

My interest in this project was reignited by experiences in the RELAMPAGO field campaign, sponsored by the National Science Foundation, in collaboration with the Department of Energy, NOAA, and NASA. Every scientist has a eureka moment, sometimes when they least expect it. For mine I would like to give special thanks to Dr. Kristen Rasmussen, because her wonderful stories at lunch in Villa Carlos Paz inspired me to look further into my senior thesis proposal and turn it into an amazing project. Finally, I would like to thank the AOS administration: Dee VanRuyven, Chelsea Dahmen, Sue Foldy and the

wonderful graduate student community for making these past two years an amazing experience and for their research support that helped me through the development of this project.

“No solo las grandes mentes cambian este mundo, sino las que creen, crecen y trabajan en él, para ser del mismo un mundo, limpio, sano, seguro y feliz para vivir”. Frase que desarrolle como estudiante de escuela superior y aun identifica la persona que soy hoy. Quisiera comenzar por agradecer a mi familia Ayala, por darme todo el amor y apoyo incondicional durante todos estos años. Especialmente a mi mamá y a mi tía, que han sido los motores que han aportado a que yo este aquí. Ningún estudiante llega al nivel que esta sin maestros que sirvan de escalones para llegar al éxito. Quisiera agradecer especialmente a mi escuela CIMATEC, su administración en aquel momento y su profesorado por darme esas herramientas que me prepararon académicamente para mi desarrollo profesional. En especial a Raquel Rodríguez, Eva Torres y Milagros Carire por el apoyo tanto académico como personal. Gracias a la campaña internacional de RELAMPAGO, al Ministerio de Ciencias y Tecnología de la Provincia de Córdoba y a la Universidad Nacional de Córdoba por permitirme la estadía en Argentina y permitirme colaborar con Andrés Lighezzolo y Agustín Martina que aportaron en el proceso de desarrollo de este proyecto. Finalmente, pero no menos importante, quisiera agradecer especialmente a la Dra. Lucia E. Arena, quien ha sido la codirectora de este proyecto, el cual vio este proyecto crecer, trabajo arduas noches conmigo en el desarrollo de este proyecto y me ha extendido su hogar y hospitalidad en Argentina, considerándome un miembro mas de su familia y esperando con ansias el próximo paso luego de este proyecto.

This thesis is dedicated to my grandma; may her gentle soul rest in peace.

Esta tesis esta dedicada a mi abuela, que en paz descansa.

## **Abstract**

Falling hailstones are some of the most destructive natural phenomena in convectively active regions of the world. Cordoba Province in Argentina is a region of severe storms of worldwide relevance because the storms that initiate in this area are characterized by tremendous vertical development characterized by significant rainfall of giant hail from 5 to 10 cm, including a recent record of 17.5 cm in the city of Carlos Paz in 2018. Previous studies of hail formation and detection rely on satellite snapshots or modeling studies, but lack hail validation, instead relying on proxy metrics. Here, to address this limitation, we collected hail in the Cordoba region from a record-breaking hail event and from the RELAMPAGO field campaign. The two case studies allow us to evaluate hail detection algorithms with actual verification of hail properties. Specifically, we sought to evaluate how well satellite hail detection algorithms and background large-scale meteorological conditions predict the likelihood of large hail development in Argentina. Using data from the C-band Córdoba radar (RMA1) and GOES-16, we were able to identify a multicell organized mesoscale convective system developing at 22:00 UTC on December 13<sup>th</sup> in 2018 producing hail at 02:20 UTC in Villa del Dique after it advances over a mountain range. Brightness temperature analysis showed a gradual decrease of brightness temperatures through time starting at 200 K in the earlier development stages and then 190 K before a hail event. On February 8<sup>th</sup>, we identified an unorganized multicellular convective system developing at 16:00 UTC (southern cell) over the plains in the San Luis Province while a second convective cell develops at 18:00 UTC (northern cell) and within 45 minutes showed a significant vertical development and has multiple hail events in Villa Carlos Paz and nearby cities. Brightness temperature analysis showed a gradual decrease of brightness temperatures

through time starting at 210 K in the earlier development stages for the northern cell and then 195 K before a hail event. The southern cell didn't reach these lower temperatures, showing temperatures ranging from 210-215 K. During these events, giant hail (greater than 5 cm) were observed in both mountainous and valley settings, for both February 8<sup>th</sup> and December 13<sup>th</sup> even though the local national weather service warnings did not predict hail fall for convective storms on either date. Crystallographic analysis of hail samples from both hailstorms showed a similar number of rings internally and a large number of air bubbles. Through our analysis of verified hailfall, the December 13<sup>th</sup> case shows that in fact under large-scale conditions and these types of MCS, hail can fall over las Sierras de Cordoba. But we also found a hail-producing case where these large-scale ingredients were not present. The results from this comparison between two hail-producing cases gives us the motivation to look further at these different types of environments and cases that can produce hail in this region. Ultimately, the long-term goal is to better understand unique aspects of hail formation and challenges to hail forecasting in this region, especially given that these hail-producing systems formed in two different environments and neither were forecasted to hail that day.

Keywords: hailstone, severe storm, bubbles, brightness temperatures.

## **Table of Contents**

<b>ACKNOWLEDGMENTS .....</b>	<b>I</b>
<b>DEDICATION.....</b>	<b>III</b>
<b>ABSTRACT.....</b>	<b>IV</b>
<b>TABLE OF CONTENTS .....</b>	<b>VI</b>
1.1. MOTIVATION.....	1
1.2. BACKGROUND.....	3
1.2.1. <i>Hail Development</i> .....	3
1.2.2. <i>Types of convective systems producing hail in Cordoba</i> .....	4
1.2.3. <i>Ingredients supporting these storms type</i> .....	7
1.2.4. <i>Attempts to infer hail from data</i> .....	9
1.2.5. <i>Research Questions/Objectives</i> .....	10
<b>2. METHODS .....</b>	<b>12</b>
2.1. CHOICE OF CASES TO STUDY .....	12
2.2. CONVECTIVE STORM IDENTIFICATION AND TRACKING .....	12
2.2.1. <i>Satellite</i> .....	12
2.2.2. <i>Radar</i> .....	15
2.3. <i>HAIL CHARACTERIZATION</i> .....	16
2.4. ENVIRONMENTAL DATA .....	17
2.5. STORM WARNINGS .....	18
<b>3. RESULTS .....</b>	<b>19</b>

3.1.	DECEMBER 13-14.....	19
3.1.1.	<i>Convective characteristics</i> .....	19
3.1.2.	<i>Convective evolution</i> .....	20
3.2.	FEBRUARY 8 <sup>TH</sup> .....	22
3.2.1.	<i>Convective characteristics</i> .....	22
3.2.2.	<i>Convective evolution</i> .....	24
3.3.	HAIL CHARACTERIZATION .....	26
3.4.	ENVIRONMENTAL CONDITIONS SUPPORTING HAIL-PRODUCING CELLS .....	27
3.4.1.	<i>December 13-14</i> .....	27
3.4.2.	<i>February 8<sup>th</sup></i> .....	32
<b>4.</b>	<b>DISCUSSION</b> .....	<b>36</b>
<b>5.</b>	<b>CONCLUSIONS/FUTURE WORK</b> .....	<b>44</b>
<b>6.</b>	<b>REFERENCES</b> .....	<b>47</b>
<b>7.</b>	<b>TABLES</b> .....	<b>52</b>
<b>8.</b>	<b>FIGURES</b> .....	<b>54</b>

## **1. Introduction**

### **1.1. Motivation**

Falling hailstones are some of the most destructive natural phenomena in convectively active regions of the world. In the U.S., hail damage is the costliest natural hazard in terms of insured losses of homes, businesses, automobiles, aircraft, and agriculture (Dennis and Kumjian 2017) with individual storm damages in extreme cases exceeding 1 billion dollars (Höller and Reinhardt 1986; Kunz et al. 2018). In other parts of the world, such as India, hail can decimate crops and fauna, such as a 2014 Maharashtra storms that affected thirty-five species of birds and nine species of mammals (Narwade et al. 2014; Bal et al. 2014). In Europe, because of the lack of temporal and spatial records of large hail, most climatological studies about hail over Europe do not concern large hail (larger than 5 cm). This is because European weather stations typically do not record hail sizes (Punge and Kunz 2016; Pucik et al. 2019). Pucik et al 2019 through a compilation of limited hail reports through Europe found that that hail impacts could be correlated to the size of the hailstone. Damage to crops and trees were most frequently associated with hail sizes ranging from 2 to 3 cm while damage to roofs, cars and windows were typically reported with larger hail between 4 to 6 cm. To reduce the impact of these losses, it is essential to advance forecasting of hail by improving weather model processes and satellite detection involved in hail formation, development, and environmental conditions that anticipate hail threats.

Cordoba Province in Argentina is a region of severe storms of worldwide relevance as shown by (Zipser et al. 2006) using satellite minimum IR brightness temperatures as proxies for intense storms. These storms are characterized by tremendous vertical development (crossing the tropopause reaching 18 km), generating a significant amount of precipitation leading to floods, strong destructive winds accompanied by tornadoes, intense electrical storms and produce large hailstones. These are some of the meteorological phenomena in the southeastern part of Southeast South America (SESA), which makes this region the most intense convective systems in the world. However, there's a lack of ground-based data to observe and understand these convective systems. Current forecasts for hail formation and development have significant challenges. Its difficulty comes from the limited knowledge of the main environmental and storms internal controls on hail size. Additionally, there is no robust conceptual model that explains processes responsible for why some storms produce extremely large hail while others produce large accumulations of small hail. The international field campaign RELAMPAGO-CACTI in 2018-19 focused on studying these events and try to better understand convective systems in Argentina. It provides ground-based datasets and ground validation of hail reports, starting to look at the production of severe weather and the role of terrain processes in initiating and developing organized convective systems.

## 1.2. Background

### 1.2.1. *Hail Development*

Hailstones are pellets of ice formed inside a convective storm (Rogers and Yau 1989). Their development is typically three to four miles above the surface (in warm seasons), where air temperatures range from  $-10^{\circ}$  to  $-30^{\circ}$  C. Hail starts to develop as water vapor condenses in the updraft and then freezes if conditions are sufficiently cold, forming embryos (e.g., snow or frozen raindrops), that collect supercooled cloud droplets becoming into a hailstone (Browning et al. 1976); extreme rimming could also have the same result. Hail growth is possible by the re-entering of hailstones in a strong updraft after falling some distance, carried through the cloud again in moist air, growing another layer, and falling again following a recycling process until the updraft cannot support the weight of the hailstone which then makes it fall to the surface. However, more recent studies hypothesize that instead of a “recycle cycle” through the cloud, most growth occurs on one pass through the updraft, suggesting that the key to large hail is large supercooled liquid water content and residence time (Kumjian et al. 2019). Levi and Aufdermaur 1970 and Knight and Knight 1970 established a relationship between air temperatures and hail ring growth where they found that ring growth is highly dependent on the surrounding air temperature in the cloud. Optimal hail growth is dependent on five key characteristics: 1) appropriate updraft strength and breadth to facilitate the suspension of hailstones/embryos, 2) sufficient amounts of supercooled liquid water, 3) temperatures conducive to hail growth, 4) the size and number of embryos such that the particles are balanced in the updraft and competition does not deplete the total water content, and 5) trajectories that take these embryos through the optimal growth environments (Dennis and Kumjian 2017). It’s still unknown where the hail

is falling out with respect to the strong updraft, with recent models such as in Kumjian et al. 2020 predicting that giant hail found in Argentina is only possibly supported in the main updraft and falling under it.

### *1.2.2. Types of convective systems producing hail in Cordoba*

Previous studies have aimed to understand the seasonal variability of convective systems in Argentina. Vidal 2014 looked at different precipitation systems through precipitation features (PF) using the Tropical Rainfall Measuring Mission (TRMM) database from January 1998 through December of 2010 (13 years). He characterizes precipitation features into four categories: large precipitation systems with deep convective cores, large precipitation systems with shallow convective cores, small precipitation systems with deep convective cores, and finally small precipitation systems with shallow convective cores. Vidal found that austral summers (DJF) explain most of the precipitation in South America because of the large events associated with large precipitation systems with deep convective cores, specifically in northeastern Argentina. Mulholland et al. 2018 took a similar approach, but additionally used operational ground-based radar data between May 2015 and May 2017 to validate TRMM PFs and similar to Vidal, he found that austral winter months of May–September were characterized by the fewest number of events, with a large increase in events between October and February (austral spring into summer). Finally, (Bruick et al. 2019) focusing in hailstorms in this region, through a 16-year observational period of TRMM PFs also found a maximum frequency of hail occurring during the austral warm season (October–March). This study only inferred hail-producing storms from satellite data and did not have actual ground-validation of hail.

The mode of convection (discrete vs multicellular) has been shown to directly affect the production of severe weather (Dial et al. 2010). Previous studies in the United States, such as Smith et al. 2012, have shown that most tornado activity and hail reports are associated with super cellular convection. More specifically, Blair et al. 2017 suggest that there is “a strong bias for supercell thunderstorms to frequently produce the largest hail compared with other convective morphologies (Nelson 1987; Miller et al. 1988; Johns and Doswell 1992; Duda and Gallus 2010; Dawson et al. 2013)” The non-super cellular convection mode is associated with smaller-diameter hailstones. However, multiple limitations have previously made it difficult to study convective mode and severe weather in Argentina such as the lack of high spatial and temporal radar data, surface and upper-air observations, and standard severe weather reporting.

To get more insight into the convective mode and severe weather in Argentina, research done by Mulholland et al. 2018 separated different convective modes into four categories using the C-band radar (RMA1) located in Córdoba city during austral springs and summer from 2015 to 2017. The categories were: *Multicell Unorganized* events which displayed cells that were  $\leq 25$  km from one another with reflectivity  $\geq 30$  dBZ, **Multicell-organized (MCS)** events which displayed a region of contiguous reflectivity  $\geq 30$  dBZ over a horizontal distance of  $\geq 50$  km and contain at least one  $\geq 50$  dBZ reflectivity core, *Discrete Non-Supercell* events which displayed non- or weakly rotating cells that were  $> 25$  km apart from one another with reflectivity  $\geq 30$  dBZ and finally *Discrete Super-Cell* events which displayed clear rotation for  $\geq 15$  min with reflectivity  $\geq 30$  dBZ and were typically associated with reflectivity hook echoes. This research found two-thirds of its sample size was

characterized as a multicellular convective storm also agreeing with satellite observations analyzed by Bruick et al. 2019 showing, that the majority of the hail-producing storms inferred from the satellite were organized multicellular convection.

The “Sierras de Cordoba” is a mountain range located in central Argentina, much older than the Andes (from the Tertiary), forming from the Lower Paleozoic. Due to their age, they are strongly eroded. There is one orographic formation at the southern boundary between San Luis and Cordoba Province and the rest of the formations extend north to the west of the Cordoba Province at the same latitude as La Rioja and Cartamarca Provinces. This mountain range is composed of 4 main chains of mountains: Sierras Chicas, Sierras Grande, Sierras de Pocho and Sierra de Comechingones, which can reach an altitude up to 2882 meters above the seal level. Vidal 2014 found that convective systems that developed within the “Sierras de Cordoba” initiated at the end of the day between 21 and 00 Z and had a long convective life, ranging from 24 up to 60 hours. Furthermore, Mulholland et al 2018 found that there is a distinct bimodal structure in the temporal distribution of convective initiation, with its first peak occurring between;1400 and 1900 UTC (1100–1600 LST) and the second peak occurring between 2300 and 0600 UTC (2000–0300 LST) for all convective modes. Bruick et al 2019 examined the diurnal cycle of hailstorms in sub-tropical South America and found that hailstorm activity begins to increase early in the afternoon (1700 UTC; 1400 LT) and continues through the next morning.

### *1.2.3. Ingredients supporting these storms type*

Alvarez et al. 2015 found that regional circulation anomalies mainly over southern South America can be influenced by the large-scale extratropical circulation anomalies in turn induced by the convection enhanced or suppressed by the Madden–Julian oscillation (MJO) over tropical western Pacific-Indian tropical oceans. During December, January and February (DJF), warm anomalies are present over the extratropical part of the continent from phase 6 to 1, when anomalous downward motion is favored over the SESA region. Alvarez found that during austral summers, there's an increased chance of precipitation in the SESA regions potentially favored by upper-level convergence over tropical South America and a cyclonic anomaly around its southern tip, both being circulation responses to MJO activity.

The trade winds in the Caribbean split into another branch which, influenced by the presence of the continent and the mountain barrier, flows southwestward to Venezuela, Colombia, and northern Peru reaching speeds higher than  $10 \text{ m/s}^{-1}$  over a narrow extent known as Llanos. This jet is referred through the literature as the northern branch of the South American Low-Level Jet (Jones 2019). It is well documented that the SALLJ has a strong influence on the development of deep convection over the SESA region (Salio et al. 2002; Vidal 2014; Rasmussen and Houze 2016; Mulholland et al. 2018; Bruick et al. 2019; Jones 2019). The decelerating leading edge of the flow promotes strong convergence of the horizontal wind field, thus allowing low-level moisture to ascend into the free troposphere. If it occurs in an unstable synoptic-scale environment, it can result in the development of large MCSs (EUMeTrain).

Rasmussen and Houze 2016 discuss how moisture fluxes controlled by the strength of the SALLJ, dry air subsidence from the westerlies traversing the Andes Mountains, and lee cyclogenesis are important elements for the occurrence of convective systems developing over las Sierras de Cordoba. “Enhanced moisture flux of warm and moist low-level air from the Amazon basin via the SALLJ is being capped by mid- to upper-level dry air subsidence from the westerlies traversing the Andes Mountains. Lee cyclogenesis then induces a north-south pressure gradient that helps bring air from the SALLJ into the foothills of the Andes instead of its climatological position to the east.” Low- to midlevel flow around the southern Andes converges with the SALLJ (Rasmussen and Houze 2011), which is collocated with the Sierras de Córdoba, forming the optimal region for convective initiation in subtropical South America. Thus, while the Sierras de Córdoba help focus and initiate convective storms, they happen to exist in an ideal location to intercept converging air masses from various sources.

Previous work suggests that the topographic relief of mountains is a critical element for hail formation in deep convective systems occurring near mountains. Levi et al. 1989 showed that convective systems that developed in this region are “lineal convective systems” that move from the southwest to the north of the Cordoba Province and that the ascending atmospheric movement is improved by the forced convergence caused by mountain slopes, which is a favorable situation to generate deep convective clouds. Terrain modification runs by Rasmussen and Houze 2016 showed how reducing or increasing the topographic relief of the Andes would affect convective initiation, on how convective system would propagate over this area, on the flow modification of low-level synoptic disturbances, and the average convective available potential energy and convective inhibition values available for

convection systems developing in this region. Other studies such as (García-Ortega et al. 2009) looked at two hailstorm studies and found out that regional topography was one element that played a key role in triggering convection over the Andes. (de la Torre et al. 2011) found a relationship between mountain waves and the development of deep convection in the Mendoza region near the Andes. This study concluded that mountain waves could be the main forcing for convection developing in the Mendoza region, through the analysis of Convective Available Potential Energy (CAPE) and Convective Inhibition (CIN) indices. On the other hand, other authors such as Teitelbaum and D'Andrea 2015 showed that mountain waves do not play any role in the production of deep convection and hailstorms, at least in the cases they focused on rather having large scale ingredients, similarly discussed in Rasmussen and House 2016, may play a bigger role for convective initiation in this region.

#### *1.2.4. Attempts to infer hail from data*

Visible and infrared measurements can be exploited to get a more comprehensive mapping of hail occurrence (Bauer-Messmer and Waldovel 1997; Ravinder et al. 2013; Merino et al. 2014). This data set has the potential for detection and nowcasting of hailstorms in particular regions (Ribeiro et al. 2019). When characterizing convective clouds producing hail, it is essential to geographically locate each hail sample. According to Roca and Ramanathan 2000 and KONDURU et al. 2013, brightness temperatures are directly associated with the type of cloud. Müller et al. 2018 showed how a strong vertical updraft could be inferred from the cooling rate, defined by the temporal change of the brightness temperatures of the cells between two subsequent satellite images. To have hail in a convective cloud, we need a strong vertical updraft that can support the weight of a large

hailstone, and by then we can use the brightness temperatures to infer if a convective system could support hail and how big could be. From a radar's perspective, the reflectivity of hail is going to depend upon whether the outside surface is wet, dry, or if there is any water enclosed in the hail. Dry hail tends to show lower reflectivity than wet hail from the same size; this comes from the different dielectric constant of ice and water. The reflectivity from a single hailstone or a collection of stones falling through similar conditions at the same location can change as it falls from above the melting level to below melting level (Rinehart 2010).

#### *1.2.5. Research Questions/Objectives*

Previously discussed studies are prominently from satellite snapshots or modeling studies and they are using proxies without hail validation. The only study that uses ground-based radar data is Mulholland's et al 2018 but is only for a few seasons. All these studies are limited in the fact that there not a lot of continuous ground-based observations or hail validation that relate to what they are discussing. So, these proxies are presented in a more statistical sense, but it is unclear if they are representative of the evolution of storm that produces hail in this region? For this study we have collected hail in the Cordoba region from a record-breaking hail event and from during RELAMPAGO which gives us a novelty aspect of having actual verification of hail events from two case studies. Given the hail reports, can we look at how well can satellite hail detection algorithms and background large-scale meteorological conditions predict the likelihood of large hail development in Argentina? We hypothesize that a combination of satellite and radar data will allow us to adequately identify hail events in a convective system and that large-scale ingredients are necessary for hail

development in the cloud. To start looking at this problem we will: (1) identify the storm mode, timing, and location of hail-producing storms, (2) describe the hail characteristics to look for similarities and differences, (3) describe temporal and spatial evolution using satellite and radar to see if previously discussed thresholds help determine where and when the hail formed, (4) describe the large-scale conditions favoring the development of these storms and (5) have a discussion including these storms to their warnings done by the local National Weather Service.

## **2. Methods**

### **2.1. Choice of cases to study**

February 8<sup>th</sup> and December 13<sup>th</sup> in 2018 were primarily chosen for analysis because we were able to collect giant hailstone samples from both case studies (as shown in Figure 2.1.1) to validate observations from satellite and radar images. Note that they both occur within times of the year when previous studies such as Vidal 2014 and Mulholland et al 2018 showed these convective systems were frequent and also Bruick et al. 2019 suggested hail is frequent in this region. Hail reports that were associated with available hail samples were available using data collected through a Ministry of Science and Technology of the Cordoba Province program, "Cosecheros de Granizo" (Arena and Crespo 2019). Other hail reports were found through a mix of social media platforms such as "Twitter", "Facebook", and local newspapers online.

### **2.2. Convective storm identification and tracking**

#### *2.2.1. Satellite*

To identify and track the storm, we used specific channels from the satellite GOES-16. This satellite has a spatial resolution of .5 km for channels of .64  $\mu m$  in the visible spectrum, 1 km for other channels in the visible and near IR, and 2 km for channels greater than 2  $\mu m$ . Data is available every 15 minutes. The channel 5 (1.6  $\mu m$ ) "snow/ice" band is used for daytime cloud, snow, and ice discrimination, and was used in this analysis to identify possible hail zones in the cloud. Channel 10 (7.3  $\mu m$ ) gives information about lower mid-level atmospheric flow and can help identify jet streaks. It is used in this analysis to look

at the low and mid-level moisture in the atmosphere in the location studied. Channel 11 (8.4  $\mu\text{m}$ ) or “cloud-top phase” band is commonly used to determine the microphysical properties of clouds. This channel is used to analyze the area in kilometers squared of each convective system in both case studies and also used to define and track convective cores of each storm. Finally, Channel 13 is also known as the “clean” infrared because its low sensitivity to water vapor is used to identify when and at what time clouds become convective. Specific channel information was taken from the online GOES R ABI information guides by NOAA and NASA. Channels 5, 10 and 13 were picked for the information they provide to the analysis of this project (including measurements of convective activity and environmental conditions), and channel 11 was picked based on the relationship previously established by Müller et al. 2019, and the need of strong updraft to support giant hail in the cloud discussed by Kumjian et al. 2020.

We will use channel 11 brightness temperatures thresholds previously defined by Roca and Ramanathan 1999 and Konduru et al. 2013 to: calculate the area of each convective system, identify the overshooting top of a convective system which we will call “convective core” and track the convective storm through time. During these two case studies, giant hail was collected and recorded in Villa Carlos Paz (VCP) and nearby towns, and Villa del Dique (VDD) (Figure 2.1.1). We correlated the satellite information with the hail sample records and identified the genesis of the convective process. Firstly, satellite images were filtered to only show minimum brightness temperatures of 250 K to calculate each storm's area before, during, and after a hail event demonstrated in Figure 2.2.1. In this procedure, spaces within the storms (area with brightness temperatures greater than 250 K) were subtracted. To look at the temporal evolution of the cloud top area for both case studies in February and December,

satellite images were filtered to temperatures below 200 or 205K to infer the updraft intensity of the cloud and visualize the system's isolated convective core as shown in Figure 2.2.2 (b). It should be noted that the trajectory obtained with this method will have a systematic shift in the direction of the winds. Pixels showing brightness temperatures thresholds with three or more pixels in the image were considered to be included in the total area.

This same procedure was carried out at the following times: 18:00, 18:15, 18:30, 18:45, 19:00, 19:15, 19:30, 19:45, 20:00 UTC for February 8<sup>th</sup> and 01:45, 02:00, 02:15 UTC for December 13<sup>th</sup>. Next, we used a brightness temperature threshold of 211 K and for any grouping of pixels that met that threshold, we calculated the midpoint of that grouping to locate and track the “core” of the storm as shown in Figure 2.2.2 (c). This temperature is explicitly used because at 18:00 UTC it is the only pixel available for the northern convective cell on February 8<sup>th</sup>. However, with this method we realized that this midpoint using 211 K didn't always coincide with the actual overshooting top of the storm defined as the pixel with minimum brightness temperature. Therefore, we instead used a minimum brightness temperature threshold of 205 K and the same midpoint approach (Figure 2.2.3) to locate and track the core of the storm.

We assume that it is possible to compare the coordinates of the convective cores (minimum brightness temperature less than 205 K) with those of the hail fall on the ground, since: (1) the hailstones are large (following Pruppacher and Klett 1980, the terminal velocity of a 17.5 cm hail is 33 m/s, which in an approach of free fall at that velocity would give a fall time of 1 min. This time is compared with the hailstorms that have been followed for one hour. (2) The parallax between the cloud top (approximately 10km of high) and the height of the GOES 16 satellite orbit (35786 km) is negligible (0.03%). (3) The advancing speeds of

the storms range from 10 to 37 km/h, therefore the storm travels 4 to 10 km per satellite image which is much higher than the 2km resolution for GOES-16 infrared channels.

### 2.2.2. Radar

Radar data used for this project came from the C-band Córdoba radar (5.4-cm wavelength) RMA1, a dual-polarization Doppler weather radar. This radar system was designed and manufactured by INVAP–South America and is operated by the National System of Meteorological Radars for the “Servicio Meteorológico Nacional” (SMN) of Argentina. The product we use in this project is referred to as COLMAX. This is calculated taking as a reference the reflectivity values of radar cells at some particular elevation and then comparing these with the values of the cells at a different elevation that coincides with the vertical projections of the reference cells. The maximum reflectivity values found in the vertical projection of each of the reference cells are saved and are what we see in COLMAX images. These images are available every 10 minutes. For both case studies, we are using 70 dBZ as our threshold values to identify hail areas in the convective cloud (also referred to as “convective cores”), because reflectivity is proportional to the diameter of the hydrometeor to the 6<sup>th</sup> power (Rinehart 2010) so a large hail stone will have a high reflectivity because of its size, as well as due to higher concentrations of hydrometeors which we can assume it has a high probability of hail. Reflectivity-based thresholds discussed in Mulholland et al 2018 will be used to determine the convective mode. It’s worth mentioning that the radar was not calibrated for the storm on February 8th until later that year for the RELAMPAGO field campaign.

### *2.3. Hail Characterization*

Hail was collected in various localities during hail events registered on February 8 and December 13 of 2018 as shown in Table 1. Many locations reported hail fall through social media and in some of those locations hail samples were collected. Each time hail samples were located, Argentinian citizens collected the hail, took a picture with their hands or some other object as a reference, then stored them in their fridges ( $-13\text{ }^{\circ}\text{C}$ ) and contacted us to recover the samples. This hail collection and conservation procedure became an Argentine provincial citizen science program “Cosecheros de granizo Córdoba” from October 2018.

Once we knew about the hail report, we drove to the location. We recorded the location coordinates, the time the sample was collected, and if it rained before, during, or after the hail. We record the name of the person who collected the sample and then signed a document where this person transfers the hail sample ownership to us for laboratory analysis. We record the temperature of the freezer where the hail was kept. We then transfer the hail sample that is kept in a nylon bag to a thermally reinforced cooler where the temperature is controlled at  $-15\text{ }^{\circ}\text{C}$ . Each sample is then classified and identified with the name of the person who collected the sample. Once it reaches the laboratory, it is then transferred to a cold chamber with a controlled temperature of  $-15\text{ }^{\circ}\text{C}$ . This temperature is chosen because the crystallographic structural changes are very slow (the significant changes in crystallographic structure at this temperature may not start to happen after a year or more).

To start processing samples, the subzero chamber had to previously be turned on for a few hours before the analysis (minimum 4 to 5 hours). Once it was running and reached the temperature needed to process the samples ( $-12^{\circ}\text{C}$ ), we then had to use the right clothing (coats, winter pants, and gloves) to work on the cold chamber. Once ready, we then took the

hail samples and got in the chamber quickly (to not let the cold air out and keep the chamber at the temperature needed). Once in the chamber, the hail is measured (the lengths of the lobes, the height and the width), its symmetry is observed, we weigh the sample, then it is glued with water (ultra-filtered and over-cooled) to a glass section and then with the same over-cooled water we stick it to a metal section. We then proceeded to cut the hail sample with a diamond incrustated cutting disk of 10 cm of diameters with a cutting width of 2 mm into sections (one section will be stored away, and the other section will be used for analysis). It should be noted that we cut the hail sample approximately 2 millimeters over the equatorial symmetric plane. Once the hail section is cut, the flat area is then polished with a microtome.

After gently polishing one side of the section keeping side even to prevent the alteration of the structure of the hailstone, and once we had a top view of the embryo, we take multiple pictures. Then we do a surface plastic replicate of that side of the hail (Higuchi and Yosida 1966). A specific solution of formvar diluted in 4% 1-2- dichloritan is applied gently over the flat surface already polished and then left in a sealed low humidity container and with silica gel at room temperature of  $-12^{\circ}\text{C}$  to dry for a minimum of 40 minutes. Once the replica is dry, the replica is then removed, placed on thin glass, covered with an acetate film, and then analyzed under a light transmission microscope with white light.

#### 2.4. Environmental data

Multiple weather stations for surface observations (pressure, wind speed, and wind direction) one-hour prior, during, and one-hour after a hail event where used for this analysis that is managed by SMN. All these stations can be visualized in Figure 2.4.1. Isobaric charts

at 1000, 850, 700, 500, and 250 mb at 12Z for South America were used and available from the University of Wyoming. Operational soundings were used mainly from Cordoba Airport and Santa Rosa Airport at 12Z from an online source in Argentina. Large scale Daily composites for February 8<sup>th</sup> and December 13<sup>th</sup> from the Physical Science Laboratory NCEP/NCAR reanalysis datasets were used, specifically: specific humidity anomaly composites for South America at 850 mb, stream functions anomalies for .8458 and .2101 sigma and wind vector mean composites at 1000, 850, 700, 500 and 250 mb. Finally, surface station observations and soundings at 12 and 22 Z from the RELAMPAGO field campaign were used for the December 13<sup>th</sup> case analysis.

## 2.5. Storm warnings

Storm warnings can normally be accessed through the official governmental page of SMN. The organization keeps warnings 365 days after issued, after this time the reports are available by request. They also have a Twitter account, where they post periodically warnings for different cities in Argentina. Because we tried to access these warnings a year later from both case studies, we were able to access warnings through Twitter and have them to compare their forecast with our result for each day.

### **3. Results**

#### **3.1. December 13-14**

##### *3.1.1. Convective characteristics*

The general temporal evolution of the December 13 storm is shown through satellite images from Channel 13 in Figure 3.1.1. Hail collected corresponds to 02:15 UTC in Villa de Dique in Río Tercero reservoir and graupel in the city of Córdoba at approximately 03:00 UTC. However, no information is recorded of hail fall except in the indicated region; this might be because the storm developed during the night, which limits the number of people able to record the event. Note that because the storm develops at night, channels in the visible spectrum are not available. In Figure 3.1.1, particularly at 22:00 UTC (32 degrees S, 67 degrees W), there is a small northern cell (also referred as the western cell) forming over the plains of the San Luis Province (marked by a white circle), with another notable formation to the southeast (also referred to eastern cell). This western connective cell is the one that has hail reports associated with its convective core before it merged with the eastern cell and then heading north. After the western cell passes over the “Sierras de Comechingones” (which happens at 00:00 UTC) 2 hours and 15 minutes later a hail event is registered in Villa del Dique in Río Tercero. Based on Mulholland’s radar-based thresholds (analysis shown in Figure 3.1.2; at 02:00 and 02:20 UTC) for the different convective modes described, I was able to identify that the convective cell responsible for the hail event in Villa del Dique was a Multicellular organized mesoscale convective system because it displays a region of contiguous reflectivity  $\geq 30$  dBZ over a horizontal distance of  $\geq 50$  km and contains at least one  $\geq 50$  dBZ reflectivity core. It’s worth mentioning that the storm was not tracked after

03:00 UTC because it already merged with the eastern cell, making it difficult to discriminate against each other, so the convective mode only describes the convective system before and during the hail events discussed previously.

### *3.1.2. Convective evolution*

Brightness temperature analysis using thresholds previously described (Figure 3.1.3) showed a gradual decrease of brightness temperatures through time showing brightness temperatures of 200 K in the earlier development stages of the western convective cell (previously marked by a white circle) down to 190 K and lower brightness temperatures before a hail event, and again after it merges with the western convective cell. The convective core was located southwest with respect to the location where the hail fell. Because of the limitation of the satellite images only being available every 15 minutes, we were not able to see the position of the convective core at the exact time of the hail event. Concerning the area evolution, the western cell (Figure 3.1.4) it developed from 104325 km<sup>2</sup> at 01:45 UTC, 123887 km<sup>2</sup> at 02:00 UTC to 235697 km<sup>2</sup> at 02:15 UTC, 5 minutes before the hail event in Villa del Dique, and the eastern cell (Figure 3.1.5) showed area values of 107923 km<sup>2</sup> at 01:45 UTC, 103925 km<sup>2</sup> at 02:00 UTC and 235697 km<sup>2</sup> at 02:15 UTC. No difference between the satellite data for this hail-producing storm compared to the eastern cell was apparent on this day; both cells increased with area and both cells saw decreasing brightness temperatures over the mountains but with these two metrics we were not able to distinguish between the cell producing the hail and the one that presumably did not due to the limitation of confirmed hail reports.

Based on the location of the hail event (Figure 3.1.2; shown by an orange star), we could identify the convective core associated with the hail we collected. With this information I took a similar approach for the radar data as I did with the satellite images from channel 11. We zoomed in to the area near where the hail occurred and identified areas of reflectivity reaching at least 70 dBZ in Figure 3.1.6 (because this threshold is a good indicator that there is hail in the cloud) which we are referring to as “convective cores”. We identified one convective core at 02:10 UTC, no convective cores during the hail event at 02:20 UTC, and 1 convective core 10 minutes later (Figure 3.1.6). This pattern was not compared to the eastern cell that is not associated with hail events on this event. This pattern makes sense because, at 02:15 UTC, we are seeing low brightness temperatures of 190 K in the same region as these high radar reflectivities which means that we could potentially have a strong enough updraft that is supporting giant hail development in the cloud.

On December 12<sup>th</sup> between the hours 13:00 and 15:00 LST, for areas within the north and east of Argentina, warnings were issued for strong storms and intense rains with intense lightning activity, intense gusts wind, and hail fall. Also on December 12<sup>th</sup> at 16:00 LST for locations in central and southern of Córdoba, east and center La Pampa and finally the central and southern San Luis, SMN issued warnings for severe weather due to an unstable humid air mass prevailing in the area accompanied with intense rains, electrical activity, strong gusts winds, and hail fall. Finally, there was the last warning on December 13<sup>th</sup> at 05:00 LST for the southeast area of Córdoba, forecasting storms and intense rains for the morning of December 13<sup>th</sup>, extending to December 14<sup>th</sup> with rainfall reaching 50 and 150 mm. SMN forecasted hail on the 12<sup>th</sup> but focused primarily on heavy rainfall for the 13<sup>th</sup>/14<sup>th</sup> and no mention of hail for that later period. This event occurred toward the end of the

RELAMPAGO campaign and was a mission to study the mesoscale organization of convection later in the evening. Forecast models during the campaign overall struggled with capturing the timing and location of convection, including conditions supporting hail.

### 3.2. February 8<sup>th</sup>

#### 3.2.1. *Convective characteristics*

The general temporal evolution of the February 8<sup>th</sup> storm is shown through satellite images from Channel 13 in Figure 3.2.1. Hail collected corresponds to 18:50, 19:20, 19:20, 19:30, 19:45 UTC in Icho Cruz, Villa Carlos Paz (San Lorenzo Street, Tupungato Street, Tokio Street), and San Nicolas respectively. However, no information is recorded of hail fall for the southern cell; this might be because it advances over a remote area where there is a limited population able to report any hail fall. According to the Figure 3.2.1, a distinctive cell develops over the plains in the San Luis province (32 degrees S, 67 degrees W) and then advances south of Córdoba to the east and then to the north. At 16:00 UTC it reaches the “Sierras de Comechingones” similarly seen on December 13. Likewise, at 17 UTC, the beginning of the formation of a new northern cell that advances eastward through the Sierras de Córdoba is evident. This cell evolves, independently of the previous one, and is associated with large hail that was collected and recorded. This case is different from December 13, because here we have two cells that are developing independently in two different locations (southern cell over the plains as seen on December 13 vs northern cell over las sierras de Pocho, which is part of las sierras de Cordoba.

Radar-based thresholds (analysis shown in Figure 3.2.2) for the different convective modes described, I was able to identify that the convective cell responsible for the hail event in different locations in Villa Carlos Paz and San Nicolas was a Multicell Unorganized event because it displayed cells that were  $\leq 25$  km from one another with reflectivity  $\geq 30$  dBZ. It's worth mentioning that I did not follow the northern convective cell after the last hail report recorded, so this convective mode only fits this multicellular structure system before and at 19:45 UTC. After this time, it merges with the southern cell and advances to the northeast. Using the criteria strictly from reflectivity, we do observe the typical characteristic of a supercell. We can see the hook echo at 19:20 UTC and based on Kumjian et al 2020 analysis on this case that went into more detail of the radar data, he also concluded that this case had supercell characteristics.

Satellite images from Channel 5 were analyzed to track the storm and identify zones in the cloud which could potentially have hail (Figure 3.2.3). Black dots in Figure 3.2.3 show the presence of ice in this region at the time at which hail was recorded and collected with an amplification of the image to the maximum limit resolution. These figures were correlated with hail reports from social media and articles from local newspapers and a TV news channel. Images at 18:45 UTC show that the "ice zone" represented by black dots is located in Icho Cruz where the first hail event was reported. The second image at 19:00 UTC shows how the ice zone increased its spatial distribution, with a "boomerang" shape area and black spots 10 to 15 km south of Icho Cruz. The following image at 19:15 UTC, 5 minutes before a hail event, shows the black spot area near San Lorenzo and Tupungato. The ice zone expanded significantly in straight-line south of San Nicolás, and some new black spots

emerged to the east of the storm. Finally, at 19:30 UTC, we can observe how the ice zone are moving northeastward, 20 km from Cordoba.

### 3.2.2. *Convective evolution*

Brightness temperature analysis using thresholds previously described showed a gradual decrease of brightness temperatures through time showing brightness temperatures of 210 K in the earlier development stages of the convective system down to 195 K of minimum brightness temperatures before a hail event, and areas of low brightness temperatures increase spatially after it merges with the southern convective cell. The convective core from the northern convective cell was located southeast (as shown in Figure 3.2.4) with respect to the location where the hail fell. This is a similar pattern to what was found during December 13<sup>th</sup>. We initially plotted San Lorenzo, Tupungato, and Tokio because they were the only locations, we had hail samples from. Icho Cruz and San Nicolas were found after I noticed that the convective core was positioned southeast of where we collected hail. On February 8<sup>th</sup> and December 13<sup>th</sup> hail events happened northward of the convective core. Concerning the area evolution of the northern cell (Figure 3.2.5), we observed a rapid growth (within 1 hour and 45 minutes, the area jumped from around 4000 km<sup>2</sup> to around 20,000 km<sup>2</sup>). The southern cell, on the other hand, was more extensive spatially (Figure 2.2.6) speaking but it didn't have as low of brightness temperatures as the northern cell had (southern cell showed 210-215 K vs northern cell showing 200-195 K). This pattern suggest that the southern cell didn't have as deep of vertical development as the northern cell and therefore, we assumed it was going to have either small hail associated with it or lower chances of having a hail event. After it reaches 19:45 UTC, it merges with the northern cell, and shortly after the rest of it

dissipates. However, we don't have any confirmation that it hailed because it's happening in a remote area. Even though it didn't show the same characteristics seen in the northern cell on this day and the western cell on December 13<sup>th</sup>, we can't validate whether if it had a hail event or not.

Based on the location of the hail event (shown by multiple colored stars in Figure 3.2.2), we could identify the convective core in radar that was associated with the hail we collected. With this information I took a similar approach as I did with images from channel 11 in identifying a convective core and relating that location to the hail report. We zoomed in to the area near the hail reports on this case and identified areas of radar reflectivity reaching or higher than 70 dBZ in Figure 3.2.7 (because this threshold is a good indicator that there is hail in the cloud). In figure 3.2.7, we see an increase of the number of convective cores after the first hail event, and then it decreased 10 minutes after where we had our second and third hail events then it maintained the same number of convective cores through the 5th hail event as well. Is very interesting that we are observing more convective cores with > 70 dBZ reflectivity present in this cell, compared to the cell on December 13<sup>th</sup>. We also observe that we do see a pattern somewhat different from the overshooting top in satellite images. Here we can see that the convective core is located southwest of the hail events.

Two warnings were made by SMN, one on February 7<sup>th</sup> concerning high temperatures reaching 35° and 40° C in the central regions of Argentina with rain and isolated storms in the area. It was also mentioned that by February 9 there was going to be a temperature drop because of a cold front passing over the area then. There was a second warning on February 8<sup>th</sup> for the Mendoza region (Zona Cordillerana de Cuyo) and north Argentinian region for persistent precipitation. SMN stated a warning that there was going to be a development of

heavy rain and isolated storms with a variety of intensities until the morning of the next day. In regions reaching 4000 meters, storms were expected to produce periods of intense rain and snow. Regions that were going to experience intense convection included: La Rioja, Catamarca, Salta, and Jujuy. Similarly, to December 13<sup>th</sup>, SMN forecasted the development of strong isolated storms over the mountains but didn't forecast hail for this event as well.

### 3.3. Hail Characterization

Table 2 shows a summary of the hail characterization analysis. For samples collected in Villa Carlos Paz, we had 40 samples of hailstones collected that fell from 19:00 to 19:45 UTC on February 8<sup>th</sup> from an Unorganized multicellular convective system with minimum brightness temperatures of 195 K just before hail fall. The northern cell average area for the hail events was 9832 km<sup>2</sup>. The minimum diameter found in the sample group was 3 cm, while the maximum diameter was 17 cm. The prevailing geometric shape was spherical for all hailstones, lobes were present, we found micrometric bubbles, and also giant bubbles which makes the density of the hailstone spongy. For samples collected in Villa del Dique, we only had one hailstone that fell at 02:00 UTC on December 13<sup>th</sup> with minimum brightness temperatures of 190 K before the hail fall associated with a multicellular mesoscale convective system. The western cell area was 154638 km<sup>2</sup> before the hail event. The diameter for this hailstone was 8 cm, with a spherical geometric shape. Lobes were present, we found micrometric bubbles, and also giant bubbles which also made the density of this hailstone spongy. Finally, the last sample group that was registered in Cordoba city at 03:00 UTC associated with minimum brightness temperatures of 195 to 190 K was also associated

with a multicellular mesoscale convective system. Our sample size was composed of 8 graupel showing a minimum diameter of .8 cm and a maximum diameter of 1.3 cm.

### 3.4. Environmental conditions supporting hail-producing cells

#### 3.4.1. *December 13-14*

As seen in Figure 3.4.1, relative humidity composite reanalysis has an anomalous area of humidity extending from west Brazil to the northeastern part of continental Argentina at the 850 mb level. Similarly, we observe the same pattern on images from channel 10 with important moisture concentrations over west Brazil and west, and south continental Argentina. A distinctive high humidity area is observed central east of Argentina even though we don't see clouds in the satellite images at this time in this region of higher humidity. Also, there are anomalously high areas of humidity west of Brazil and southern Argentina and also a mass of warm dry air advancing over the Andes seen on channel 10. Satellite images are temporally sequenced in close to hail events.

Based on the analysis the 850 hPa isobaric chart at 12 UTC on December 13<sup>th</sup>, we observe a low-pressure system over central northwest of continental Argentina (fitting with previous descriptions of the North Argentinian low described in (Celeste Saulo and Nicolini 1999), which is typically located around 36 S-66 W), and another located over the Atlantic southeast of Brazil. We also observe oceanic high-pressure systems west of Chile, east of Argentina and south of Uruguay, and a third system east of Brazil. We looked at radiosonde observations at 850 mb level, then overlaid the wind patterns as arrows on the isobaric chart at the same level. Previous analysis shows that there are westerly mid-level winds at 10 kt west of the Andes, a northeasterly flow at the same speed, and a third Antarctic flow coming

from the southwest which is justified by the position of high- and low-pressure systems in this area. Based on the temperature and wind analysis there is a switch in wind direction, with a warm airflow coming from the north and converging with a cold air mass coming from the south (as shown in Figure 3.4.2). With this information and that in the satellite images we were able to see the convection forming along the cold front, there is a clear stationary cold front located in this region, which is preventing the warm northerly flow from moving further south making it an area of convective initiation on this day.

In Figure 3.4.3, as in previous figures, we are observing the same low-pressure system northwest of continental Argentina and another located in the Atlantic southeast of Brazil. We also observe oceanic high-pressure systems west of Chile, east of Argentina and south of Uruguay, and a third system east of Brazil. Both soundings at Cordoba Airport and Santa Rosa Airport are showing a strong northerly flow at 15 kt. Shown isobaric charts at 1000 hPa at 12 UTC shows a trough over continental Argentina (low-pressure system fits the description of aforementioned Northern Argentinian Low from literature), specifically with its peak on the lee side of the Andes which is expected to support cyclogenesis and a ridge (high-pressure system) east coast of continental Argentina and Uruguay which fits with the wind observed from the soundings. Anomalously high cyclonic circulation from the trough and anti-cyclonic circulation from the ridge from the trough and ridge observed might support the northerly flow we are observing at the surface. Finally, 1000 mb composite vector winds from NCAR reanalysis are showing the expected pattern that the geostrophic wind would have under these conditions and go along with what we are seeing with surface observations and pressure map also showing a weak westerly flow from the Pacific (4 to 5 m/s which is approximately 10 kt).

As seen in Figure 3.4.4, there is an important low-pressure system in the center of Argentina associated with the convective system studied. The sounding from Cordoba Airport taken at 12z is showing a strong northeasterly wind flow at 35 kt while the Santa Rosa sounding taken at the same time is showing a slight tilted northwesterly flow at 25 kt. Also, at 850 hPa, CSU sounding was taken at 22z on December 13<sup>th</sup>, launched east of Cordoba city, which is also showing a strong northerly wind flow. Wind composite mean reanalysis shows more intensive flows concentrated in the northeastern part of Argentina which would be the area expected to have strong currents to have a rich moisture source. Westerly flow from the Pacific is still observed with a weaker flow over the northern half of Argentina after it hits the Andes, and a stronger flow crossing over la Patagonia.

At 700 hPa, shown in Figure 3.4.5, soundings at Cordoba and Santa Rosa are showing the North-westerly flow which is also seen in the pressure map. They also show 30 kt northerly winds at 750 hPa in both sounding sites. We start seeing a stronger southeasterly flow from the Pacific windward side of the Andes and then a northwesterly flow on the lee side. This could be the orographic deflection of the mid-level winds by the Andes. At this level, there is also a second though south of Brazil east of Argentina and Uruguay showing maximum wind speeds of 27 m/s. At 500 hPa, soundings at Cordoba and Santa Rosa are showing the same pattern seen in 700 hPa with stronger mid-level jets, which is also seen on the pressure map and wind vector reanalysis (figure not shown).

Finally, Figure 3.4.6 is showing data at 250 hPa. Soundings from Cordoba and Santa Rosa are showing a northwesterly flow of 80 and 90 kt. Pressure maps at this level show stronger southeasterly flow from the Pacific windward side of the Andes and then a northwesterly flow on the lee side. A similar pattern is observed in wind vector reanalysis.

We also observe two jet streaks located at the windward side of the Andes and the second one on the lee side with average speeds of 55 m/s.

Multiple surface station observations were analyzed and compiled into Figure 3.4.7 for December 13<sup>th</sup> as well. At 22:00 LST, Cordoba readings are showing a northeasterly flow, Pilar read a northwesterly flow, while Merlo registered a westerly flow, and finally San Luis and Rio Cuarto showed southeasterly flow and a southerly flow respectively. At 23:00 LST, Cordoba now shows a northeasterly flow, Pilar a southerly flow, Merlo recorded a westerly flow, and San Luis and Rio Cuarto showed a southeasterly and southwesterly flow respectively. Finally, on December 14<sup>th</sup> at 00:00 LST, Cordoba station reported winds coming from the southwest, Pilar registering a southeasterly flow, Merlo a constant westerly flow, Villa Dolores registered a southerly flow, San Luis and Rio Cuarto showing a westerly and southwesterly flow respectively.

All of the results discussed previously point to the presence of the South American Low-Level jet which is the main factor to provide all the moisture from the Amazonian basin to the area studied. Firstly (Figure 3.4.8), in the NCEP/NCAR relative humidity composite reanalysis we observed a large anomalous area of high humidity that extends from west Brazil to northern central Argentina. Then wind patterns 1 km above the surface produced by the low and high-pressure systems are potentially supporting the low-level jet as seen in NCEP/NCAR .84 sigma stream function analysis showing a strong cyclonic anomaly west of continental Argentina (associated with the trough west of the Andes) and a significant anti-cyclonic anomaly east of Argentina (associated with the ridge south of Brazil over the Atlantic).

As discussed in (Jones 2019), SALLJ wind speeds exceeding  $10 \text{ m s}^{-1}$  are maximum at 850 hPa (1-2 km above the surface), which we are observing at our previous analysis at this level. Finally at 250 hPa (around 10 km above the surface), as described in Salio et al. 2002, pressure maps at this level show stronger southeasterly flow from the Pacific windward side of the Andes and then a northern westerly flow on the lee side with two jet streaks located at the windward side of the Andes and the second one on the lee side with average speeds of 55 m/s. An upper-Level Jet upwind of the Andes decelerates as it crosses the mountains. The NW-SE upper-level jet streak produces a direct ageostrophic circulation on its entrance region. The interaction between the low-level branch and the LLJ reinforces the convergence at the left entrance region of the ULJ facilitating the development of convection in this area. This favors a meridional indirect ageostrophic circulation in its exit region. Its low-level branch, a northerly wind flow, then reinforces the SALLJ (that goes along with what we are observing at 850 hPa but having maximum speeds at 750 hPa). Furthermore, as the upper jet crosses the Andes, the ensuing subsidence on the lee of the mountains induces heating and negative pressure anomalies at low levels which are associated with the NAL (which a similar described feature was observed at 1000 and 850 hPa).

All these elements discussed previously reflect what has been described by Salio et al. 2002 associated with a Chaco event. Its duration varies more frequently from 1 to 5 days (similar northern flow was observed for five consecutive days as shown by wind vector reanalysis shown in Figure 3.4.9). Circulation features and the thermodynamic field shown by this event have a specific maximum contrast of air masses in a latitude close to  $39^{\circ}\text{S}$  (as observed in Figure 3.4.4 wind vector reanalysis ), presence of a trough centered on  $70^{\circ}\text{W}$  within a baroclinic wave train penetrating from the Pacific Ocean, and a maximum of heat

and moisture over northern Argentina and Paraguay. During the CJE, there is an important flux of moisture and convergence at low and mid-levels that is about 10 times more intense than the summer mean. This clear moisture flux of moist low-level air from the Amazon basin via then is then capped by mid- to upper-level dry air subsidence from the westerlies traversing the Andes Mountains as seen in satellite from channel 10. Lee cyclogenesis then induces a north–south pressure gradient that helps bring air from the SALLJ into the foothills of the Andes, creating an optimal region for convective initiation.

#### *3.4.2. February 8<sup>th</sup>*

Figure 3.4.10 shows that the relative humidity composite reanalysis shows an anomalous area of humidity extending north of Chile, northwestern Argentina around 30 S, 68 W showing 15%, and finally south of Chile at 850 mb level. Similarly, as seen in December 13<sup>th</sup> case study satellite images are temporally sequenced in close to hail events. The first three images are shown from channel 10 where the first red circle corresponds to coordinates around 32.25 degrees S, 67.5 degrees W, showing important isolated parcels of humidity. The second and third figures next to it with a blue circle are showing another smaller cell forming to the north as described previously. The low-pressure system seen in the isobaric chart is associated with an important humidity parcel developing into a convective cell in channel 10 (“zone of interest” represented by the dark blue square in the isobaric chart). Also, there’s a northwesterly flow at 30 kt that would support the path of this cell as seen on December 13<sup>th</sup> and following with a weaker northerly flow at 10 kt compared to our case study on December 13<sup>th</sup>. Average relative humidity shows a center of the

anomalous area of interest in the same zone as the low-pressure system in continental Argentina.

Figure 3.4.11 shows that the Cordoba sounding, and Santa Rosa sounding doesn't show a wind reading at the surface, but we can observe winds at 900 hPa level, where Cordoba sounding is showing a northwesterly flow and Santa Rosa is showing a southerly flow. Isopleths maps at 1000 hPa show two low-pressure systems located in the central northwest of Argentina and another low located southeast of Brazil. Mean wind composite reanalysis is showing a northeasterly flow around Paraguay and Uruguay, and they all converge in the northern half of Argentina (circled) which goes along with the pattern shown in sounding at 900 mb, while there's a southwesterly flow going over la Patagonia.

The Figure 3.4.12 show data at 850 hPa, the sounding from Cordoba Airport is showing a northwesterly flow in contrast with Santa Rosa which is showing south-south easterly flow. The isobaric chart wind map is showing the same low-pressure systems seen at 1000 hPa level. Mean wind composite reanalysis shows this distinctive division of winds, where the southern part of Argentina has a continuous westerly flow going over la Patagonia and continuing to the Atlantic, while the northern part of Argentina have a weak northerly flow converging with the westerly wind mentioned before which is the behavior expected based on what we observe on .84 sigma stream function analysis with an anomalous region of cyclonic rotation over the southern regions of Argentina (Figure 3.4.13).

The Figure 3.4.14 show data at 700 hPa, Cordoba Airport is showing weak southeasterly flow while Santa Rosa shows a northwesterly flow, which is the same pattern seen in the mean wind composite reanalysis data. Previously mentioned southwesterly current gets stronger coming from the Pacific before it goes over la Patagonia extending to

the Atlantic also seen in the wind composite analysis which is expected when tight isopleths are present in the southern part of Argentina. At 500 hPa, Cordoba Airport shows a southwesterly flow, and Santa Rosa shows a westerly flow. We still observe a westerly flow, with stronger jet speeds reaching the 35 m/s (figure not shown). Finally, at 250 hPa, Cordoba Airport sounding shows a Westerly flow as the Santa Rosa sounding which goes along with observation from wind vector reanalysis. No new distinctive feature is observed (Figure 3.4.15).

Multiple surface station observations were analyzed and compiled into (Figure 3.4.16) for February 8<sup>th</sup>. At 15:00 LST on February 8<sup>th</sup>, we observe a surface northeasterly flow observed by Cordoba airport and Pilar observatory and a northerly flow registered in Rio Cuarto while there's a southwesterly flow registered in Villa Dolores airport and Merlo. At 16:00 LST we observe the same pattern in Cordoba, Villa Dolores, Merlo, and Rio Cuarto while the station at Pilar shows a northerly flow. There was also a significant decrease in pressure in all; stations around the area. Finally, at 17:00 LST we observe an easterly flow observed in Córdoba, a northwesterly flow observed in Villa Dolores and Merlo, a northeasterly flow in Rio Cuarto and finally a northerly flow in Pilar. Readings at this time also showed another decrease in pressure in all stations in the area.

As shown in Figure 3.4.17, February 8<sup>th</sup> there shows a northern flow and a southwesterly flow converging with the Andes as observed on December 13<sup>th</sup>, but the northern flow observed on February 8<sup>th</sup> is 30% weaker than the one present on December 13<sup>th</sup>. Stream functions analysis of .84 sigma is showing that on February 8<sup>th</sup> there is a cyclonic anomaly located in the southern part of Argentina "Patagonia", while on December 13<sup>th</sup> there was a dipole structure of cyclonic anomalies located to the west of Argentina and

an anti-cyclonic anomaly east of Argentina, Uruguay, Paraguay and south of Brazil. As observed before, the dipole structure is playing a role in strengthening the SALLJ, but on February 8<sup>th</sup> is not present which would explain a weaker northern flow converging with a westerly flow in the southern part of Argentina. The analysis from .21 sigma stream functions is showing a cyclonic anomaly extended over Argentina with two maximum south of Argentina and south of Brazil (which would explain the two maximum wind areas observed in the wind reanalysis) for February 8<sup>th</sup> in contrast to December 13<sup>th</sup> where there was a cyclonic anomaly located southwest of Argentina but the maximum is located more to the north (central Argentina).

On February 8<sup>th</sup> the cyclonic anomaly located south of Argentina (Figure 3.4.18) would explain why the upper-level jet would be located over la Patagonia. Not having the upper-level jet converging to the north of Argentina with the Andes will not create the ageostrophic wind supporting the low-level jet, which simply creates a westerly flow in the area while on December 13<sup>th</sup> the cyclonic anomaly is located more to the north, converging with the Andes and supporting the low-level jet by the ageostrophic wind. Not having the dipole structure in the surface and not having an upper-level jet converging with the Andes creating the ageostrophic wind to enhance the low-level jet would then result in a local forcing being responsible for convection on February 8<sup>th</sup> compared to December 13<sup>th</sup>. The lack of LLJ indicates lack of large-scale moisture transport. There's also a lack of large-scale forcing also supported by the trough being located further south of Patagonia. This might suggest that the upslope flow present on February 8<sup>th</sup> is then supporting a more local forcing.

#### **4. Discussion**

This study analyzes an unorganized multicellular convective system on February 8<sup>th</sup>, 2018 (referred throughout this paper as the northern and southern convective cells), and a multicell organized MCS on December 13<sup>th</sup>, 2018, using data from the C-band Córdoba radar (RMA1) and GOES-16. During these events, giant hail (greater than 5 cm) were observed in both mountainous and valley settings, collected and recorded in Villa Carlos Paz (VCP) and nearby towns on February 8<sup>th</sup>, and in Villa del Dique (VD) on December 13<sup>th</sup>. The December 13<sup>th</sup> MCS occurred in a large-scale environment conducive to hail-producing storms and organized convection described in previous studies done by (Vidal 2014; Mulholland et al 2018; Rasmussen et al 2014; Rasmussen and Houze 2016; Bruick 2019; Teitelbaum and D'Andrea 2015). December 13<sup>th</sup> fits a lot of those synoptic large-scale ingredients previously discussed compared to February 8<sup>th</sup> which lacked this similar large-scale component.

Multiple questions arise from these case study analyses such as: Is there a difference in the storm-scale dynamics of hail fall when you have a mountainous area such as las Sierras de Cordoba, or valleys and plains such as in the boundary between Mendoza and San Luis provinces? Because the convective cells on December 13<sup>th</sup> were three times larger than the unorganized convective cells on February 8<sup>th</sup>, is there a crystallographic difference between the hail samples collected? Is there a size difference between the samples and do those size differences give us information on convective core vertical development and its relationships to larger scale forcing? How would this information fit with large scale ingredients conducive for hail producing storms? These questions are important to understand the processes contributing to hail-producing storms in this region

First, we focused on the general characterization of the convective systems on December 13<sup>th</sup> and February 8<sup>th</sup>. There are two things incorporated in this analysis. First, the location and path of the storm were described. Here we investigated the geographical difference of where these storms are happening and where they become convective. Secondly, we analyze and compare the crystallographic characteristics of hail samples collected in each of the storms.

On December 13<sup>th</sup> we see that our studied initial convective system develops over a plain (32 degrees S, 67 degrees W) advancing eastward and then going over a mountain range reaching 3000 m of height and then hailing (precipitating) in Villa del Dique. This convective system follows closely with what has been described by Mulholland et al 2018; an MCS event, multicellular, where convection initiation is happening east of the Sierras around sunset (2000-0300 UTC) and following the climatological pattern most convective storms follow in this region happening between November through February. It also follows the pattern described in Bruick et al 2019 where the hail is developing overnight also agreeing with Mulholland that it develops in a multicellular structured storm.

Compared to December 13<sup>th</sup>, on February 8<sup>th</sup> we observed a multicellular unorganized system which starts developing in the same geographical location (over the plains in San Luis), happening in the same season as expected, with the time of convective initiation happening during the first peak as described by Mulholland et al. 2018 (1100 – 1600 UTC). We observe that the southern cell is developing similarly as seen on December 13<sup>th</sup> over plains but being 3 tenths smaller than the western cell on this date. A second smaller northern cell (approximately 4 tenths smaller than the southern cell) is developing in the northern tip of las Sierras. While the southern cell is reaching Cordoba province advancing to the east as

the western cell in December 13<sup>th</sup>, a convective cloud is also forming towards las Sierras de Pocho. Once the cloud reaches the peak of las Sierras de Pocho it becomes convective (rapidly increases in depth) and continues advancing to the northeast while the southern cell once it passes over the Comechingones Mountain range it weakens and later dissipates while part of it merging with the northern cell. Wind and specific humidity analyses from both case studies show a different pattern between the two storms studied on December 13<sup>th</sup> and February 8<sup>th</sup>. This is following statistics and observations by Vidal 2014, where you observe that the development of mountain afternoon-initiated storms as seen on February 8<sup>th</sup> where it happens around in the afternoon and night because time is needed for solar radiation to lift the humidity and create a favorable environment for the formation of convective clouds.

Secondly, hail samples were analyzed for both December 13<sup>th</sup> and February 8<sup>th</sup> case studies (NOTE: there are more hailstones collected from February 8<sup>th</sup> compared to only one sample collected on December 13<sup>th</sup>). Crystallographic analysis of hail samples from both hailstorms showed a similar number of rings internally and both showing a large number of air bubbles. The hailstone collected from February 8<sup>th</sup> had a larger size (giant hailstones ranging from 9-12 cm) compared to hail samples collected on December 13<sup>th</sup>. With respect to the hail event, comparing two areas of hail events we can observe that there is more hail per square inch area on December 13<sup>th</sup> compared to February 8<sup>th</sup>. While also having in mind that on February 8<sup>th</sup> hail event produced a new hail “size” record as seen in Kumjian et al 2020.

These results may indicate there is something else besides the large-scale forcing on December 13<sup>th</sup> playing a role in keeping the hail in the cloud for a long time while having less water vapor available to form multiple larger hailstones to have bigger hailstones. Here we start to observe a specific pattern in the MCS from December 13<sup>th</sup>, where we had this

convective system developing over a plain but then going over the Comechingones mountain range showing smaller hail. On the other hand, on February 8<sup>th</sup>, the northern cell that becomes convective over “La pampa de Achala” (mountain plains in las Sierras starting at an altitude of 2000 meters) produces a bigger hail in smaller quantities compared to December 13<sup>th</sup>. Next we want to explore further the detailed vertical characteristics (showing minimum brightness temperatures less than 205 K) of these storms from these different environments (Synoptic forcing versus local forcing; February 8<sup>th</sup> is 3% of the western cell on December 13<sup>th</sup>; development and hail events occurring over and to the east of the “Sierras de Pocho” on February 8<sup>th</sup> and development over the plains and hail fall after advancing over the “Sierras de Comechingones”; the storm is displacing to the northeast at 10 km/h on February 8<sup>th</sup> and to the east at 27 km/h on December 13<sup>th</sup>) to see if it gives us any clue about the hail size and also where the hail formed in both systems.

We know that the hail size is attributed to the strength of the updraft with more extensive vertical development supporting a larger size hail. To correlate the relationship of the hail size with specific vertical development characteristics, there are theoretical models needed that are out of the scope of this project. Instead, we are focusing on correlating the temporal and spatial path of the convective cores with hailstorm events recorded based on an analysis method developed in this project. Both storms showed significant vertical development (showing cold brightness temperatures of 190 K or less, compared to non-producing hail convective systems that show brightness temperatures of 200 to 210 K). Additionally, hail events were geographically located northward of the convective core, different to what is shown in conceptual models by (Browning and Foote 1976) and observations by Kumjian et al. 2020. Because we are observing an important vertical

development, meaning that the development of the cloud is reaching and exceeded the tropopause, then it is important to then look further to see if large synoptic or local (orographic) scale forcing is promoting this deep vertical convective development.

Alvarez et al. 2015 found that regional circulation anomalies mainly over southern South America can be influenced by the large-scale extratropical circulation anomalies in turn induced by the convection enhanced or suppressed by the MJO over tropical western Pacific-Indian tropical oceans. MJO phase diagrams for both dates showed strong MJO events, making us look further and see if there is a wave pattern shown in stream functions over the Pacific. On December 13<sup>th</sup>, stream functions at .21 sigma showed a wave train propagating from the western Pacific to south America with multiple pathways of propagation. The northward propagation towards higher latitudes observed over South America is a common pathway of this Rossby wave train (Hoskins and Ambrizzi 1993). The stream function analysis also shows a high cyclonic anomaly geographically located closer to central Argentina where we observe the strong upper-level jet passing along the Andes. As described in Salio et al 2003, isobaric charts at 250 mb show stronger southeasterly flow from the Pacific windward side of the Andes and then a northern westerly flow on the lee side with two jet streaks located at the windward side of the Andes and the second one on the lee side with average speeds of 55 m/s. This upper-level Jet upwind of the Andes decelerates as it crosses the mountains producing a direct ageostrophic circulation on its entrance region then reinforcing the SALLJ. The interaction between both the ageostrophic component and the low-level jet then reinforces the convergence at the left entrance region of the previously mentioned upper-level jet facilitating the development of convection in this area.

On December 13<sup>th</sup>, a present strong cyclonic anomaly associated with a mid-level trough approaching the Andes is producing synoptic-scale lift ahead of the trough and supporting a large area of convection. The pressure gradient between this strong cyclonic anomaly and an anti-cyclonic anomaly associated with the identified low-level ridge southeast of Brazil is potentially enhancing the SALLJ, increasing the input of moisture from the Amazonian Basin (Rasmussen and Houze 2016; Vera et al. 2006; Teitelbaum et al. 2008). This is confirmed by the daily specific humidity average and dewpoints from soundings suggesting strong moisture transport by a strong low-level jet. This moisture flux provided by the low-level jet is then capped by upper-level dry air subsidence from the westerlies passing over the Andes. Additionally, as described in Rasmussen and Houze 2016 we also observe lee cyclogenesis to the foothill of the Andes creating a pressure gradient bringing air from the low-level jet to the foot the Andes and then this flow converging with the SALLJ making las Sierras de Cordoba optimal for convective initiation. These ingredients not only support convection over the area but also support hail development in these convective systems (Bruick et al. 2019; Rasmussen and Houze 2016).

Compared to December 13<sup>th</sup>, the northerly flow is present on February 8<sup>th</sup>, although it is 30% weaker. We also see the southwesterly flow going over the Andes and then converging with this weaker northerly flow at 850 mb level also found on December 13. A strong cyclonic anomaly extended over Argentina associated with an upper-level trough that is present over the southeast Pacific with a second maximum southeast of Brazil. This anomaly can be associated with two anomalously high areas observed at this level explaining why the upper-level jet would be located over la Patagonia. Also, stream function analysis

shows an anomalous area of cyclonic circulation (associated with a significantly weak lower level trough) associated with a westerly flow going over la Patagonia. It seems like everything shifted southward compared to December 13<sup>th</sup>. Not having the upper-level jet converging to the north of Argentina with the Andes will not create the ageostrophic wind supporting the low-level jet, which is simply creating a westerly flow in the area.

Additionally, not having that trough as a synoptic forcing and a ridge to the east creating the dipole structure in the surface significantly enhancing the low-level jet would then result in having a local forcing play a key-role in convection initiation over the area of the study compared to large-scale forcing being responsible for deep convection on December 13<sup>th</sup>.

In both case studies, we had environmental ingredients that were favorable for convective development, and on both of those days, we saw convection occurring over different locations that had hail reported but not forecasted. Two possible reasons could explain why the SMN did not forecast hail for these two events. Firstly, Argentina previously did not have an extensive network of surface observations for hail reports. The second reason is that Argentina's central weather service is based in Buenos Aires and we assume that have limited capacity to incorporate orographic effects into their models.

Having in mind that we don't have present this large scale forcing identified on December 13<sup>th</sup> on February 8<sup>th</sup>, we then looked into the idea of the orographic forcing that we have present on February 8<sup>th</sup> and maybe on December 13<sup>th</sup>. On December 13<sup>th</sup> after the MCS developed and advanced eastward towards las sierras showing brightness temperatures of 190 K, then showing warmer temperatures just before the hail event and then showing colder brightness temperatures after a hail event. On February 8<sup>th</sup> the southern cell developing

similarly to December 13<sup>th</sup> MCS is advancing eastward towards the mountains never showing brightness temperatures lower than 210 K while the northern cell once its convective, it already shows lower brightness temperature values of 190 K and also it shows this important vertical development for at least 2 hours while the southern cell is getting weaker as it goes over the mountain range and then dissipating. Not having a strong low-level jet raises the question of where we could have moisture to support this system. Even though the lack of data for this day and the sounding not being representative enough for the convection observed on February 8<sup>th</sup> we do observe a surface easterly flow just east of the Sierras with convergence near the lee side of the mountains that would support a local moisture source and lift to overcome that convective inhibition observed on this day. In this case, such lifting was sufficient to trigger convection as described by Teitelbaum and D'Andrea 2015 and Kumjian et al. 2020. On December 13<sup>th</sup> and February 8<sup>th</sup> mountain waves could be having a key role in convection and are also observed in satellite and local images, but further modeling of the environmental state on these two cases have to be studied further in order to associate the convection of both cases to an effect of mountain waves.

## **5. Conclusions/Future Work**

This project aimed to confirm how well can satellite hail detection algorithms and background large-scale meteorological conditions predict the likelihood of large hail development in Argentina. In both case studies, we had environmental ingredients that were favorable for convective development and on both of those days, we saw convection occurring over different locations that had hail reported but not forecasted.

Our two cases provide examples of two different kinds of convective systems that can produce hail. The December 13<sup>th</sup> case was a multicellular MCS that developed over the plains in the San Luis Province and then intensified once it advanced over las Sierras de Comechingones producing hail overnight. We observed brightness temperatures of 200 K before and 190 K after reported hail events around the convective core while its area increased over time up to the point when it hailed and then merged with a different cell. On February 8<sup>th</sup>, we saw an unorganized multicellular convective system (2.5 times smaller than case on December 13<sup>th</sup>) that developed over las sierras de Cordoba with a super cellular structure and then hailed during the evening. We observed brightness temperatures of 195 K before and during registered hail events around the convective cell while having a rapid growth through time (four times faster than the MCS on December 13<sup>th</sup>).

Previous studies that composited statistics of hail proxies from satellite identified large-scale ingredients that favored convective development and supported nocturnal hail production in this region. Through our analysis of verified hailfall, the December 13<sup>th</sup> case shows that in fact under these large-scale conditions and these types of MCS, hail can fall over las Sierras. But we also found a hail-producing case where these large-scale ingredients were not present. This February case was therefore likely influenced by orography that is

leading to afternoon initiation over the high terrain of a more super cellular type of convection that we tend to associate more with hail-producing in the US. This latter case appears to be under-reported and sampled in this region. The system developed very quickly over the mountains but with similar low brightness temperatures as December 13. Additionally, more and larger hailstones fell from the February supercell than the nocturnal MCS over the high terrain. On that same February day, we observed other cells over the mountains with warmer brightness temperatures that did not have hail reports, although it is difficult to say whether if the system did hail or not because it happened in a remote area. The brightness temperature method developed in this project is effective in identifying giant hail producing storms that develop east of the Sierras de Cordoba.

The results from this comparison between two hail-producing cases give us the motivation to look further at these different types of environments and cases that can produce hail in this region to try to better understand hail formation and forecasting in this region, especially given that these hail-producing systems formed in two different environments and neither were forecasted to hail that day. Because there is a difference in brightness temperature between the convective cell that did produce hail compared to the convective cell that didn't produce hail, we would like to go into detail of finding better thresholds to identify hail producing convective systems with other satellite products. The goal will be to use these thresholds to discriminate hail producing and non-hail producing convective systems, given verified hail at the surface, to start improving hail short-term forecast for this region.

“Storm environmental conditions (e.g., vertical wind shear, buoyancy, the vertical profile of humidity, aerosol concentration) have also been identified as important factors for changing storm structure, dynamics, and microphysics, specifically, hail formation and growth (Weisman and Klemp 1982; van den Heever and Cotton 2004; Dennis and Kumjian 2017)” from Friedrich et al. 2019. We need to put this back in the context of hail formation in general given different conditions, especially because we noticed a difference in hail size between these two cases. Previous research shows how aerosols may influence the temperature at which ice nucleation can happen in the cloud especially when you have this large scale forcing where the air source is coming from different locations versus a more localized source. Specially in this area, we do tend to see agricultural settings over the plains compared to the mountains which in the case of the more localized source it may have a great impact in hail development. Having the actual hail samples will aid in understanding this potential influence in understanding and predicting hail formation and size. The ultimate goal is to improve hail forecasting through improved understanding of the processes and ingredients in this region and how remote sensing can aid in the nowcasting aspect of determining which cells may produce hail based on that improved understanding.

## 6. References

- Alvarez, M. S., C. S. Vera, G. N. Kiladis, and B. Liebmann, 2015: Influence of the Madden Julian Oscillation on precipitation and surface air temperature in South America. *Clim Dyn*, 245–262, <https://doi.org/10.1007/s00382-015-2581-6>.
- Arena, L., and A. Crespo, 2019: Recopilación de estudios primarios de caracterización cristalográfica de granizos y de las tormentas que los originan.
- Bal, S. K., S. Saha, B. B. Fand, N. P. Singh, J. Rane, and P. S. Minhas, 2014: *Hailstorm: Causes, Damage and POst-hail Management in Agriculture*. National Institute of Abiotic Stress Management.
- Bauer-Messmer, B., and A. Waldovel, 1997: Satellite data-based detection and prediction of hail. *Atmos*, **43**, 217–231.
- Blair, S. F., and Coauthors, 2017: High-Resolution Hail Observations: Implications for NWS Warning Operations. *WEATHER FORECAST*, **32**, 1101–1119, <https://doi.org/10.1175/WAF-D-16-0203.1>.
- Browning, K. A., and G. B. Foote, 1976: Airflow and hail growth in supercell storms and some implications for hail suppression. *Q. J. R. Meteorol. Soc.*, **102**, 499–533, <https://doi.org/10.1002/qj.49710243303>.
- , J. C. Fankhauser, J. P. Chalon, and P. J. Eccles, 1976: Structure of an Evolving Hailstorm, Part V; Synthesis and Implications for Hail Growth and Hail Supression. *Mon. Weather Rev.*, **104**, 603–610.
- Bruick, Z. S., K. L. Rassumen, and D. J. Cecil, 2019: Subtropical South American Hailstorm Characteristics and Environments. *Mon*, **147**, 4289–4304, <https://doi.org/10.1175/MWR-D-19-0011.1>.
- Celeste Saulo, A., and M. Nicolini, 1999: The atmospheric conditions preceding the occurrence of a strong low-level jets east of the Andes during January 1998. Sixth International Conference on Southern Hemisphere Meteorology and Oceanography, Diego Portales Convention Center Santiago, Chile [https://ams.confex.com/ams/other/techprogram/paper\\_10720.htm](https://ams.confex.com/ams/other/techprogram/paper_10720.htm).
- Dawson, D. T., II, E. R. Mansell, Y. Jung, L. J. Wicker, M. R. Kumjian, and M. Xue, 2013: Low-Level ZDR Signatures in Supercell Forward Flanks: The Role of Size Sorting and Melting of Hail. *J. Atmospheric Sci.*, **71**, 276–299, <https://doi.org/10.1175/JAS-D-13-0118.1>.
- Dennis, E. J., and M. R. Kumjian, 2017: The Impact of Vertical Wind Shear on Hail Growth in Simulated Supercells. *JAS*, **74**, 641–663, <https://doi.org/10.1175/JAS-D-16-0066.1>.

- Dial, G. L., J. P. Racy, and R. L. Thompson, 2010: Short-Term Convective Mode Evolution along Synoptic Boundaries. *Weather Forecast.*, **25**, 1430–1446, <https://doi.org/10.1175/2010WAF2222315.1>.
- Duda, J. D., and W. A. Gallus Jr., 2010: Spring and Summer Midwestern Severe Weather Reports in Supercells Compared to Other Morphologies. *Weather Forecast.*, **25**, 190–206, <https://doi.org/10.1175/2009WAF2222338.1>.
- EUMeTrain, The South American Low-Level Jet.  
<http://www.eumetrain.org/satmanu/CM4SH/Argentina/Sallj/print.htm>.
- Friedrich, K., and Coauthors, 2019: CHAT: The Colorado Hail Accumulation from Thunderstorms Project. *Bull. Am. Meteorol. Soc.*, **100**, 459–471, <https://doi.org/10.1175/BAMS-D-16-0277.1>.
- García-Ortega, E., L. López, and J. L. Sánchez, 2009: Diagnosis and sensitivity study of two severe storm events in the Southeastern Andes. *4th Eur. Conf. Sev. Storms*, **93**, 161–178, <https://doi.org/10.1016/j.atmosres.2008.10.030>.
- van den Heever, S. C., and W. R. Cotton, 2004: The Impact of Hail Size on Simulated Supercell Storms. *J. Atmospheric Sci.*, **61**, 1596–1609, [https://doi.org/10.1175/1520-0469\(2004\)061<1596:TIOHSO>2.0.CO;2](https://doi.org/10.1175/1520-0469(2004)061<1596:TIOHSO>2.0.CO;2).
- Higuchi, K., and T. Yosida, 1966: Crystallographic Orientation of Frozen Droplets on Ice Surfaces. *Physics of Snow and Ice: proceedings*, International Conference on Low Temperature Science. I. Conference on Physics of Snow and Ice, II. Conference on Cryobiology, Sapporo, Japan, 79–93 <http://hdl.handle.net/2115/20287>.
- Höllner, H., and M. E. Reinhardt, 1986: The Munich Hailstorm of July 12, 1984—Convective development and preliminary hailstone analysis. *Beitr. Phys. Atmosph.*, **59**.
- Hoskins, B. J., and T. Ambrizzi, 1993: Rossby Wave Propagation on a Realistic Longitudinally Varying Flow. *J. Atmospheric Sci.*, **50**, 1661–1671, [https://doi.org/10.1175/1520-0469\(1993\)050<1661:RWPOAR>2.0.CO;2](https://doi.org/10.1175/1520-0469(1993)050<1661:RWPOAR>2.0.CO;2).
- Johns, R. H., and C. A. Doswell III, 1992: Severe Local Storms Forecasting. *Weather Forecast.*, **7**, 588–612, [https://doi.org/10.1175/1520-0434\(1992\)007<0588:SLSF>2.0.CO;2](https://doi.org/10.1175/1520-0434(1992)007<0588:SLSF>2.0.CO;2).
- Jones, C., 2019: Recent changes in the South America low-level jet. *Npj Clim. Atmospheric Sci.*, **2**, 20, <https://doi.org/10.1038/s41612-019-0077-5>.
- Knight, C. A., and N. C. Knight, 1970: Hailstone Embryos. *J ATMOS SCI*, **27**, 659–666.
- KONDURU, R. T., C. M. KISHTAWAL, and S. SHAH, 2013: A new perspective on the infrared brightness temperature distribution of the deep convective clouds. *J. Earth Syst. Sci.*, **122**, 1195–1206, <https://doi.org/10.1007/s12040-013-0345-4>.

- Kumjian, M. R., Z. J. Lebo, and A. M. Ward, 2019: Storms Producing Large Accumulations of Small Hail. *JAMC*, **58**, 341–363, <https://doi.org/10.1175/JAMC-D-18-0073.1>.
- , and Coauthors, 2020: Gargantuan Hail in Argentina. *Bull. Am. Meteorol. Soc.*, <https://doi.org/10.1175/BAMS-D-19-0012.1>.
- Kunz, M., U. Blahak, J. Handwerker, M. Schmidberger, H. Jurgen Punge, S. Mohr, E. Fluck, and K. M. Bedka, 2018: The severe hailstorm in southwest Germany on 28 July 2013: characteristics, impacts and meteorological conditions. *Q. J. R. Meteorol. Soc.*, **144**, 231–250, <https://doi.org/10.1002/qj.3197>.
- Levi, L., and A. N. Aufdermaur, 1970: Crystallographic Orientation and Crystal Size in Cylindrical Accretions of Ice. *JAS*, **27**, 443–452.
- Merino, A., L. López, J. L. Sánchez, E. García-Ortega, E. Cattani, and V. Levizzani, 2014: Daytime identification of summer hailstorm cells from MSG data. *Nat. Hazards Earth Syst Sci*, 1017–1033.
- Miller, L. J., J. D. Tuttle, and C. A. Knight, 1988: Airflow and Hail Growth in a Severe Northern High Plains Supercell. *J. Atmospheric Sci.*, **45**, 736–762, [https://doi.org/10.1175/1520-0469\(1988\)045<0736:AAHGIA>2.0.CO;2](https://doi.org/10.1175/1520-0469(1988)045<0736:AAHGIA>2.0.CO;2).
- Mulholland, J. P., S. W. Nesbitt, R. J. Trapp, K. L. Rasmussen, and P. V. Salio, 2018: Convective Storm Life Cycle and Environments near the Sierras de Córdoba, Argentina. *Mon. Weather Rev.*, **146**, 2541–2557, <https://doi.org/10.1175/MWR-D-18-0081.1>.
- Müller, R., M. Jerg, S. Haussler, and D. Heizenreder, 2018: *A Novel Approach for the Detection of Developing Thunderstorm Cells*.
- Narwade, S., M. C. Gaikwad, K. Fartade, S. Pawar, M. Sawdekar, and P. Ingale, 2014: *Mass Mortality of Wildlife due to Hailstorms in Maharashtra, India*. Institute for Bird Population.
- Nelson, S. P., 1987: The Hybrid Multicellular–Supercellular Storm—an Efficient Hail Producer. Part II. General Characteristics and Implications for Hail Growth. *J. Atmospheric Sci.*, **44**, 2060–2073, [https://doi.org/10.1175/1520-0469\(1987\)044<2060:THMSEH>2.0.CO;2](https://doi.org/10.1175/1520-0469(1987)044<2060:THMSEH>2.0.CO;2).
- Pruppacher, H. R., and J. D. Klett, 1980: *Microphysics of Clouds and Precipitation*. Springer Netherlands, XV, 714 pp.
- Pucik, T., C. Castellano, P. Groenemeijer, T. Kuhne, A. T. Radler, B. Antonescu, and E. Faust, 2019: Large Hail Incidence and Its Economic and Societal Impacts across Europe. *Mon. Weather Rev.*, **147**, 3901–3916, <https://doi.org/10.1175/MWR-D-19-0204.1>.

- Punge, H. J., and M. Kunz, 2016: Hail observations and hailstorm characteristics in Europe: A review. *Atmos. Res.*, 159–184, <http://dx.doi.org/10.1016/j.atmosres.2016.02.012>.
- Rasmussen, K. L., and R. A. Houze Jr., 2011: Orographic Convection in Subtropical South America as Seen by the TRMM Satellite. *Mon. Weather Rev.*, **139**, 2399–2420, <https://doi.org/10.1175/MWR-D-10-05006.1>.
- Rasmussen, K. L., and R. A. J. Houze, 2016: Convective Initiation near the Andes in Subtropical South America. *Mon. Weather Rev.*, **144**, 2351–2373, <https://doi.org/10.1175/MWR-D-15-0058.1>.
- Ravinder, A., P. K. Reddy, and N. Prasad, 2013: Detection of Wavelengths for Hail Identification Using Satellite Imagery of Clouds. 2013 Fifth International Conference on Computational Intelligence, Communication Systems and Networks, Madrid, Spain, IEEE, 205–211.
- Ribeiro, B. Z., L. A. T. Machado, J. H. Huamán Ch., T. S. Biscaro, E. D. Reitas, K. W. Mozer, and S. J. Goodman, 2019: An Evaluation of the GOES-16 Rapid Scan for Nowcasting in Southeastern Brazil: Analysis of a Severe Hailstorm Case. *WEATHER FORECAST*, **34**, 1829–1847, <https://doi.org/10.1175/WAF-D-19-0070.1>.
- Rinehart, R. E., 2010: *Radar for Meteorologists*. Fifth edition. Knight Printing Company.
- Roca, R., and V. Ramanathan, 2000: Scale Dependence of Monsoonal Convective Systems over the Indian Ocean. *J. Clim.*, **13**, 1286–1298, [https://doi.org/10.1175/1520-0442\(2000\)013<1286:SDOMCS>2.0.CO;2](https://doi.org/10.1175/1520-0442(2000)013<1286:SDOMCS>2.0.CO;2).
- Rogers, R. R., and M. K. Yau, 1989: *A Short course in cloud physics*. 3rd ed. Burlington, Mass.: Butterworth Heinemann.
- Salio, P., M. Nicolini, and A. C. Saulo, 2002: Chaco low-level jet events characterization during the austral summer season. *J. Geophys. Res. Atmospheres*, **107**, ACL 32-1, <https://doi.org/10.1029/2001JD001315>.
- Smith, B. T., R. L. Thompson, J. S. Grams, C. Broyles, and H. E. Brooks, 2012: Convective Modes for Significant Severe Thunderstorms in the Contiguous United States. Part I: Storm Classification and Climatology. *Weather Forecast.*, **27**, 1114–1135, <https://doi.org/10.1175/WAF-D-11-00115.1>.
- Teitelbaum, H., and F. D’Andrea, 2015: Deep convection east of the Andes Cordillera: four hailstorm cases. *Tellus Dyn. Meteorol. Oceanogr.*, **67**, <https://doi.org/10.3402/tellusa.v67.26806>.
- , H. Le Treut, M. Moustouai, G. C. Cabrera, and G. Ibañez, 2008: Deep Convection East of the Andes Cordillera: A Test Case Analysis of Air Mass Origin. *Mon. Weather Rev.*, **136**, 2201–2209, <https://doi.org/10.1175/2007MWR2088.1>.

- de la Torre, A., R. Hierro, P. Llamedo, A. Rolla, and P. Alexander, 2011: Severe hailstorms near Southern Andes in the presence of mountain waves. *Atmospheric Res.*, **101**, 112–123, <https://doi.org/10.1016/j.atmosres.2011.01.015>.
- Vera, C., and Coauthors, 2006: The South American Low-Level Jet Experiment. *Bull. Am. Meteorol. Soc.*, **87**, 63–78, <https://doi.org/10.1175/BAMS-87-1-63>.
- Vidal, L., 2014: Convección extrema sobre Sudamérica: estructura interna, ciclos de vida e influencia de la topografía en la iniciación. Universidad de Buenos Aires, 274 pp.
- Weisman, M. L., and J. B. Klemp, 1982: The Dependence of Numerically Simulated Convective Storms on Vertical Wind Shear and Buoyancy. *Mon. Weather Rev.*, **110**, 504–520, [https://doi.org/10.1175/1520-0493\(1982\)110<0504:TDONSC>2.0.CO;2](https://doi.org/10.1175/1520-0493(1982)110<0504:TDONSC>2.0.CO;2).
- Zipser, E. J., S. W. Nesbitt, C. Liu, and D. P. Yorty, 2006: Where Are the Most Intense Thunderstorms on Earth? *B AM METEOROL SOC*, 1057–1071, <https://doi.org/10.1175/BAMS-87-8-1057>.

## 7. Tables

Table 1: Hail events information corresponding to storms of February 8<sup>th</sup> and December 13<sup>th</sup> in 2018.

Location	Coordinates	Times of hail events (LST)	Time of hail event (UTC)	Information source	
				Sample collected	Social Media/Local News
<i>Icho Cruz</i>	-31.470844, -64.541380	15:50	18:50	No	Yes
<i>San Lorenzo Street (VCP)</i>	-31.422844, -64.497452	16:00	19:20	Yes	Yes
<i>Tupungato Street (VCP)</i>	-31.430425, -64.499612	16:00	19:20	Yes	Yes
<i>Tokio Street (VCP)</i>	-31.421580, -64.500763	16:00	19:30	Yes	Yes
<i>San Nicolás</i>	-31.435851, -64.456595	16:00	19:45	No	Yes
<i>Villa del Dique</i>	-32.201393, -64.452606	23:20	02:20	Yes	Yes

Table 2: Summary of the hail characterization analysis.

Date	February 8 <sup>th</sup> , 2018	December 13 <sup>th</sup> , 2018	December 13 <sup>th</sup> , 2018
<b>Location</b>	Villa Carlos Paz	Villa del Dique	Córdoba
<b>Time (UTC)</b>	19:00 - 19:45	2:20	03:00
<b>Min. T<sub>B</sub></b>	195	180	180 - 185
<b>Convective mode</b>	Unorganized Multicellular Convective System	Multicell Organized MCS	Multicell Organized MCS
<b>Storm area before hail event (avg. km<sup>2</sup>)</b>	9832	154638	---
<b>Hail sample quantity</b>	40	1	8 (graupel)
<b>Minimum diameter (cm)</b>	2	8	0.8
<b>Maximum diameter (cm)</b>	17 (Colossus)	8	1.3
<b>Prevailing Geometric Shape</b>	Spherical	Spherical	Spherical
<b>Lobes presence (traces)</b>	Yes	Yes	No
<b>Micrometric bubbles</b>	Yes	Yes	Yes
<b>Giant bubbles &gt;2mm</b>	Yes	Yes	----
<b>Density: spongy</b>	Yes	Yes	----

## 8. Figures

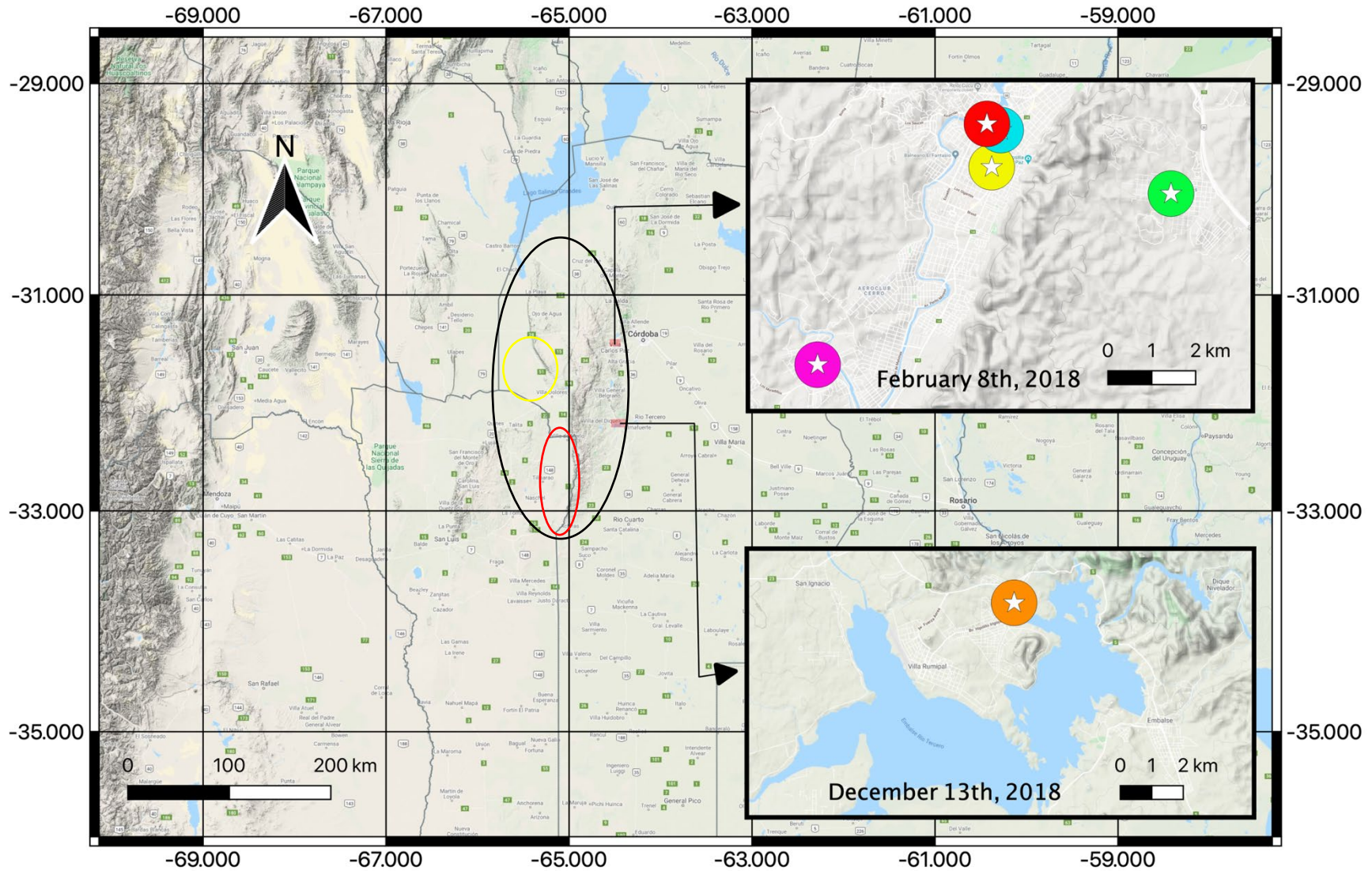


Figure 2.1.1: Map showing the “Sierras de Córdoba” (circled by a black marking) with a red circle surrounding the “Sierras de Comechingones” and a yellow circle surrounding the “Sierras de Pocho” and locations where hail reports were available.

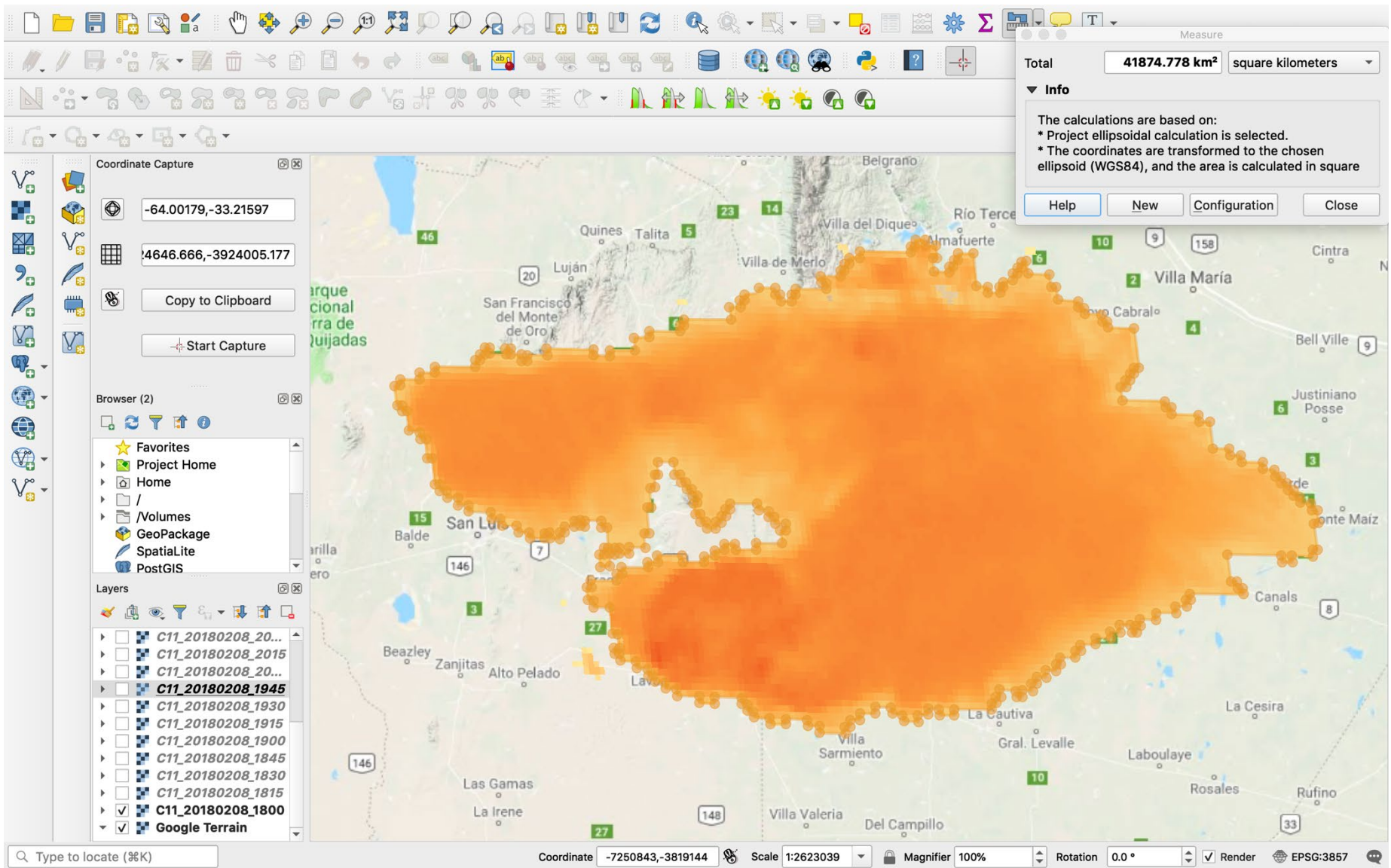


Figure 2.2.1: Example of final result of the area analysis in QGIS of northern convective cell on February 8<sup>th</sup>, 2018.

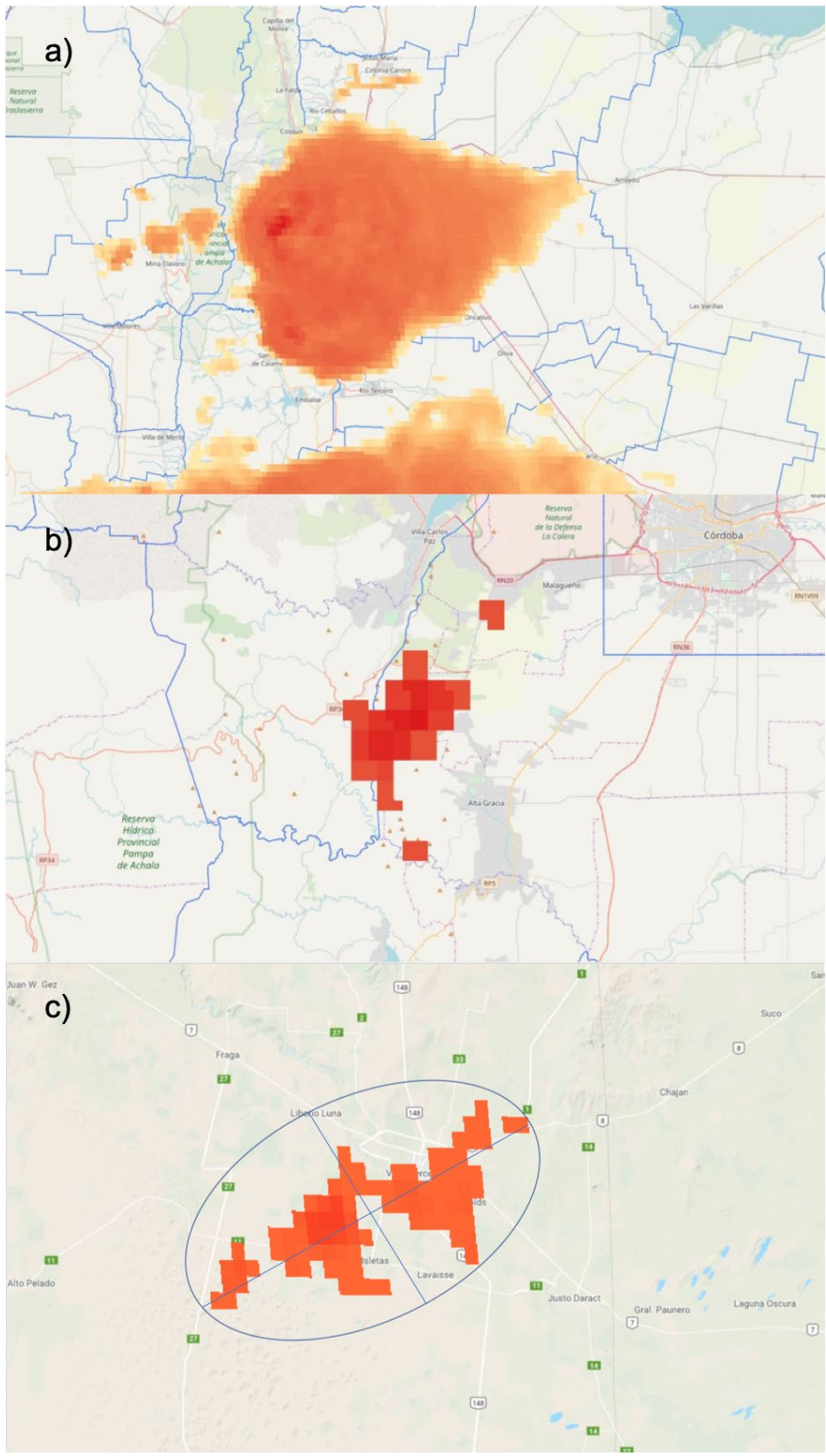


Figure 2.2.2: Channel 11 image from GOES-16 (a) analyzed considering only brightness temperatures corresponding to 205 K presented in (b) and then locating the center of an ellipsis (c).

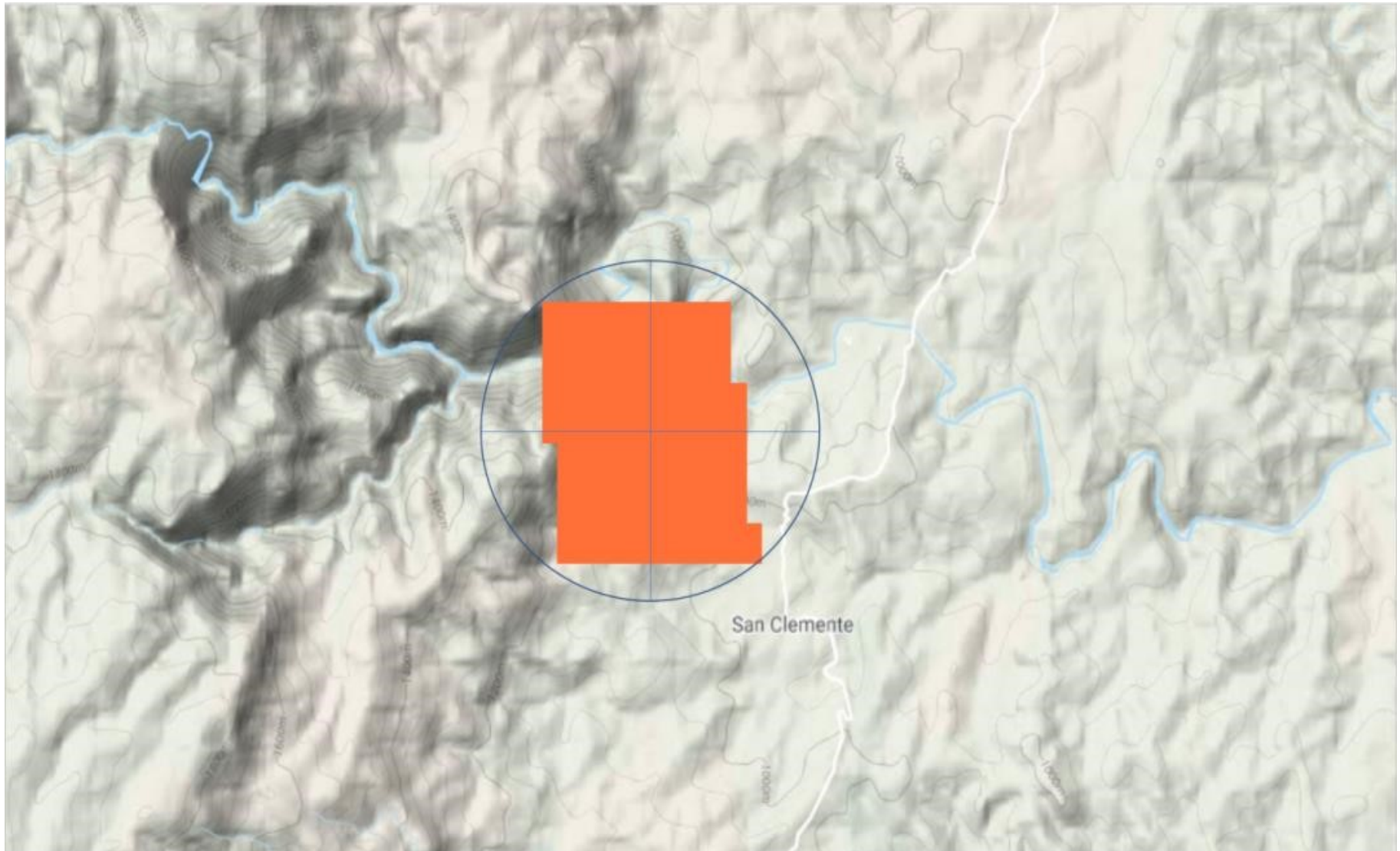


Figure 2.2.3: Analysis method used to calculate northern and southern convective system for February 8<sup>th</sup> and December 13<sup>th</sup>.

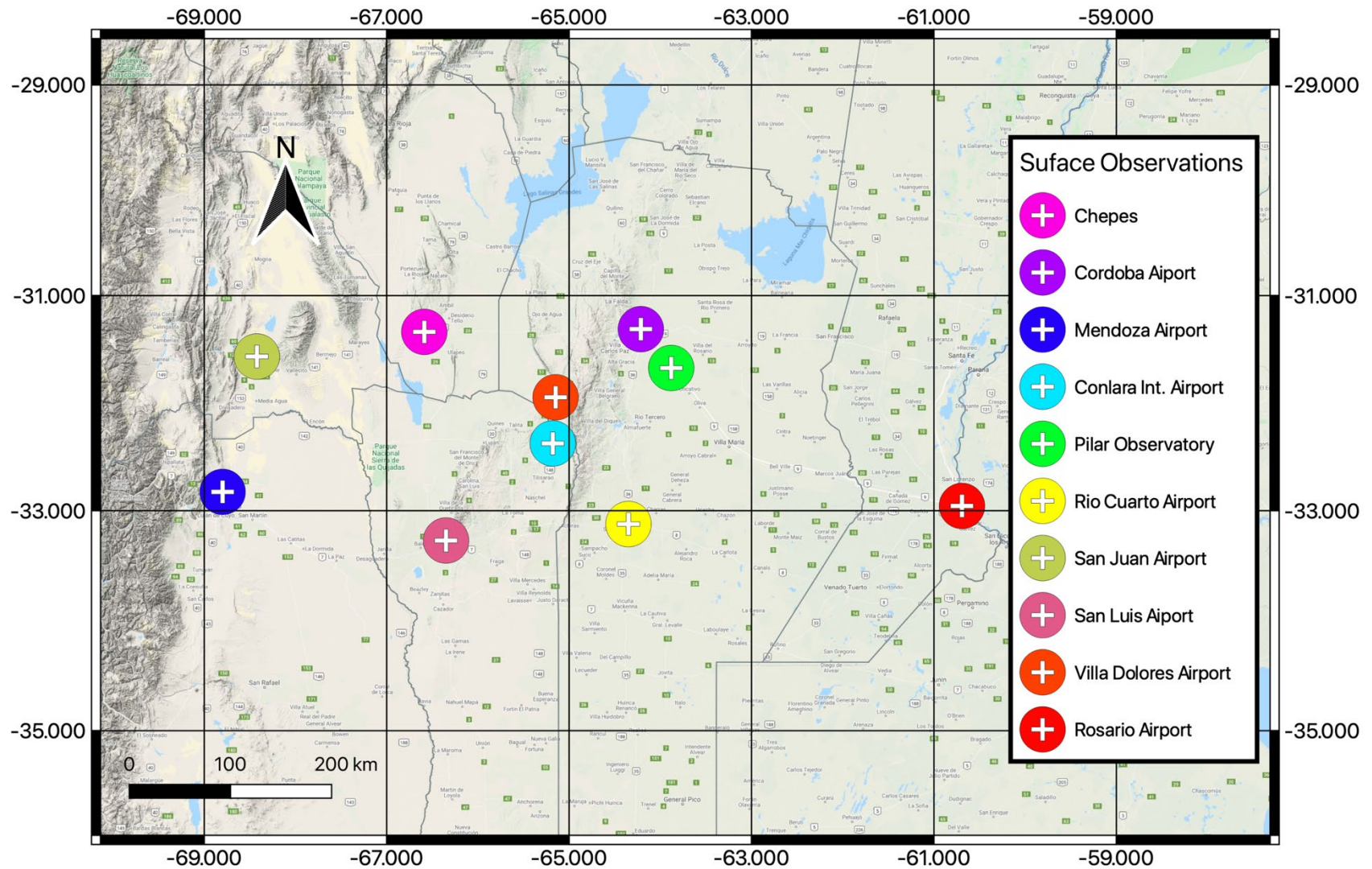


Figure 2.4.1: Weather stations managed by SMN available for surface observations.

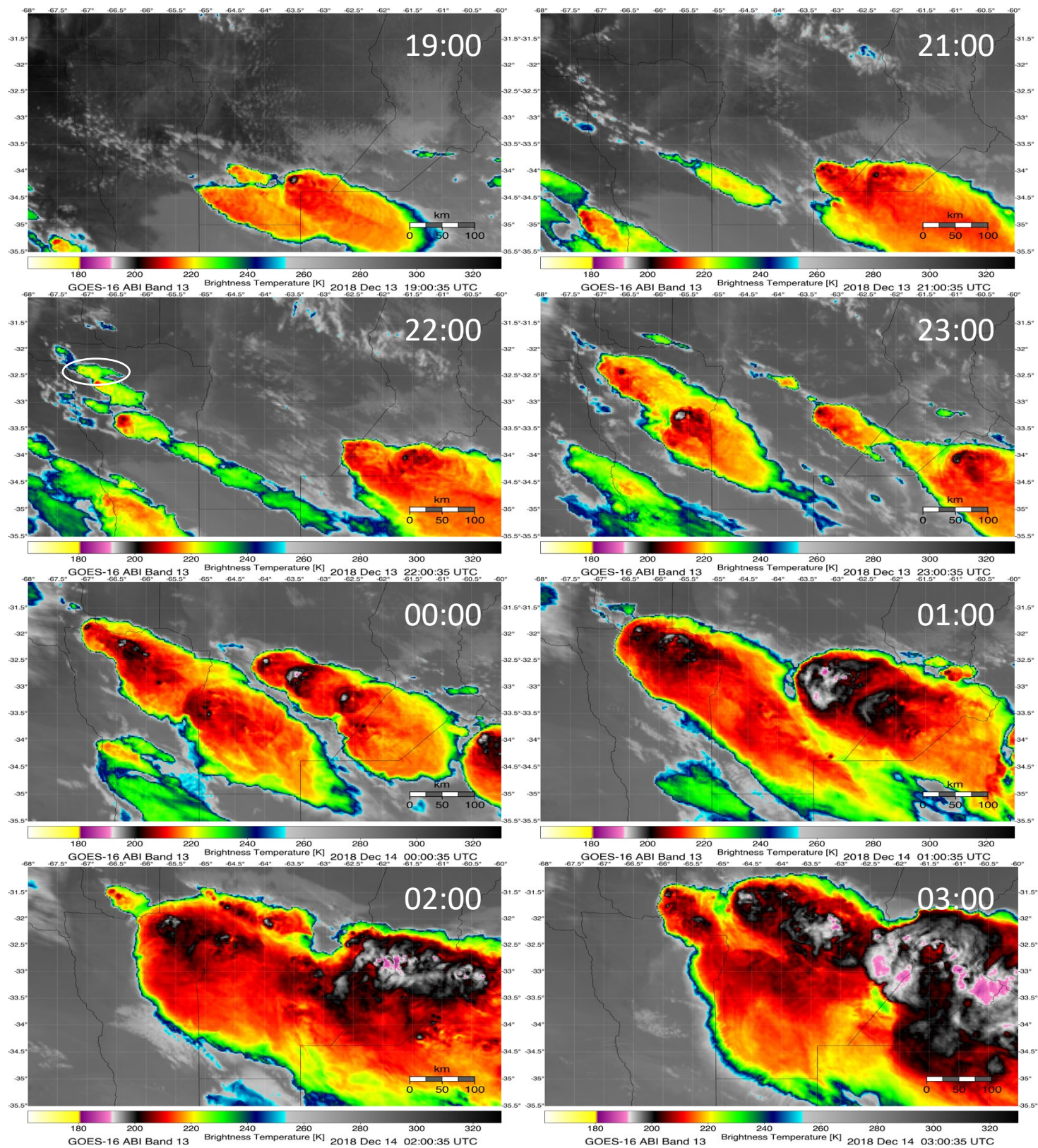


Figure 3.1.1: Images from GOES-16 showing the convective system responsible for hail fall (marked by a white circle at 22:00 UTC) studied on December 13<sup>th</sup>, 2018. As shown in Table 1, these images are just before and during the recorded hail events.

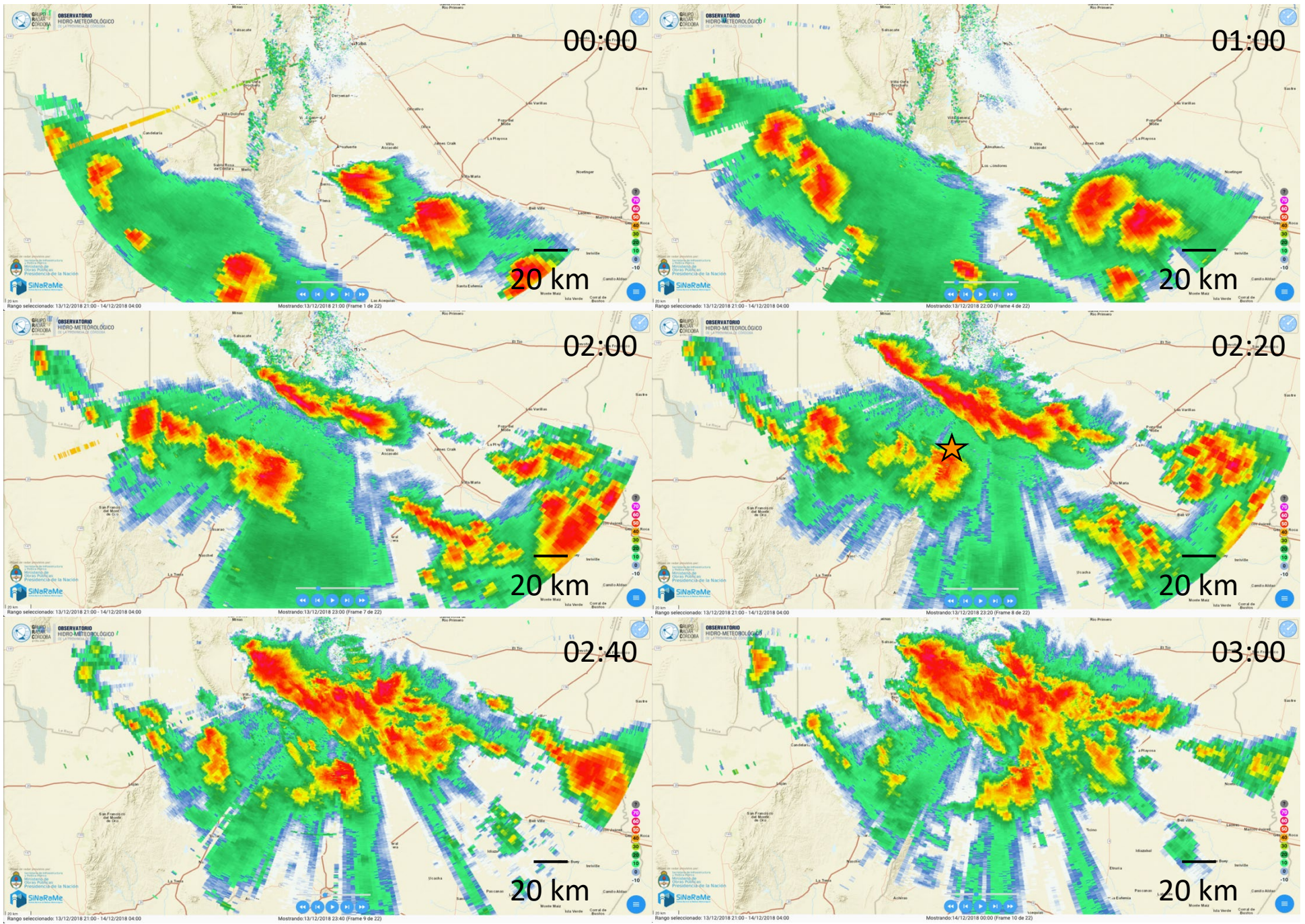


Figure 3.1.2: COLMAX images from RMA1 radar showing the temporal evolution of MCS on December 13<sup>th</sup>, 2018 and location where hail fall was reported (orange star).

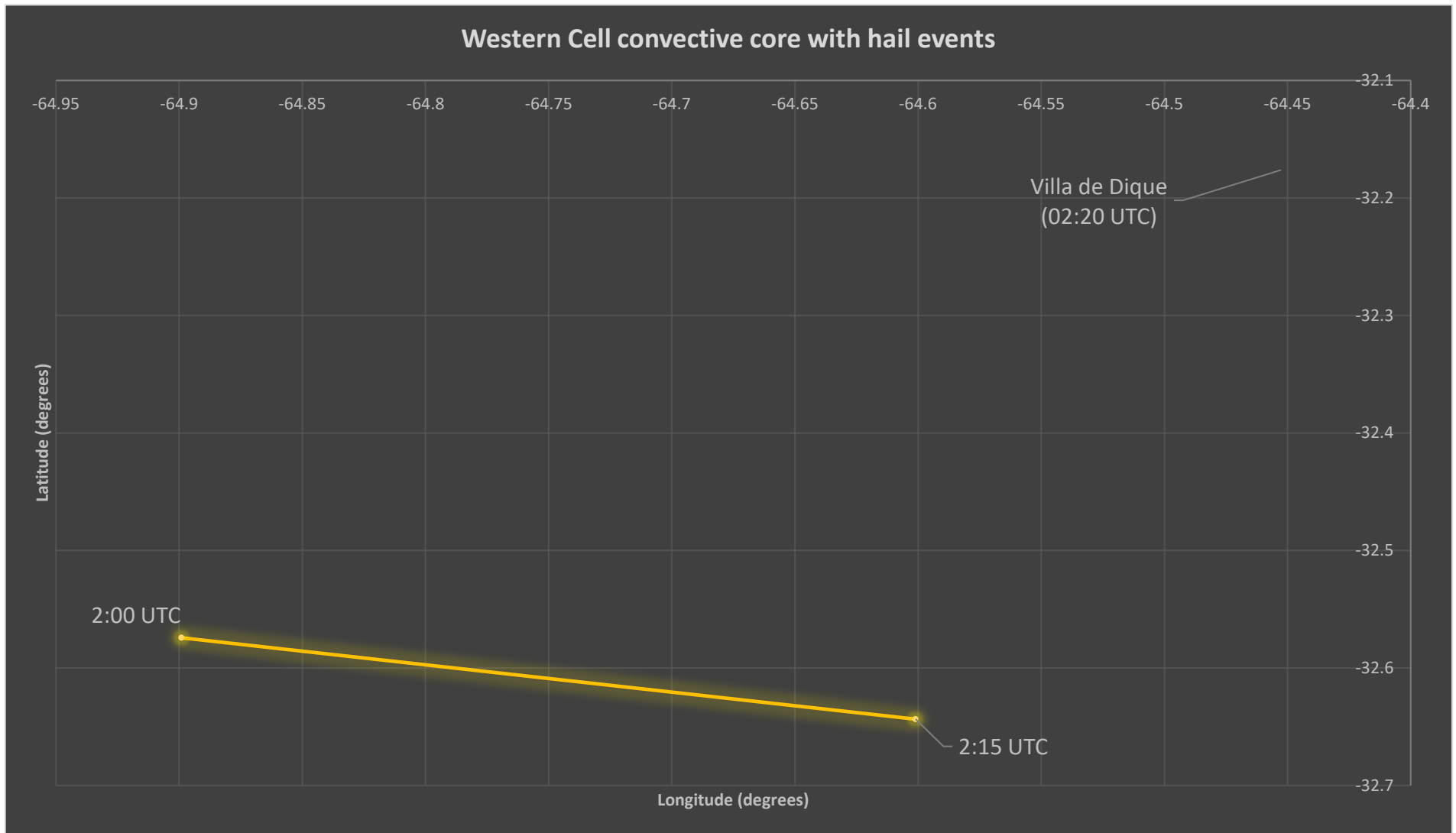


Figure 3.1.3: Western cell convective core trajectory analysis from brightness temperature evolution showing maximum temperatures of 205 K on December 13<sup>th</sup>, with respect to the hail event in Villa del Dique at 02:20 UTC.

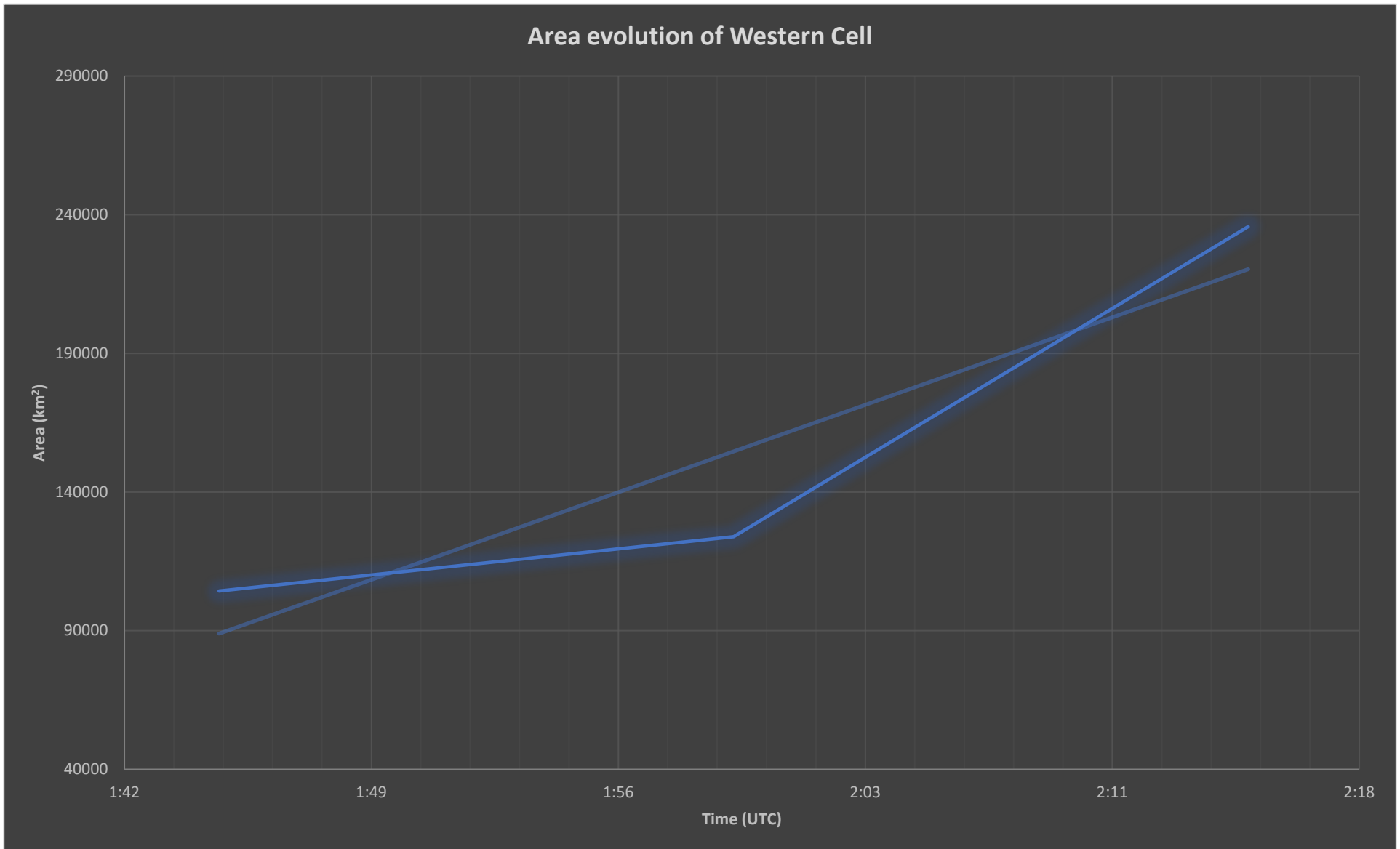


Figure 3.1.4: Western cell area evolution through time on December 13<sup>th</sup>.

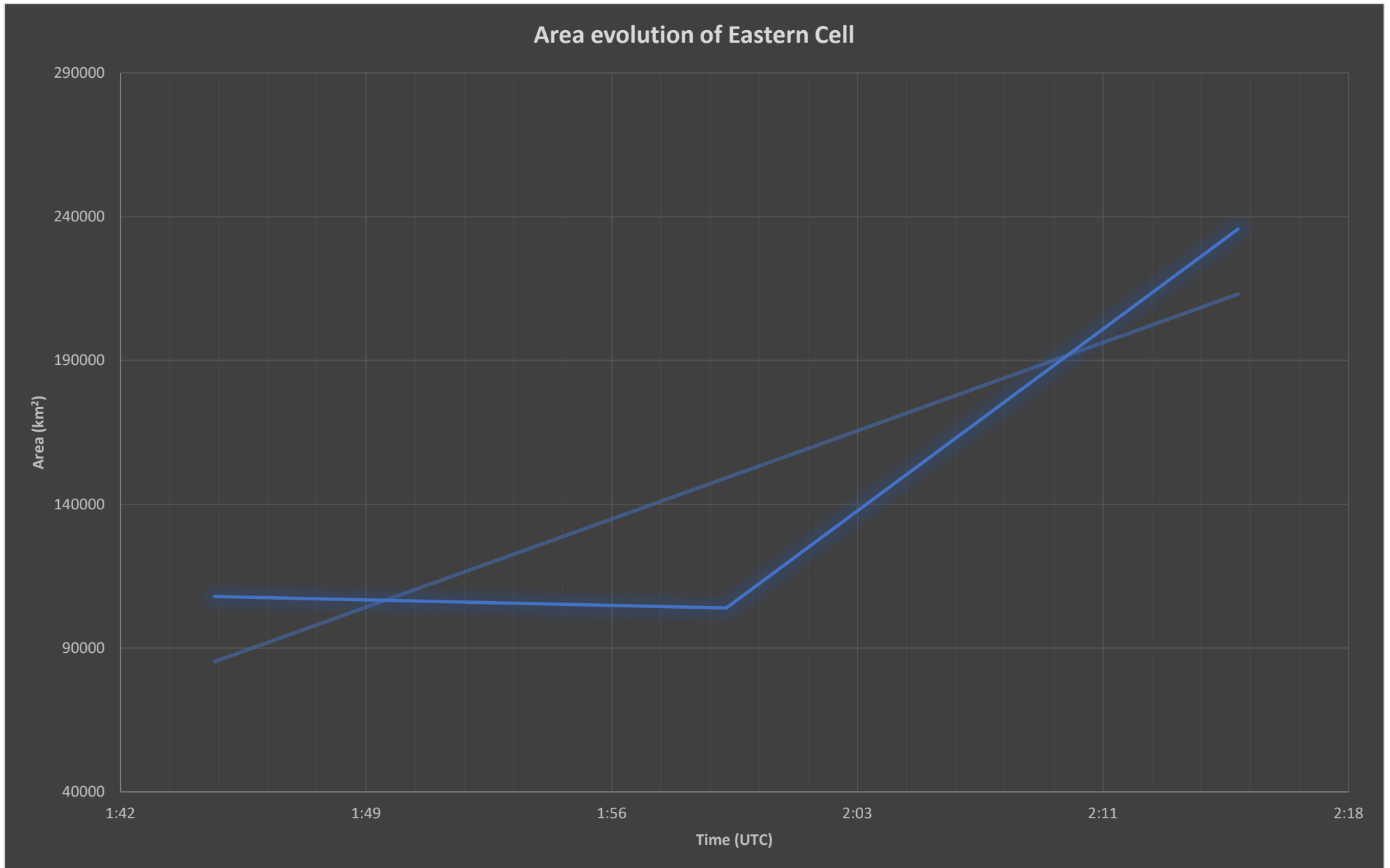


Figure 3.1.5: Eastern cell area evolution through time on December 13<sup>th</sup>.

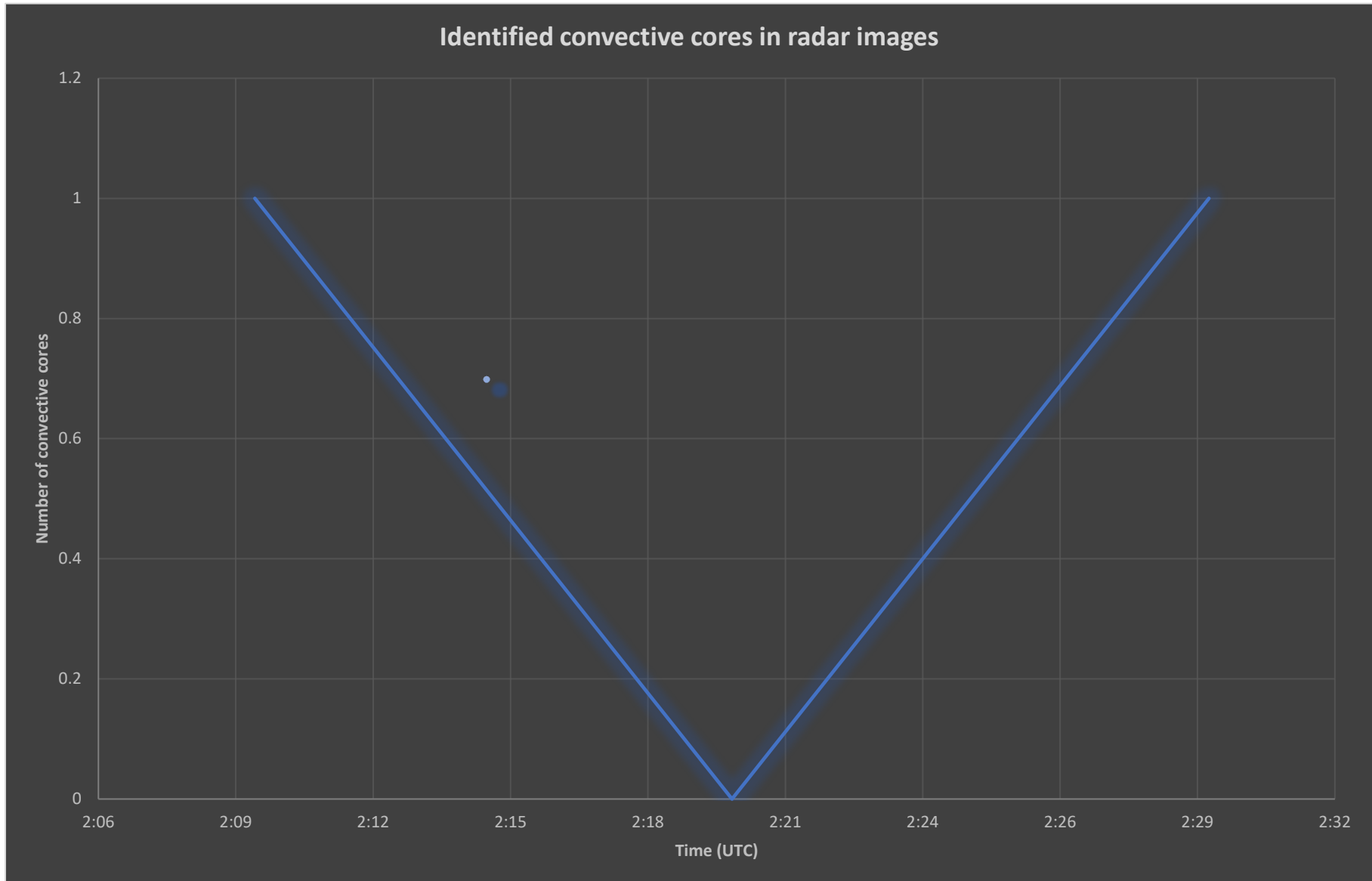


Figure 3.1.6: Convective cores identified in radar images that showed values greater than 70 dBZ in convective core in December 13<sup>th</sup>.

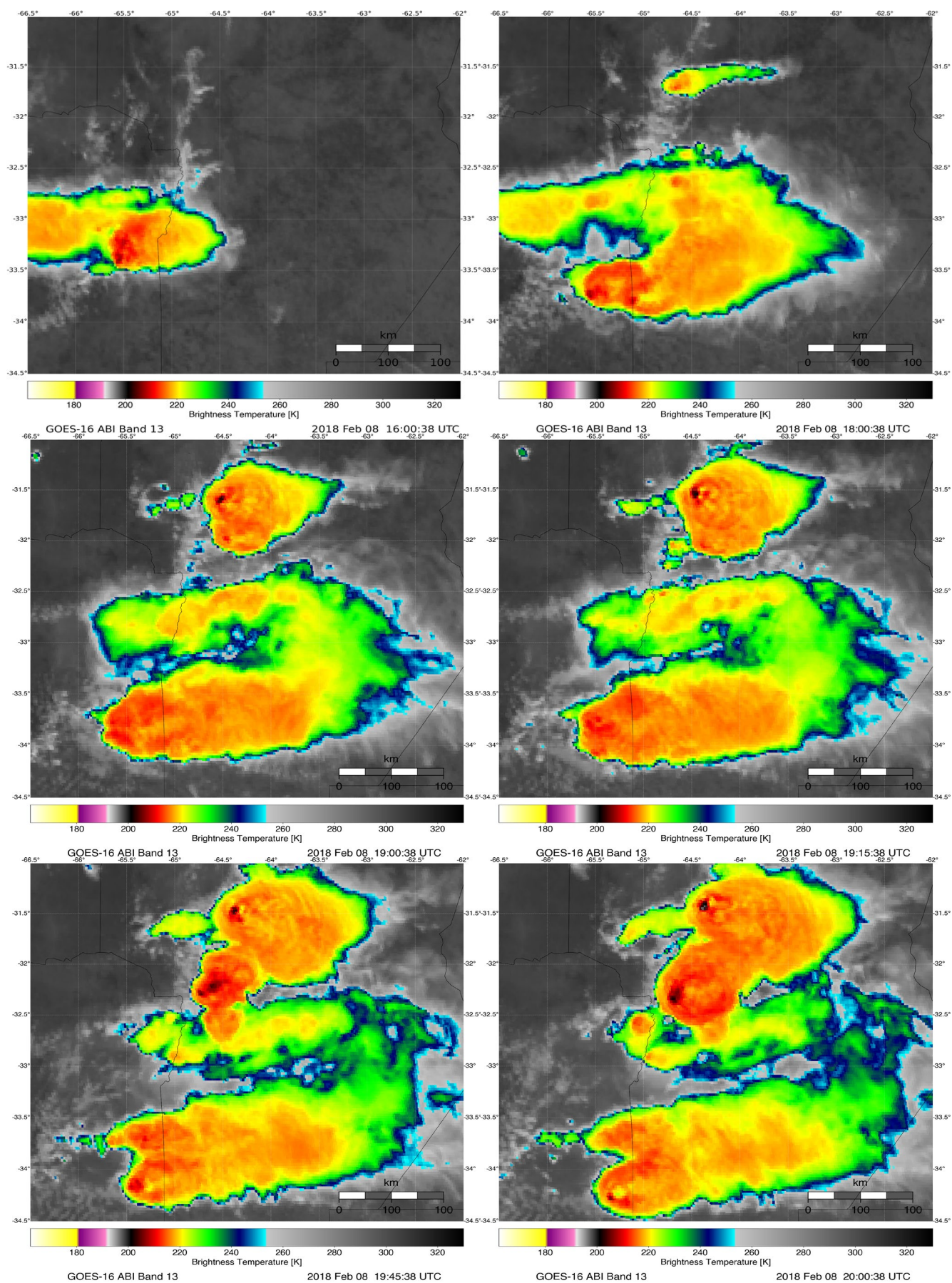


Figure 3.2.1: Images from GOES-16 and RMA1 showing the two convective systems studied February 8<sup>th</sup>, 2018. As shown in *Table 1*, these images are just before and during the recorded hailstorms.

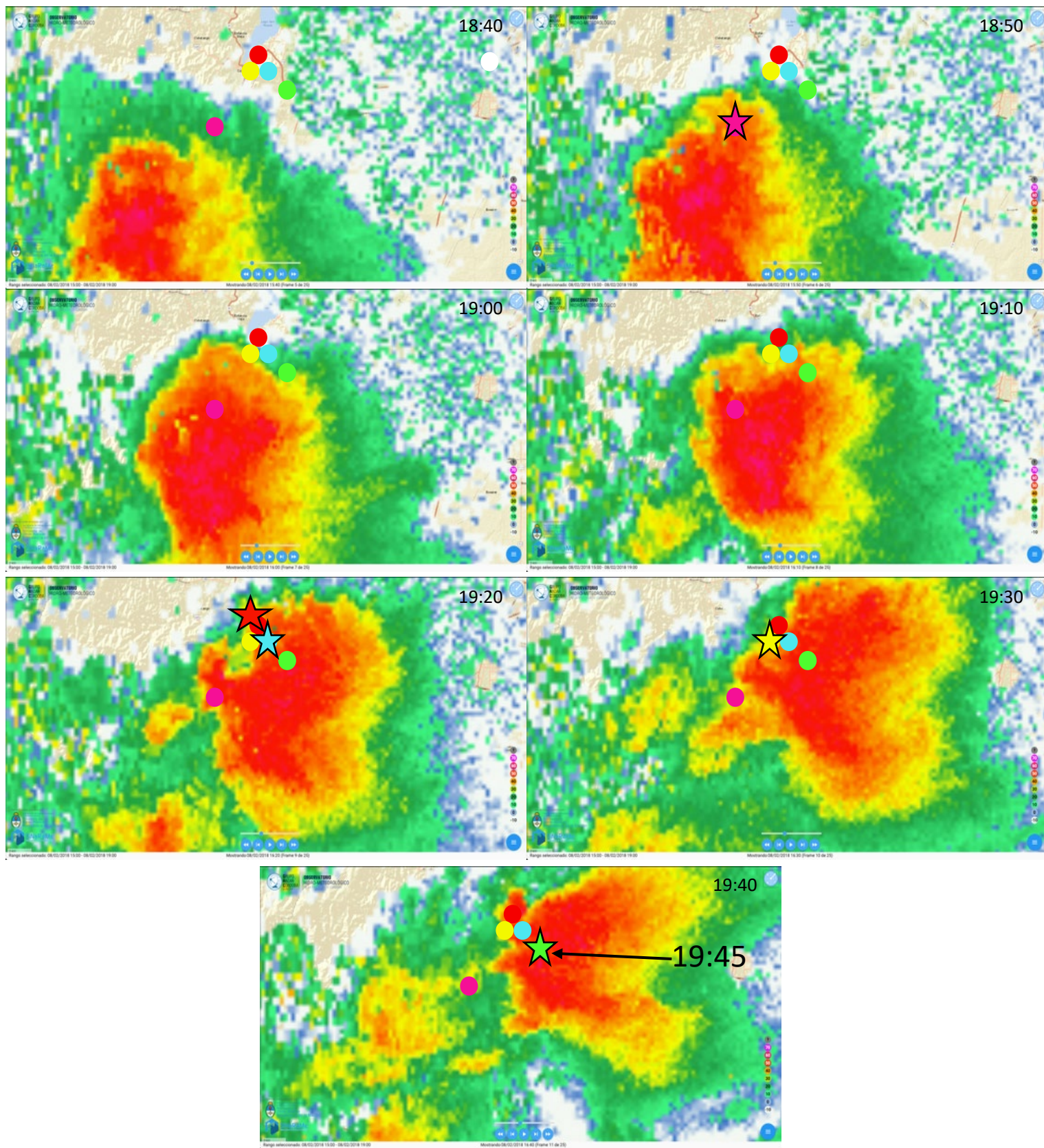


Figure 3.2.2: COLMAX images from RMA1 radar showing the temporal evolution of the northern convective system and locations where hail fall was reported. Stars represent hail fall in each of the radar images.

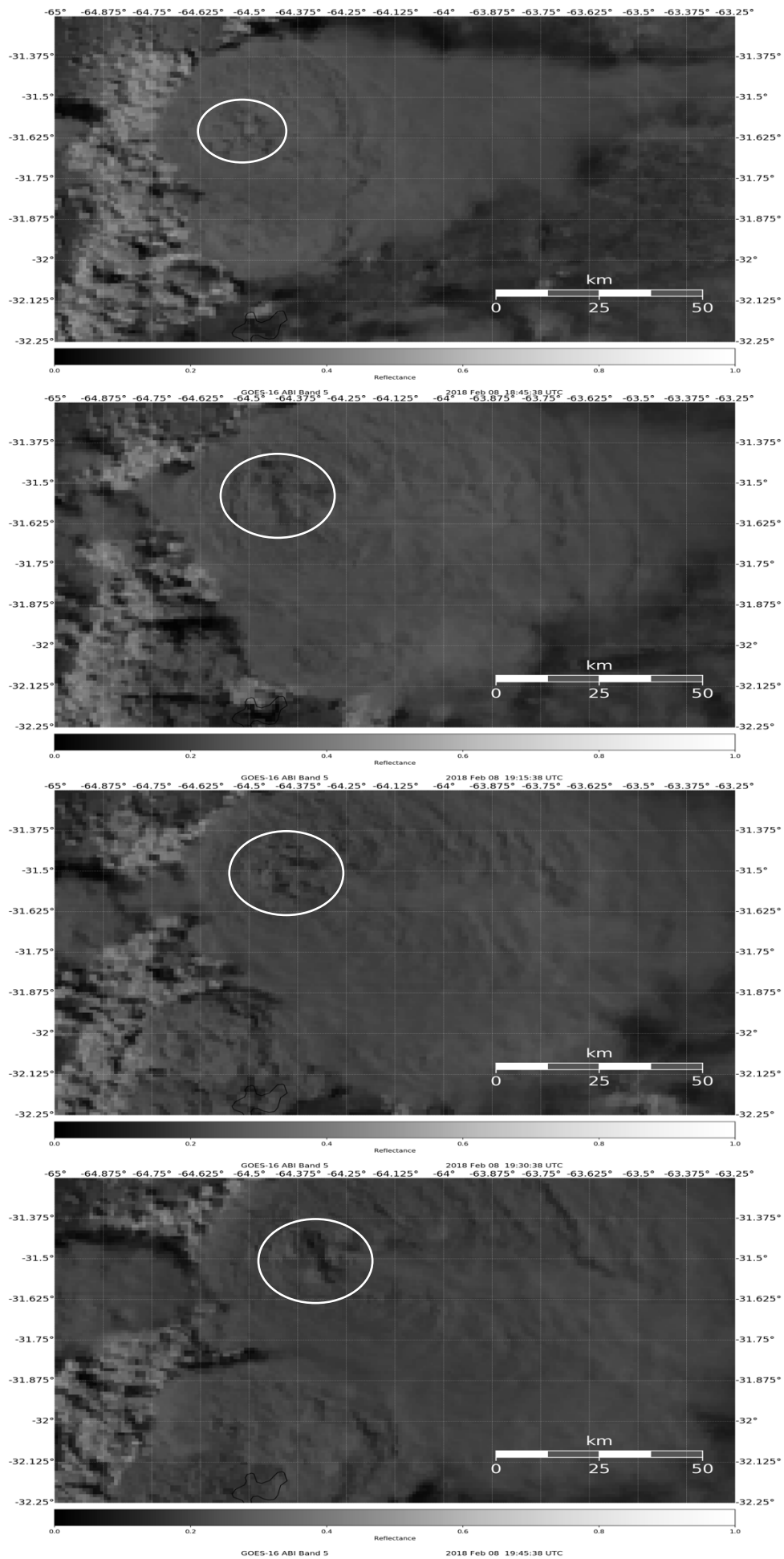


Figure 3.2.3: Channel 5 images are corresponding to times in which hail fall was recorded.

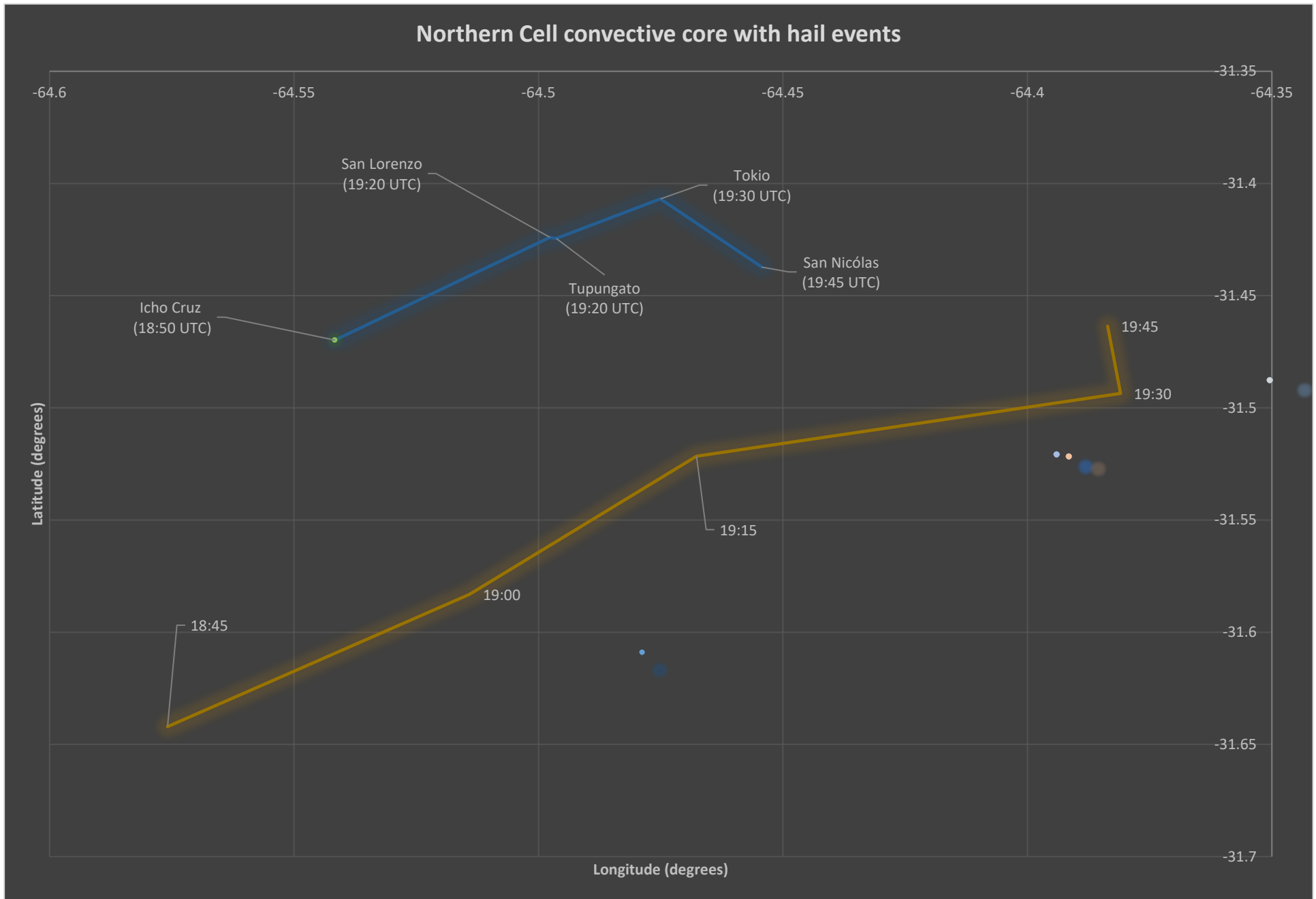


Figure 3.2.4: Northern cell convective core trajectory analysis from brightness temperature evolution showing maximum temperatures of 205 K on February 8<sup>th</sup>, with respect to the hail event in Icho Cruz, San Lorenzo Street, Tupungato Street, Tokio Street and San Nicolas at 18:50, 19:20, 19:20, 19:30 and 19:45 respectively.

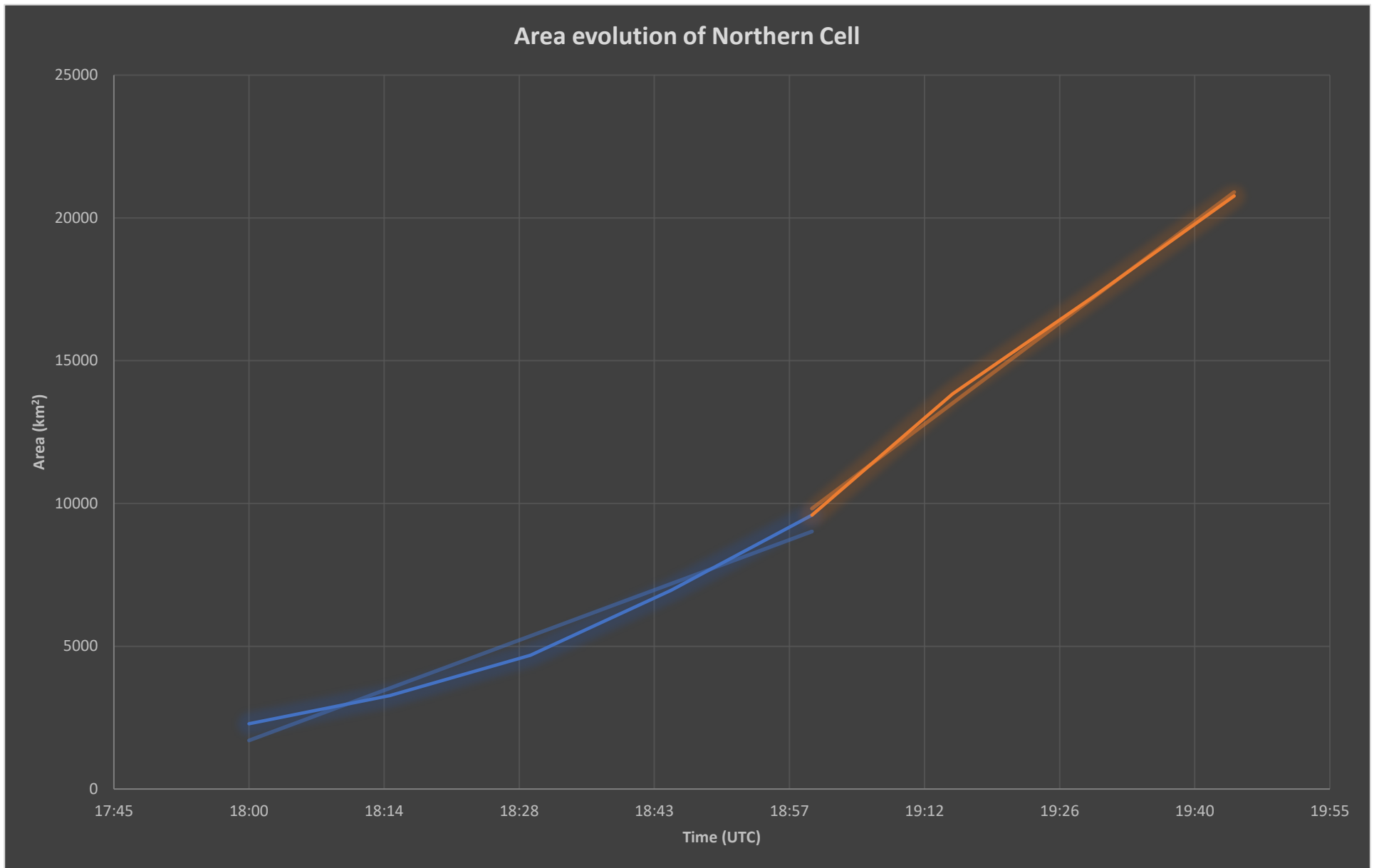


Figure 3.2.5: Northern cell area evolution through time on February 8<sup>th</sup>.

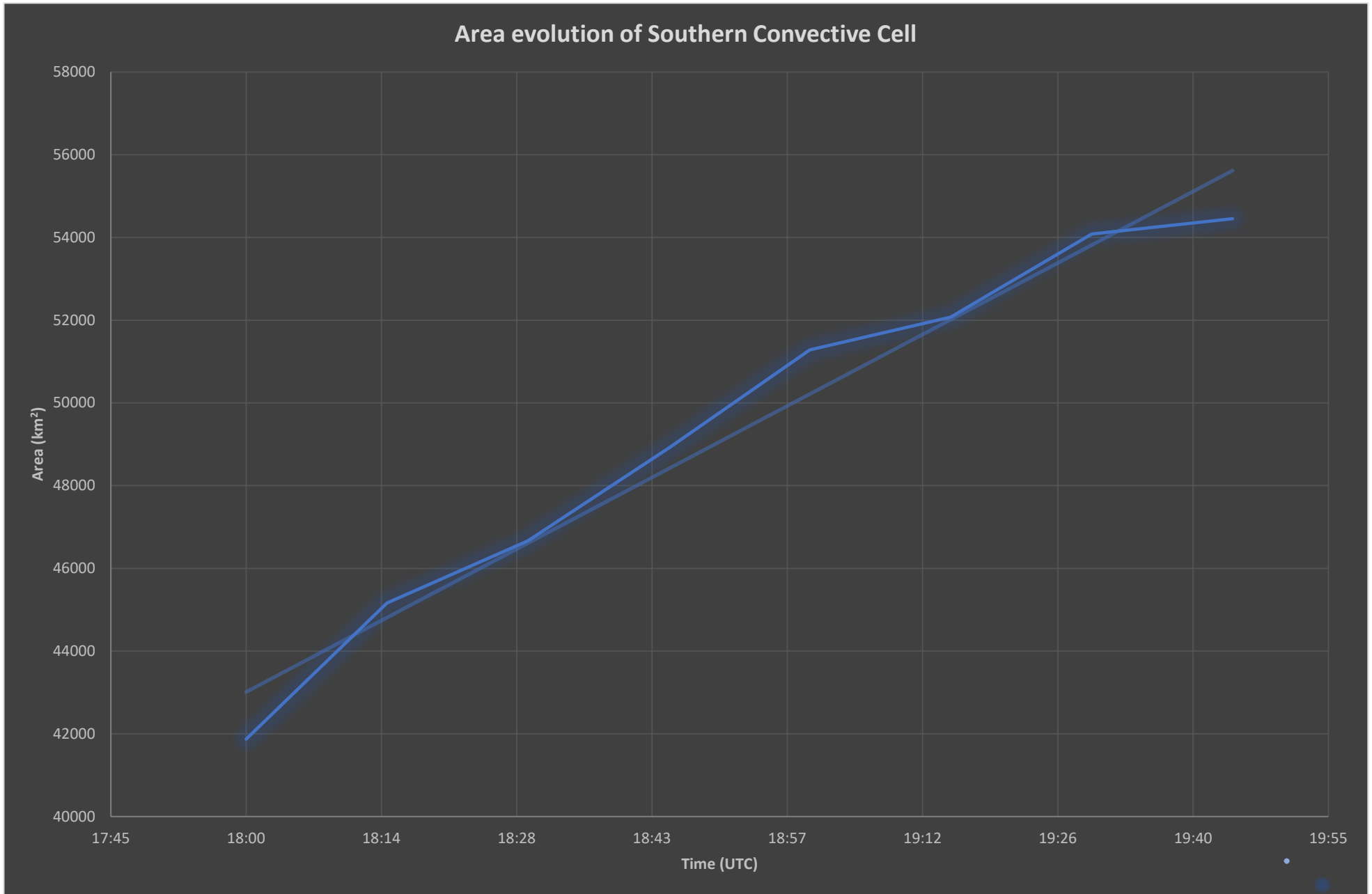


Figure 3.2.6: Southern cell area evolution through time on February 8<sup>th</sup>.

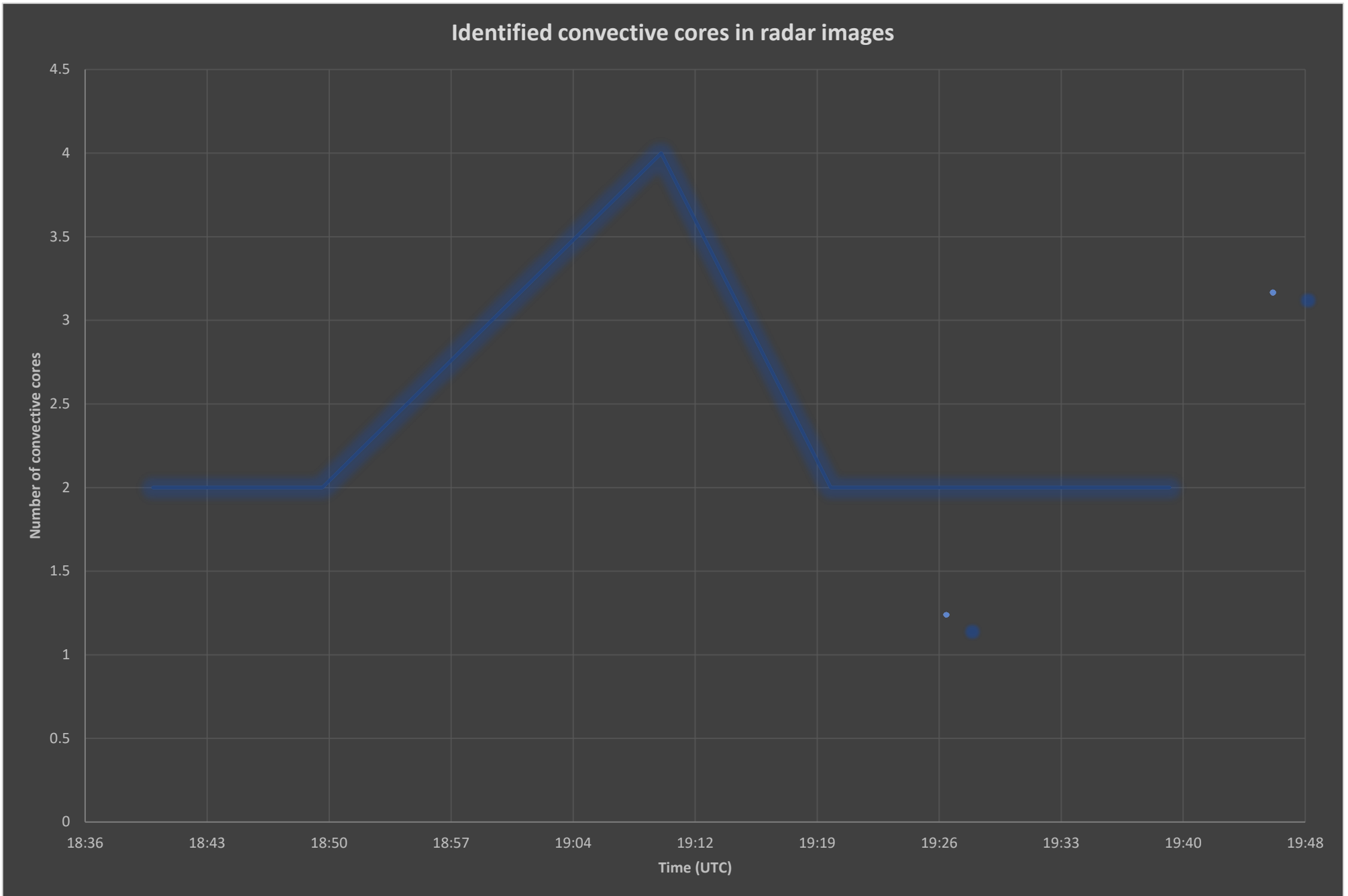


Figure 3.2.7: Convective cores identified in radar images that showed values greater than 70 dBZ in convective core in February 8<sup>th</sup>.

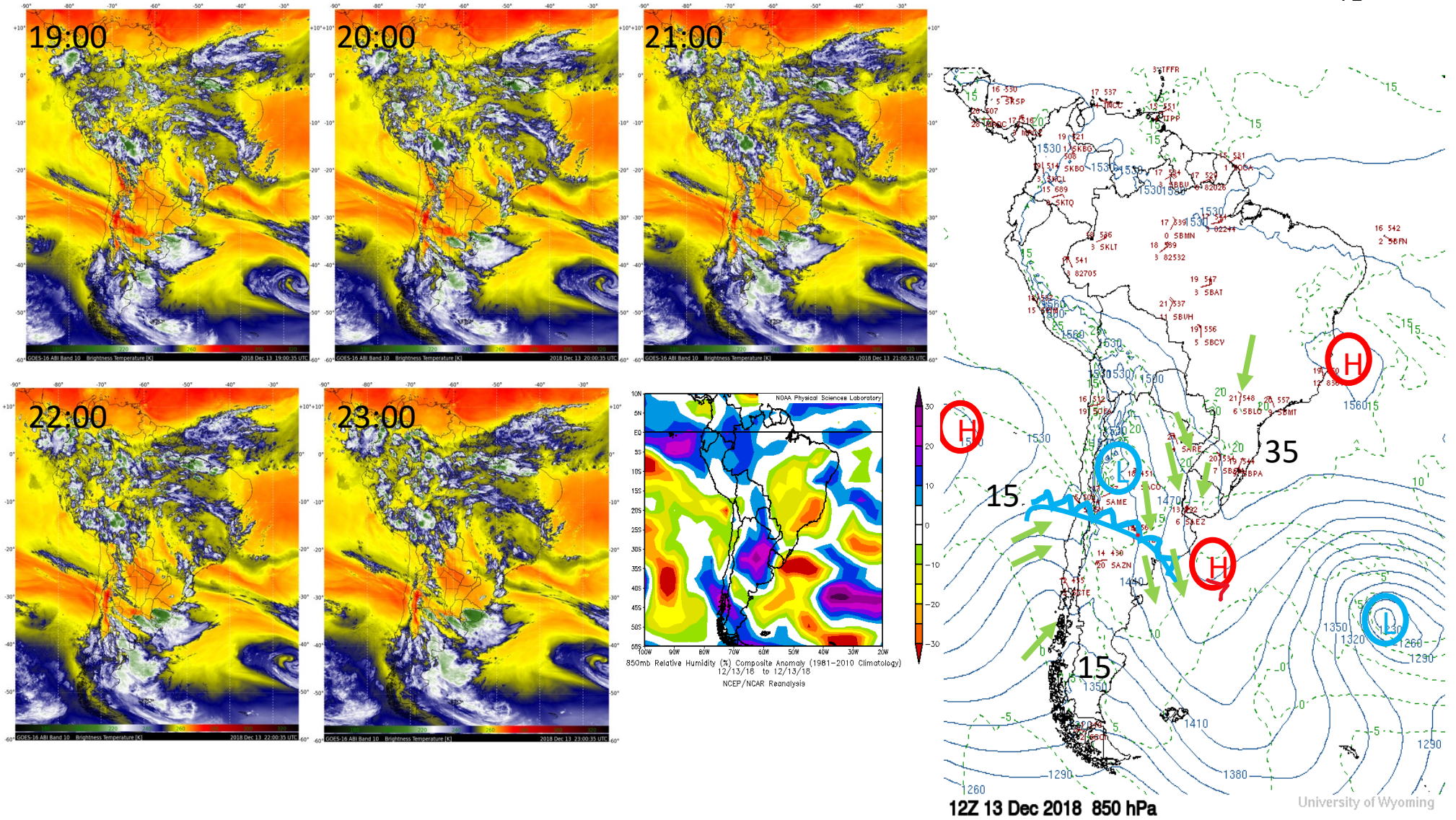


Figure 3.4.1: Images from GOES-16 channel 10 at 19:00, 20:00, 21:00, 22:00 and 23:00 UTC, relative humidity composite at 850 mb for December 13th and isobaric chart at 850 hPa at 12z for December 13<sup>th</sup>.

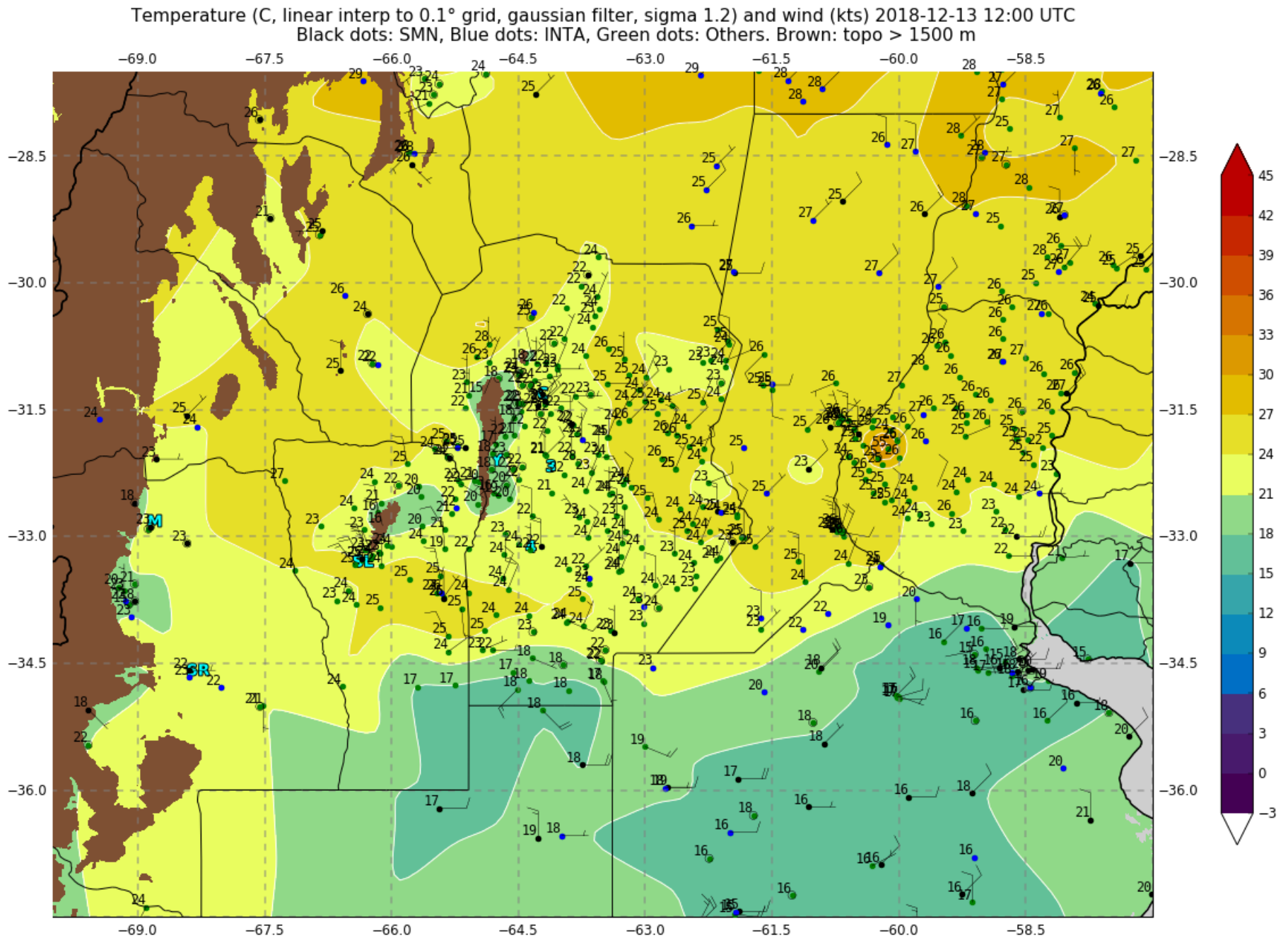
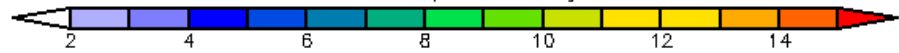
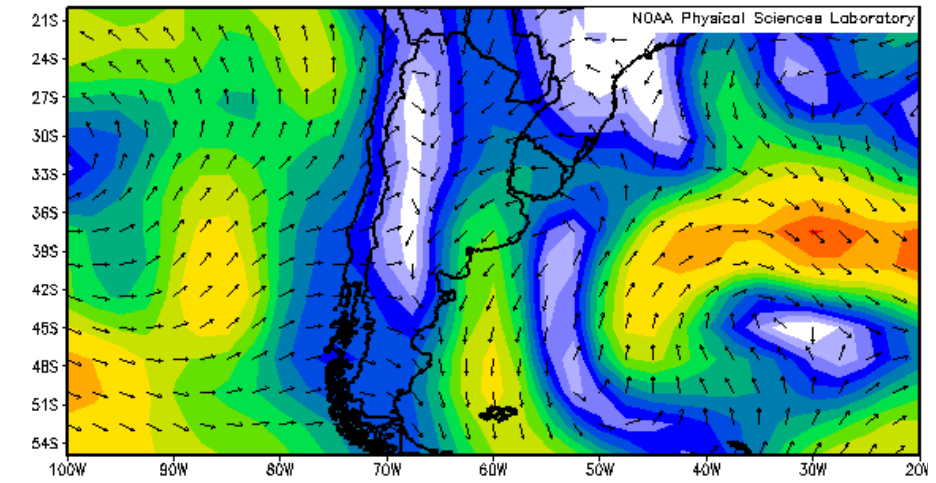
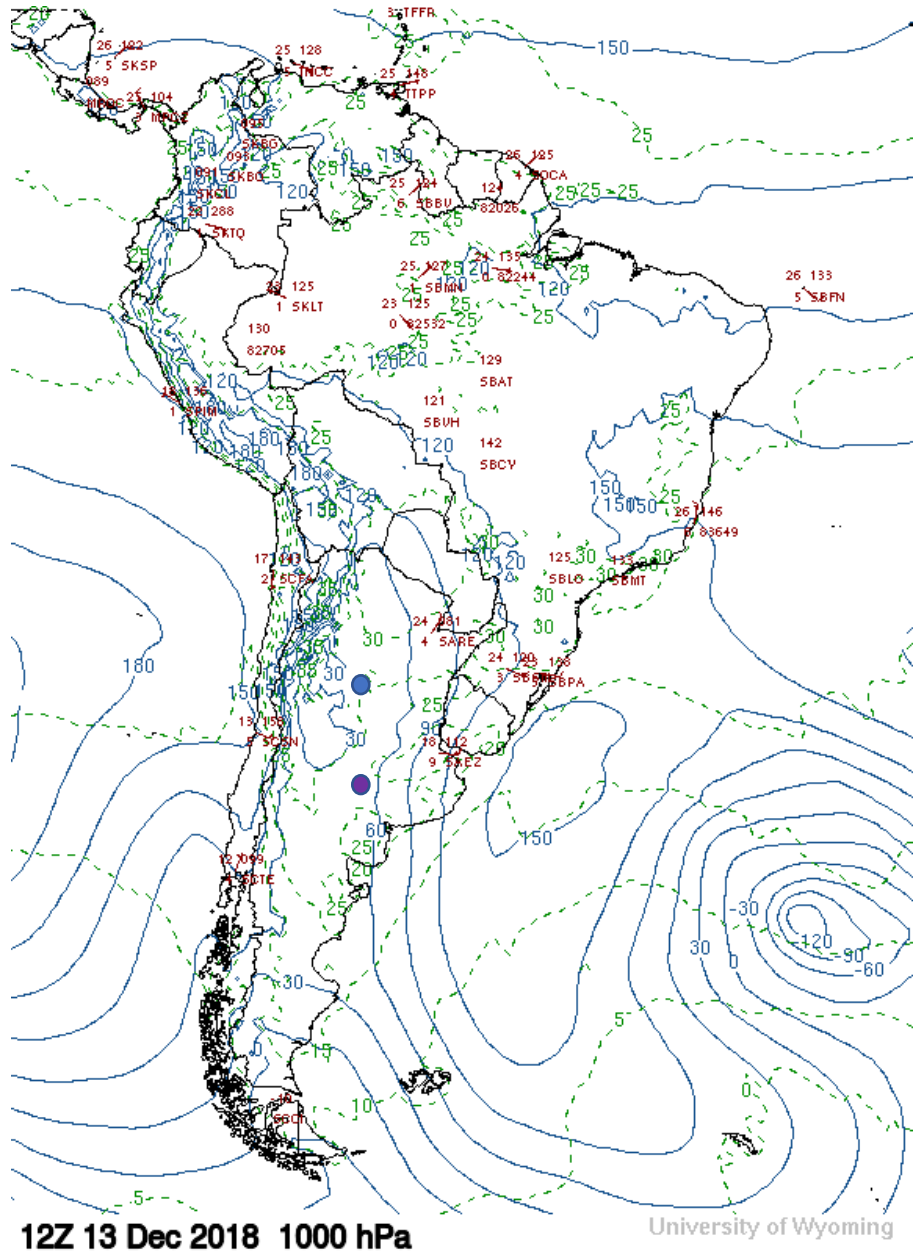
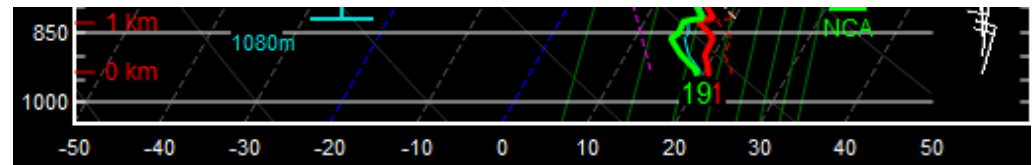


Figure 3.4.2: Surface observation taken at the RELAMPAGO field campaign on December 13<sup>th</sup>, showing a mass of warm air coming from the north east and a cold air mass coming from the south which tells us the position of the cold front in this case study.



SACO – 12z ●



SAZR – 12z ●

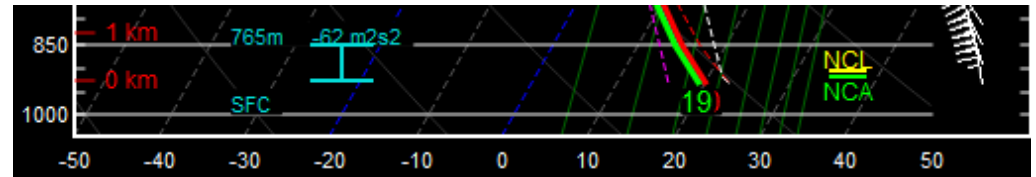
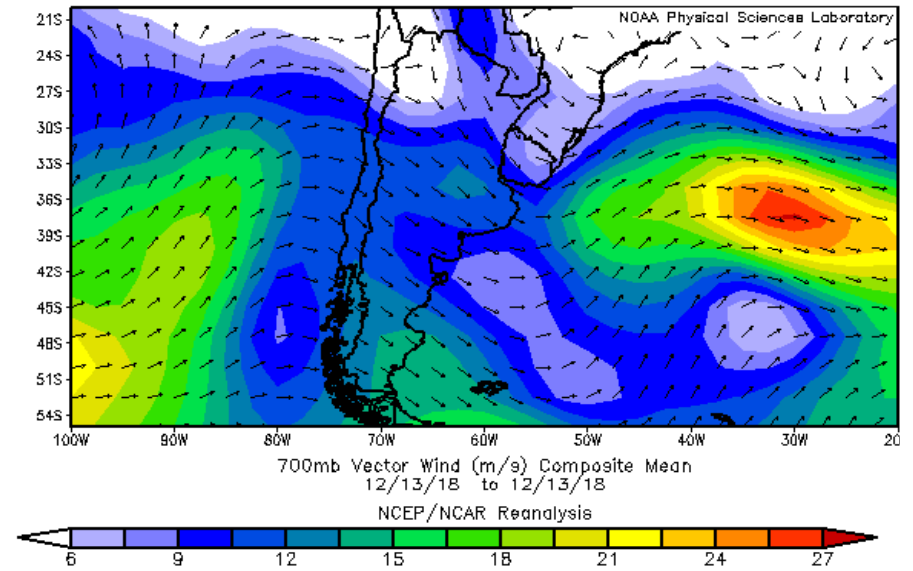
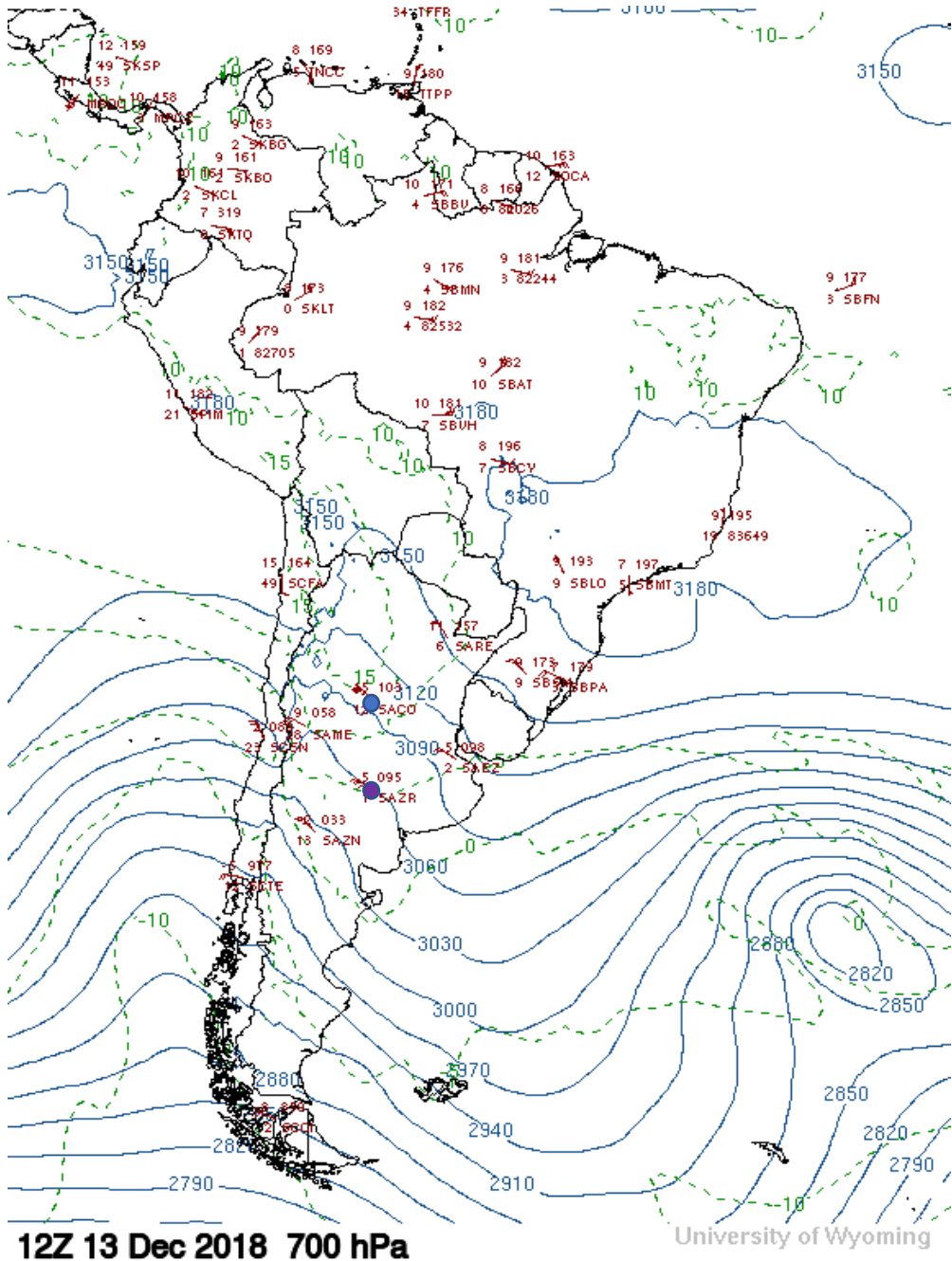
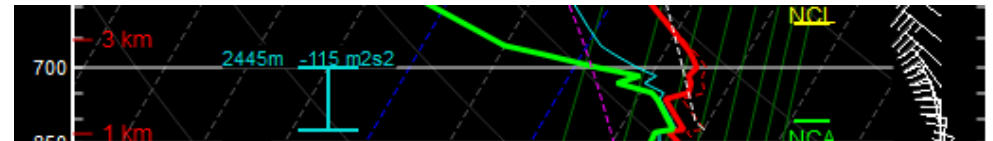


Figure 3.4.3: Isobaric chart at 1000 hPa, wind vector composites mean at 1000 mb and sections of atmospheric soundings from Cordoba Airport and Santa Rosa Airport at 12 z for December 13<sup>th</sup>. Colored dots in the isobaric chart show the location of the where radiosondes observations were taken such as: Cordoba Airport “SACO” (blue), and Santa Rosa Airport “SAZR” (purple).





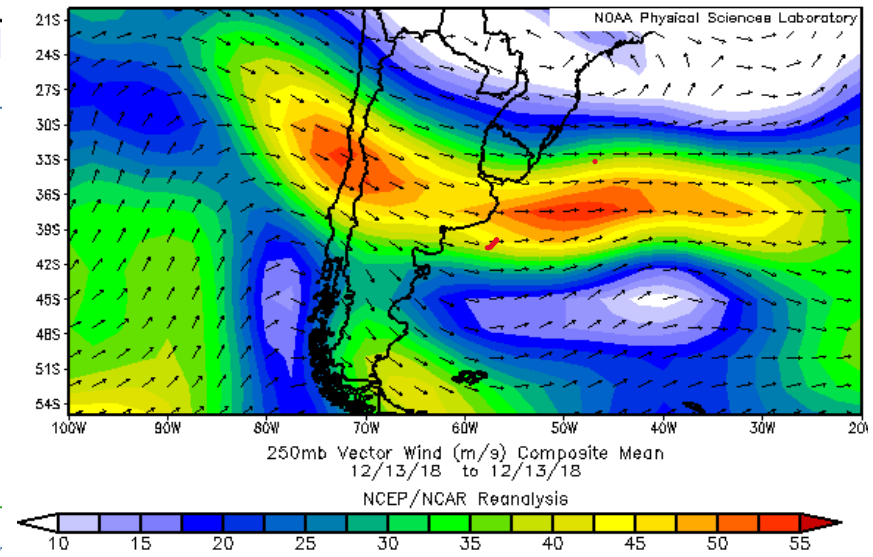
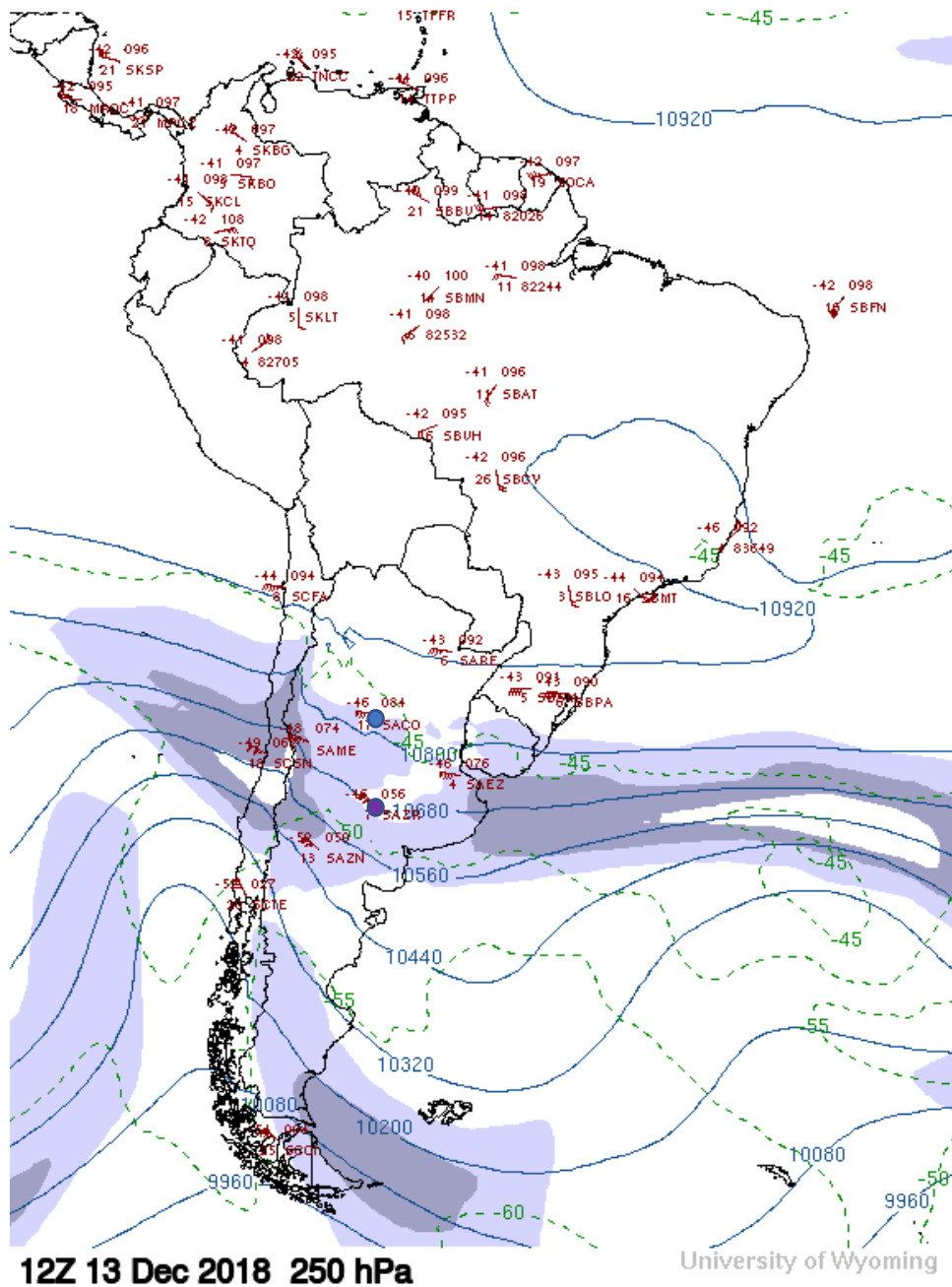
SACO – 12z ●



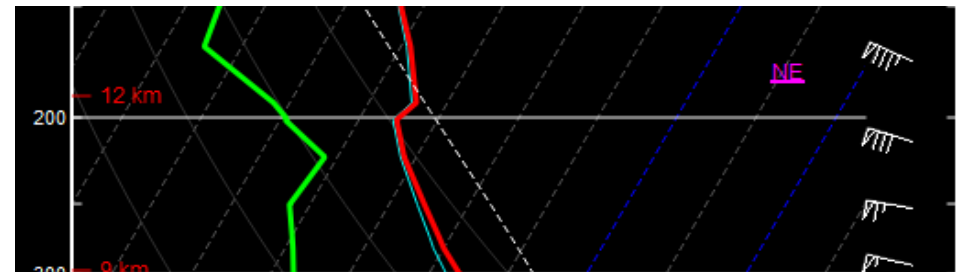
SAZR – 12z ●



Figure 3.4.5: Isobaric chart at 700 hPa, wind vector composites mean at 700 mb and sections of atmospheric soundings from Cordoba Airport and Santa Rosa Airport at 12 z for December 13<sup>th</sup>. Colored dots in the isobaric chart show the location of the where radiosondes observations were taken such as: Cordoba Airport “SACO” (blue), and Santa Rosa Airport “SAZR” (purple).



SACO – 12z ●



SAZR – 12z ●

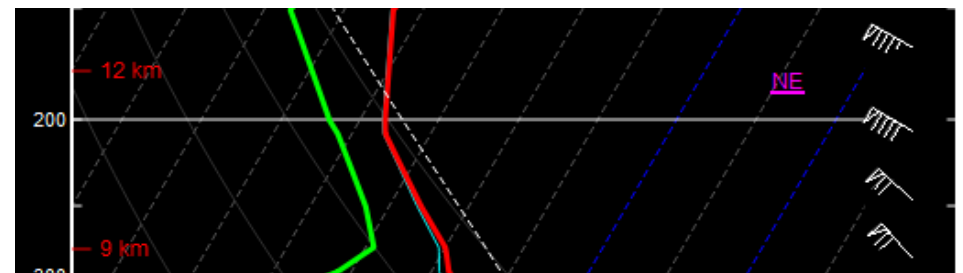


Figure 3.4.6: Isobaric chart at 250 hPa, wind vector composites mean at 250 mb and sections of atmospheric soundings from Cordoba Airport and Santa Rosa Airport at 12 z for December 13th. Colored dots in the isobaric chart show the location of the where radiosondes observations were taken such as: Cordoba Airport “SACO” (blue), and Santa Rosa Airport “SAZR” (purple).

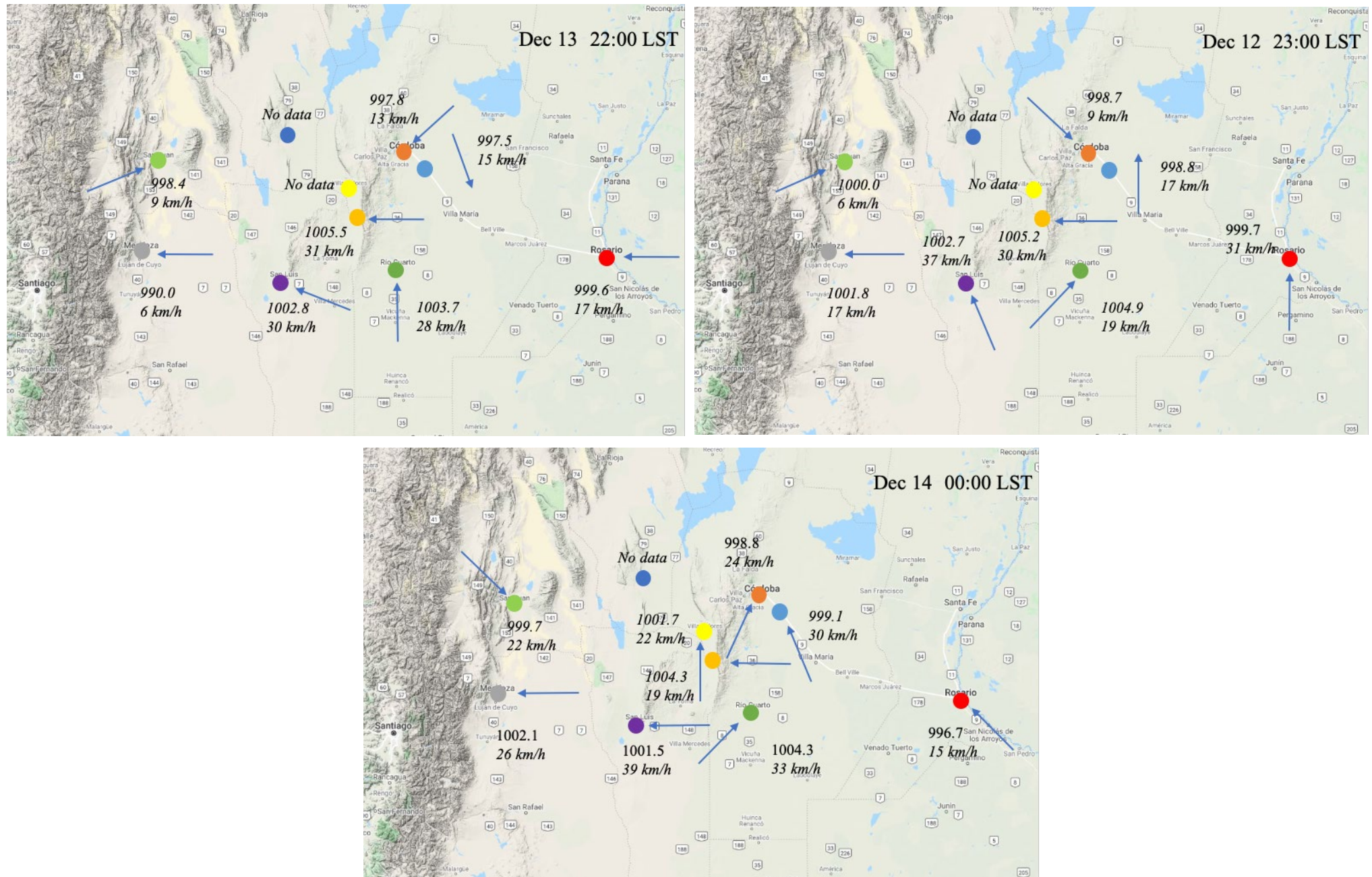
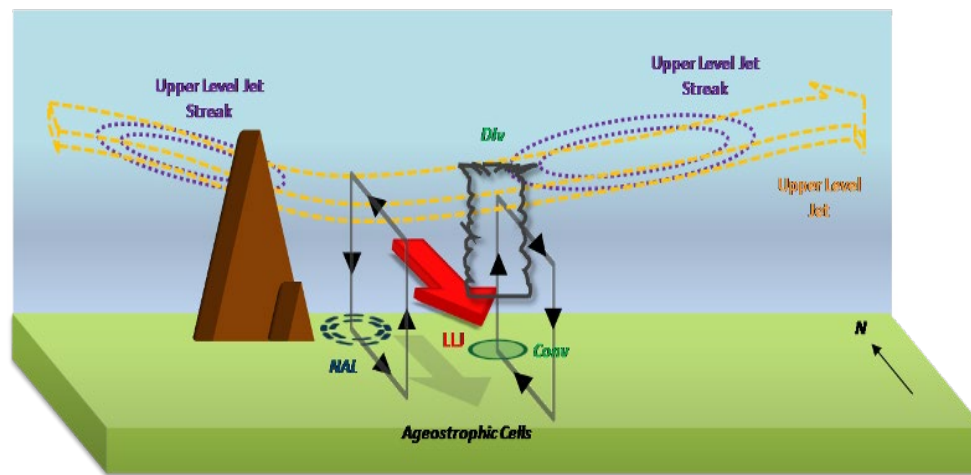
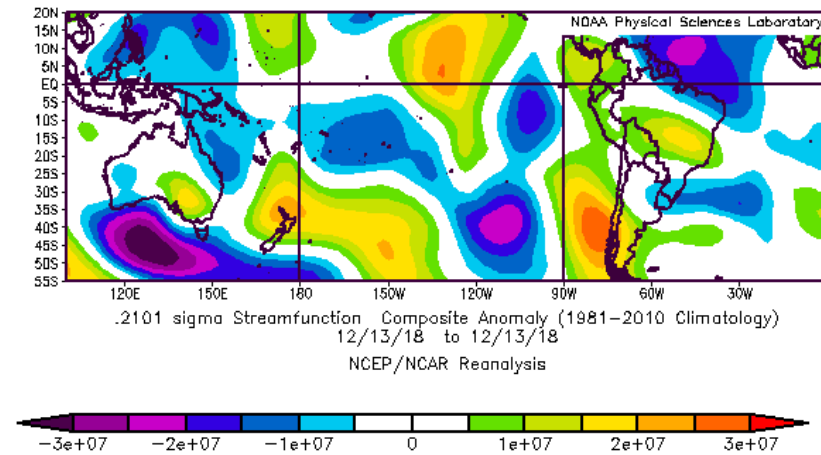
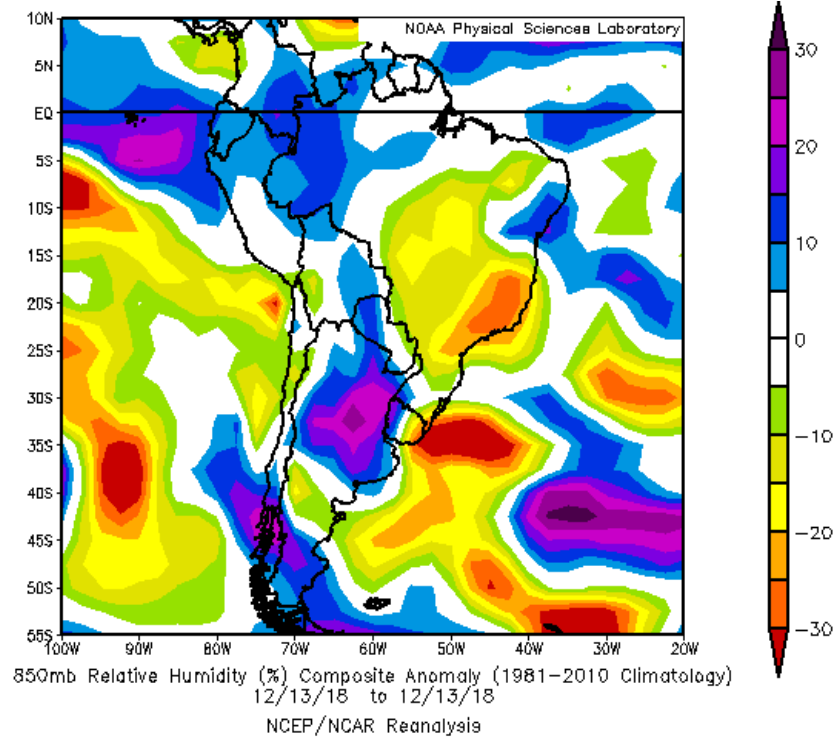


Figure 3.4.7: Pressure, wind speed and wind direction (arrow size not proportional to wind speed) observations measures in multiple weather station in the region studied for December 13<sup>th</sup>, 2018.



(EUMeTrain)

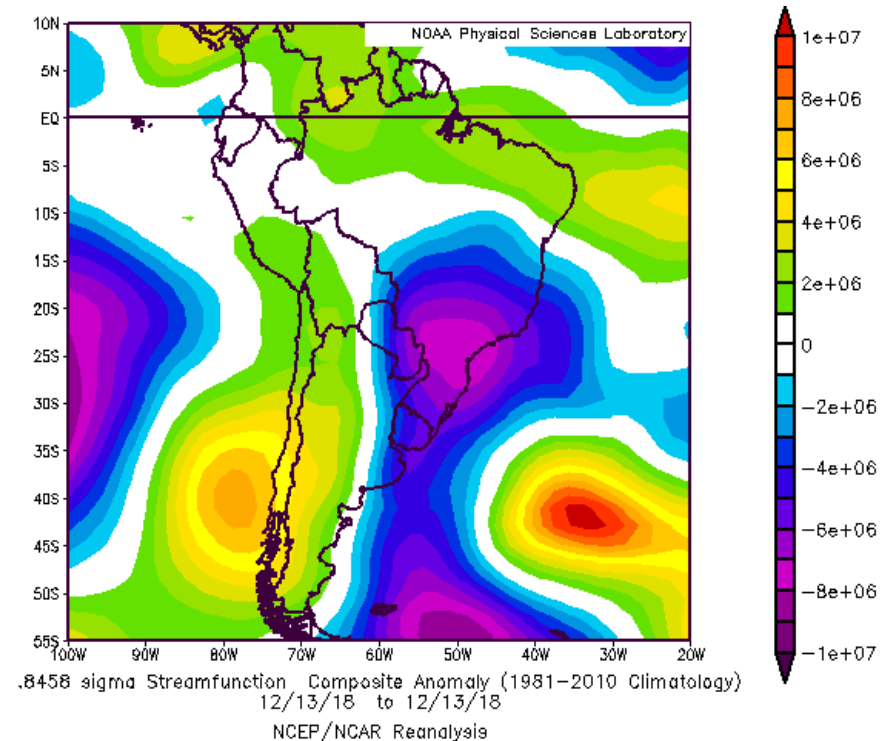


Figure 3.4.8: Top left figure is showing relative humidity composite anomalies at 850 mb, top right figure is showing .21 sigma stream function composite anomalies, bottom right figure is showing .84 sigma stream function composite anomalies for December 13<sup>th</sup>, bottom left figure is a diagram showing the interactions between the low-level jet with upper level jet streaks and north Argentinian low with respect to a convective system (brown mountains represent the “Sierras de Cordoba”)

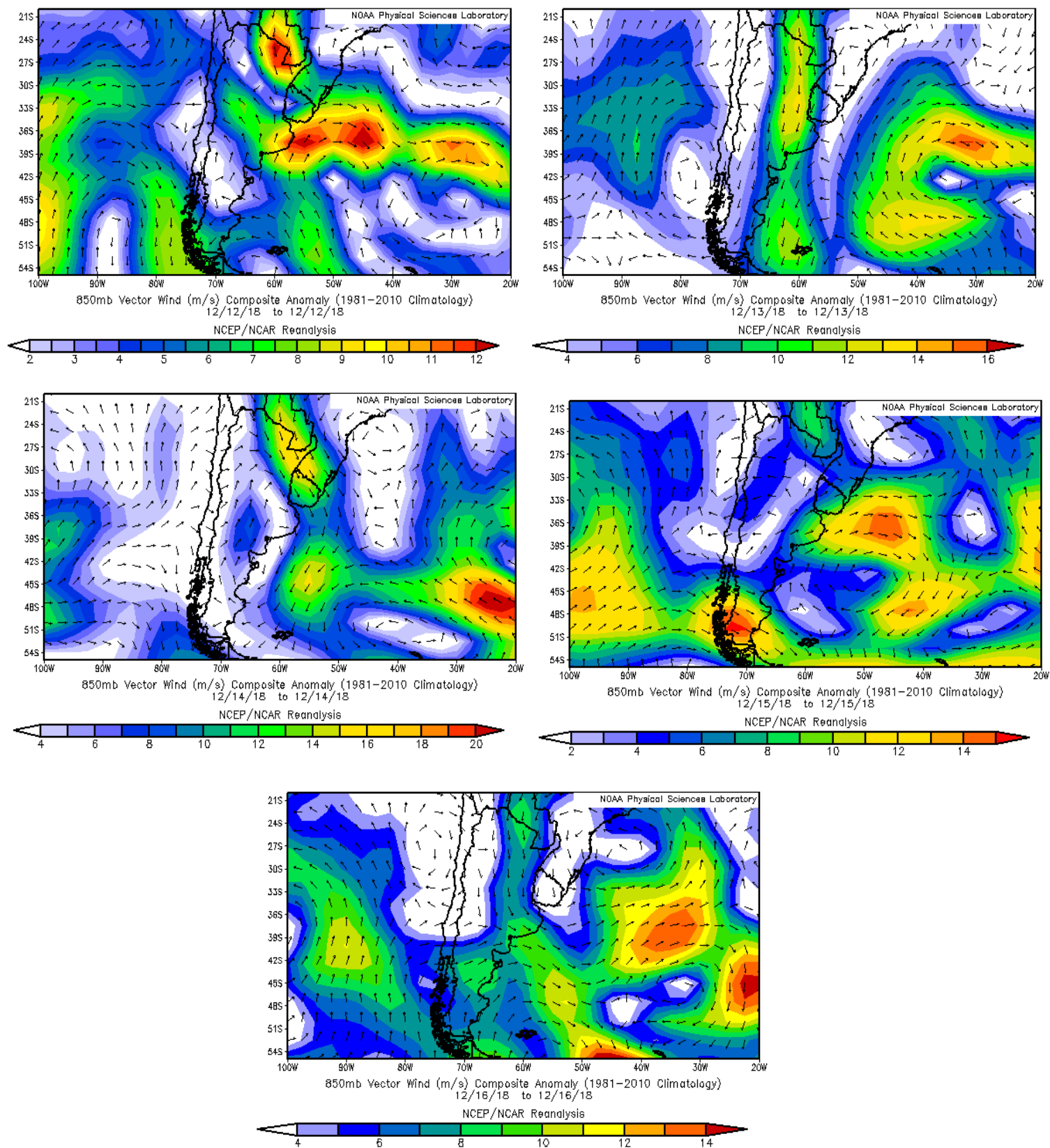


Figure 3.4.9: Wind vector composite anomaly at 850 mb showing a present northern flow for 5 consecutive days.

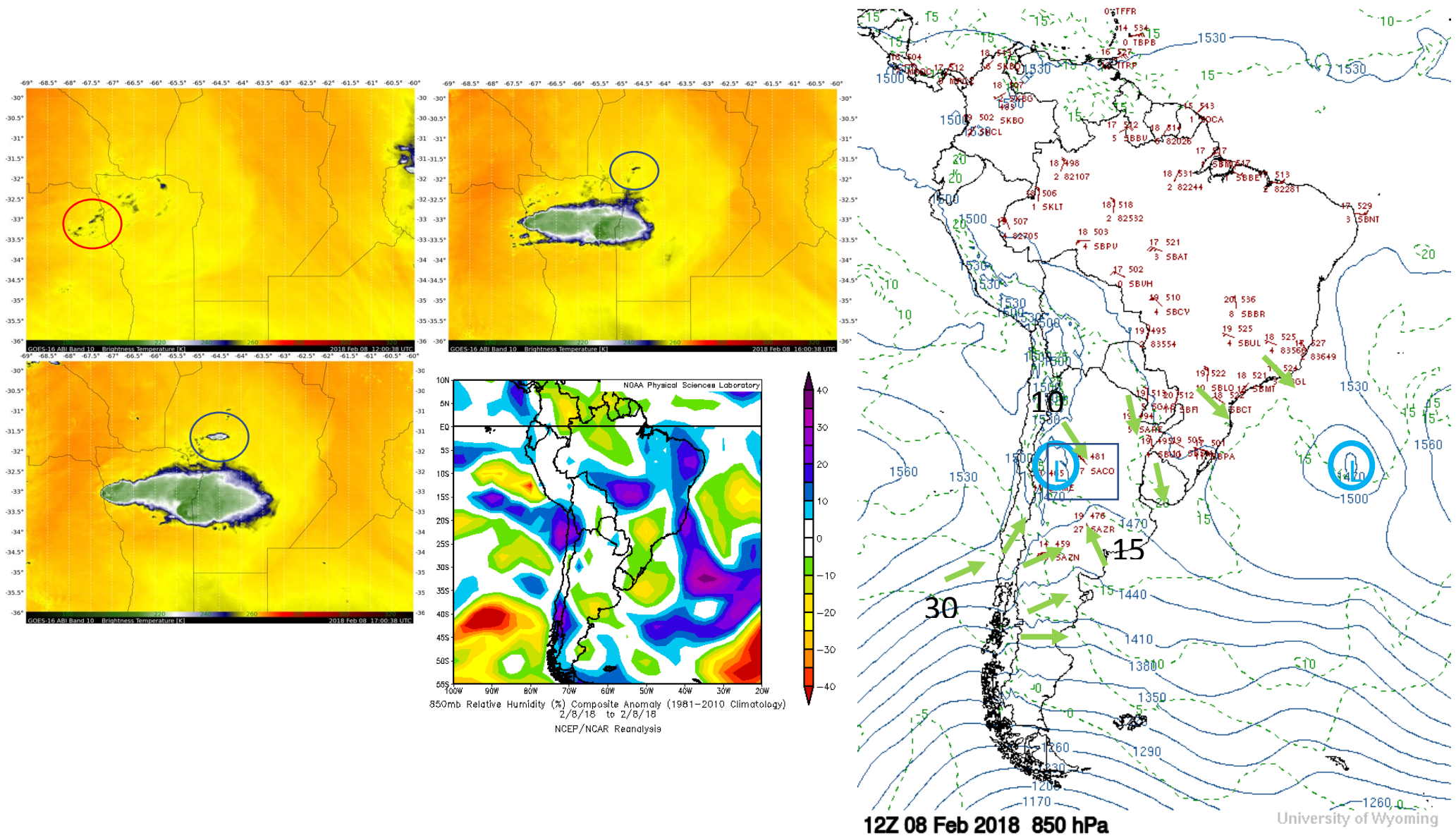
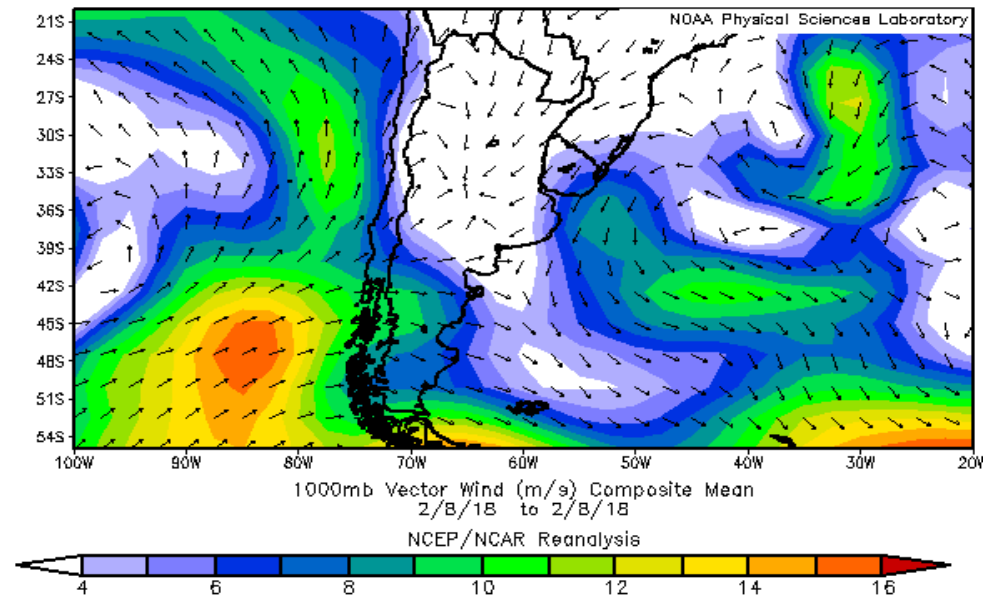
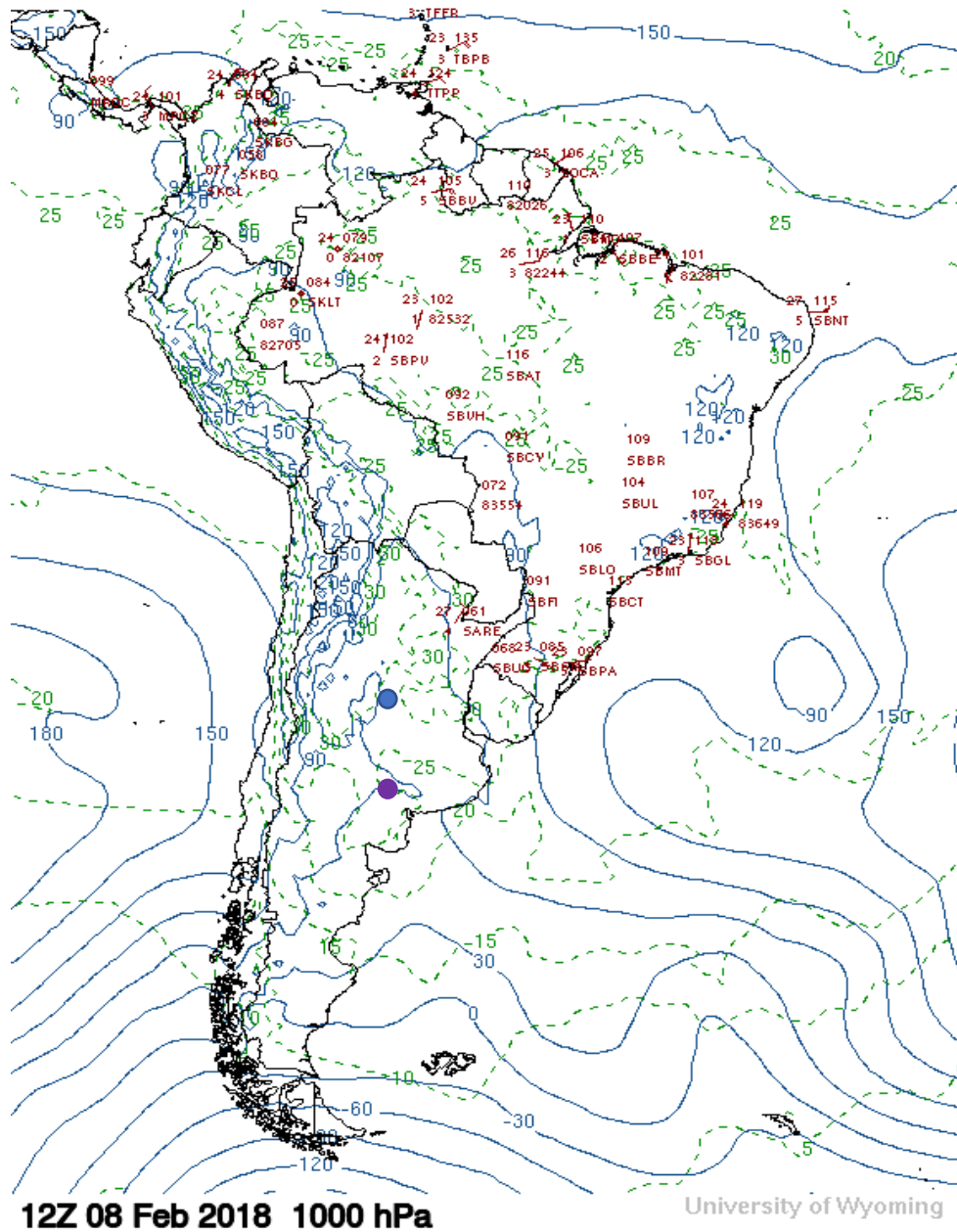
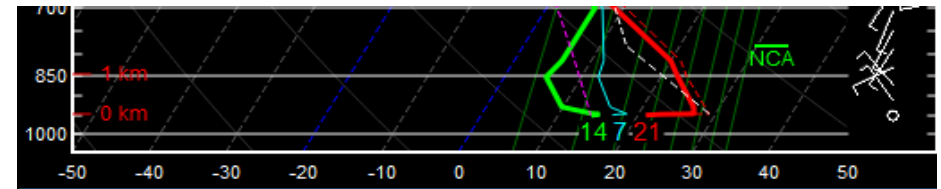


Figure 3.4.10: Right figure is an isobaric chart at 850 hPa at 12z, with a blue box showing the area shown in images from channel 10 at 12:00, 16:00 and 17:00 UTC for February 8<sup>th</sup>. Figure in the middle bottom is showing relative humidity composite anomalies at 850 mb for the same day.



SACO-12z ●



SAZR-12z ●

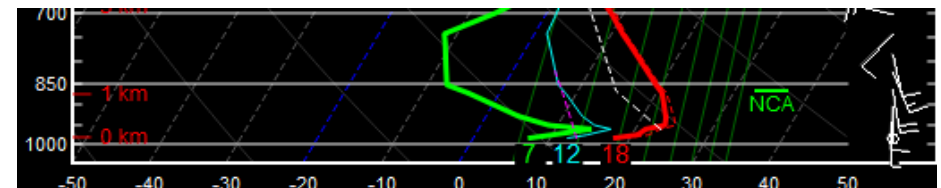
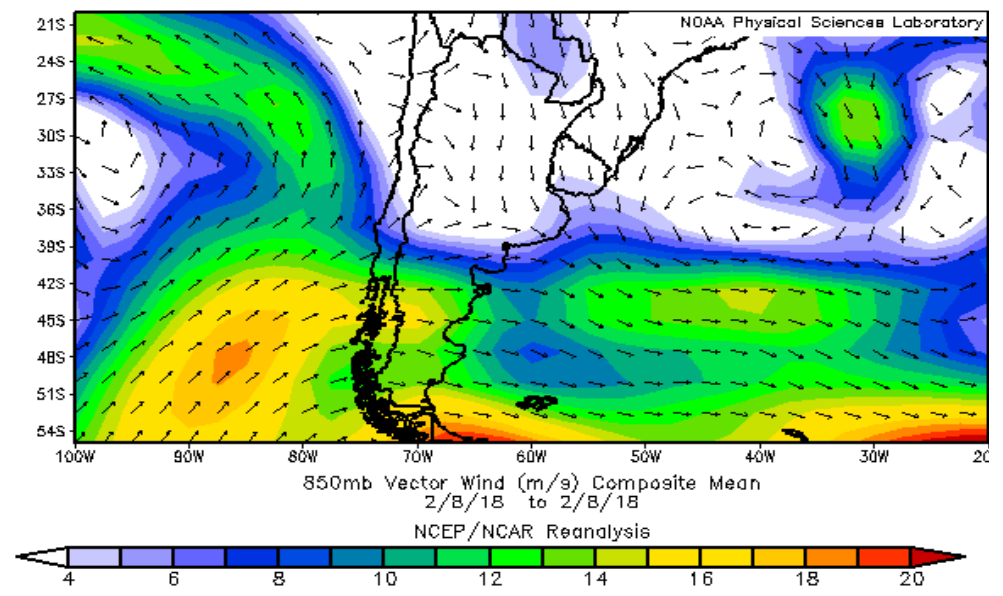
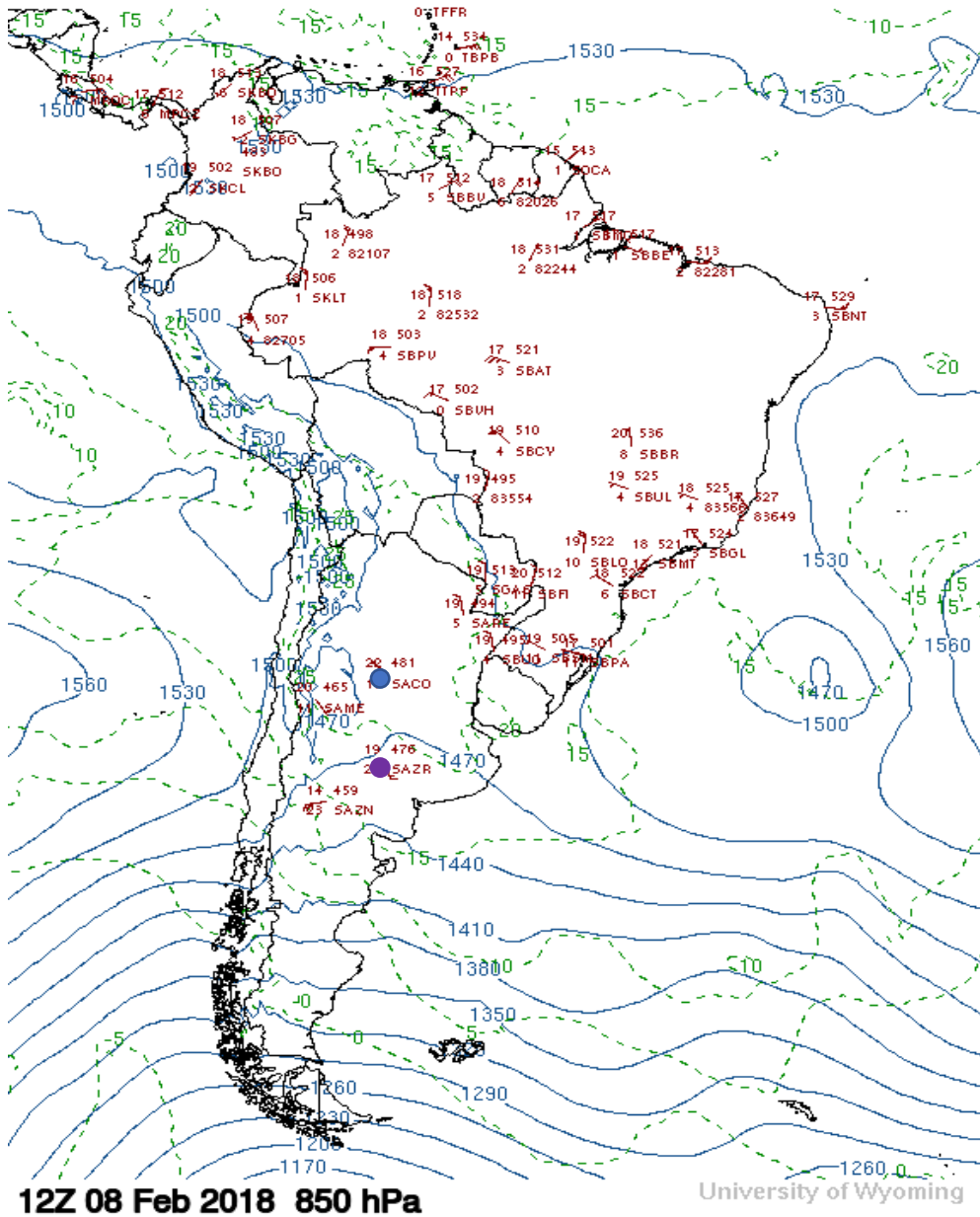
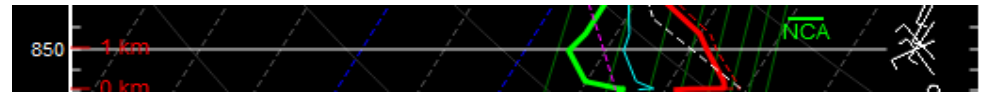


Figure 3.4.11: Isobaric chart at 1000 hPa, wind vector composites mean at 1000 mb and sections of atmospheric soundings from Cordoba Airport and Santa Rosa Airport at 12 z for February 8<sup>th</sup>. Colored dots in the isobaric chart show the location of the where radiosondes observations were taken such as: Cordoba Airport “SACO” (blue), and Santa Rosa Airport “SAZR” (purple).



SACO-12z ●



SAZR-12z ●

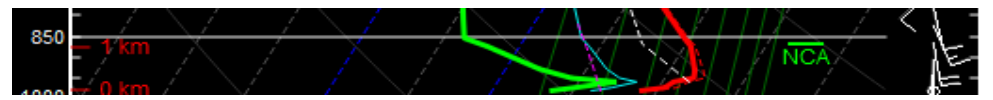


Figure 3.4.12: Isobaric chart at 850 hPa, wind vector composites mean at 850 mb and sections of atmospheric soundings from Cordoba Airport and Santa Rosa Airport at 12 z for February 8<sup>th</sup>. Colored dots in the isobaric chart show the location of the where radiosondes observations were taken such as: Cordoba Airport “SACO” (blue), and Santa Rosa Airport “SAZR” (purple).

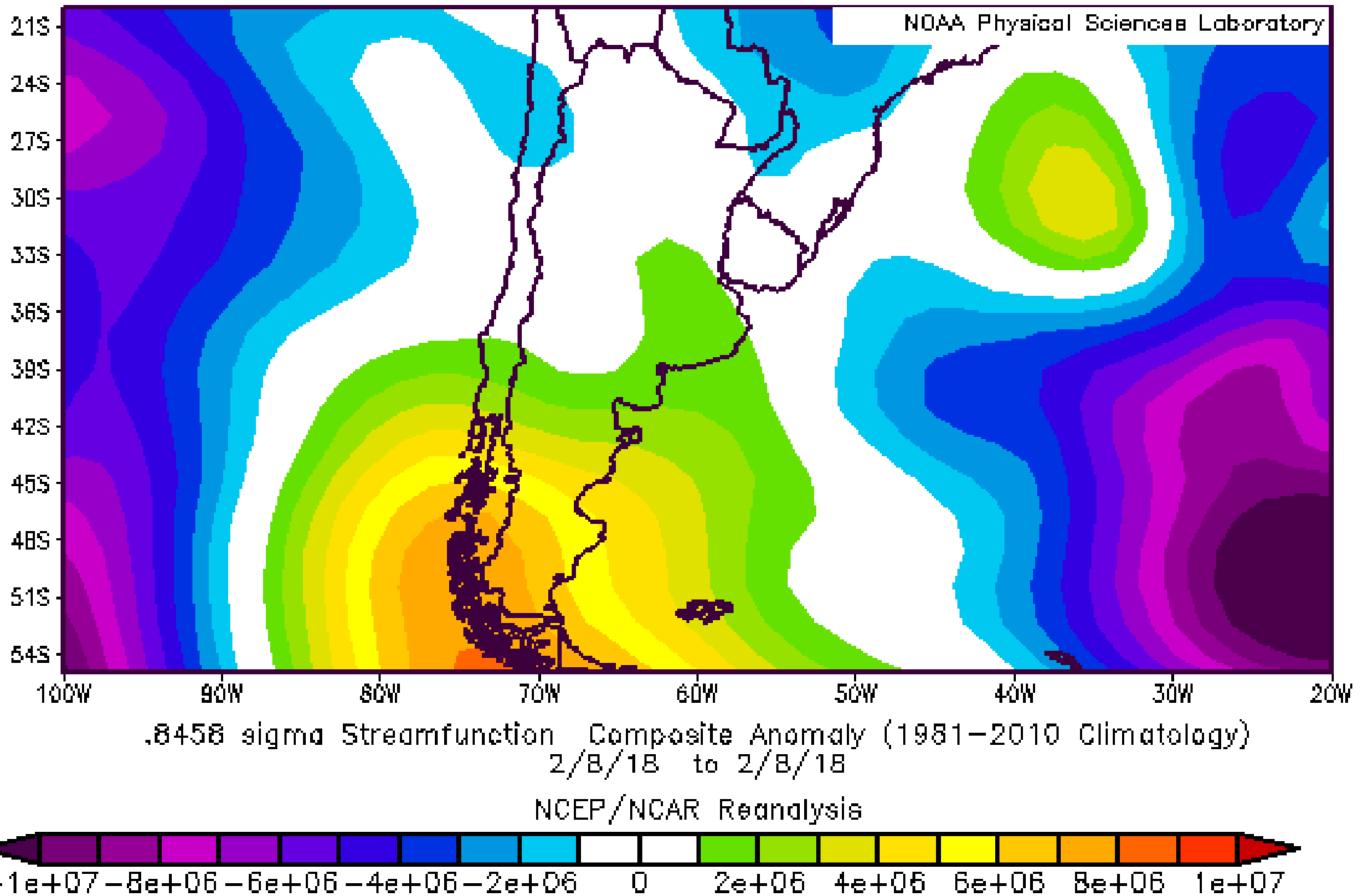
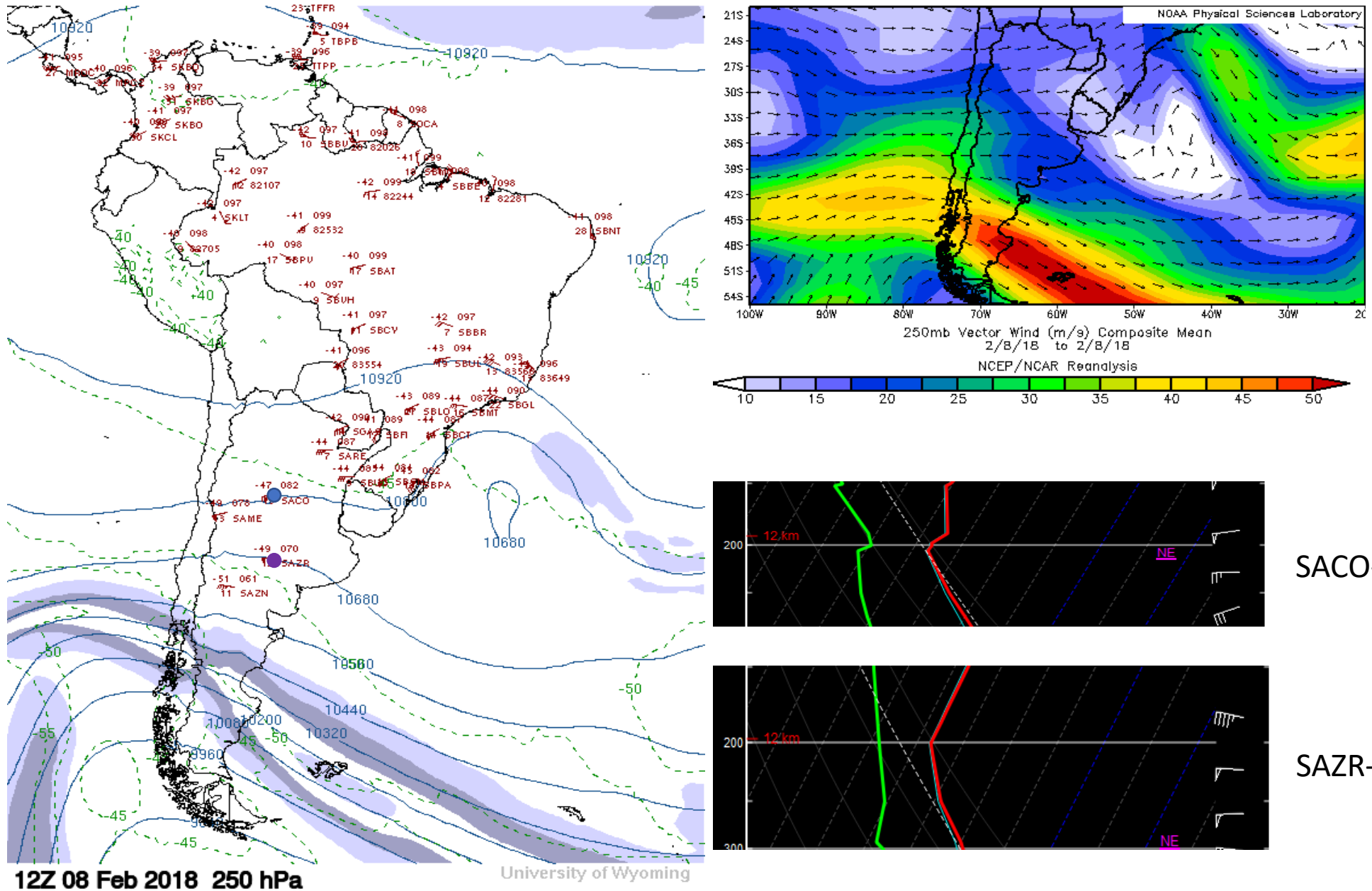


Figure 3.4.13: .84 sigma steam function composite showing an anomalously high area of cyclonic rotation south of Argentina for February 8<sup>th</sup>.





12Z 08 Feb 2018 250 hPa

University of Wyoming

Figure 3.4.15: Isobaric chart at 250 hPa, wind vector composites mean at 250 mb and sections of atmospheric soundings from Cordoba Airport and Santa Rosa Airport at 12 z for February 8<sup>th</sup>. Colored dots in the isobaric chart show the location of the where radiosondes observations were taken such as: Cordoba Airport “SACO” (blue), and Santa Rosa Airport “SAZR” (purple).

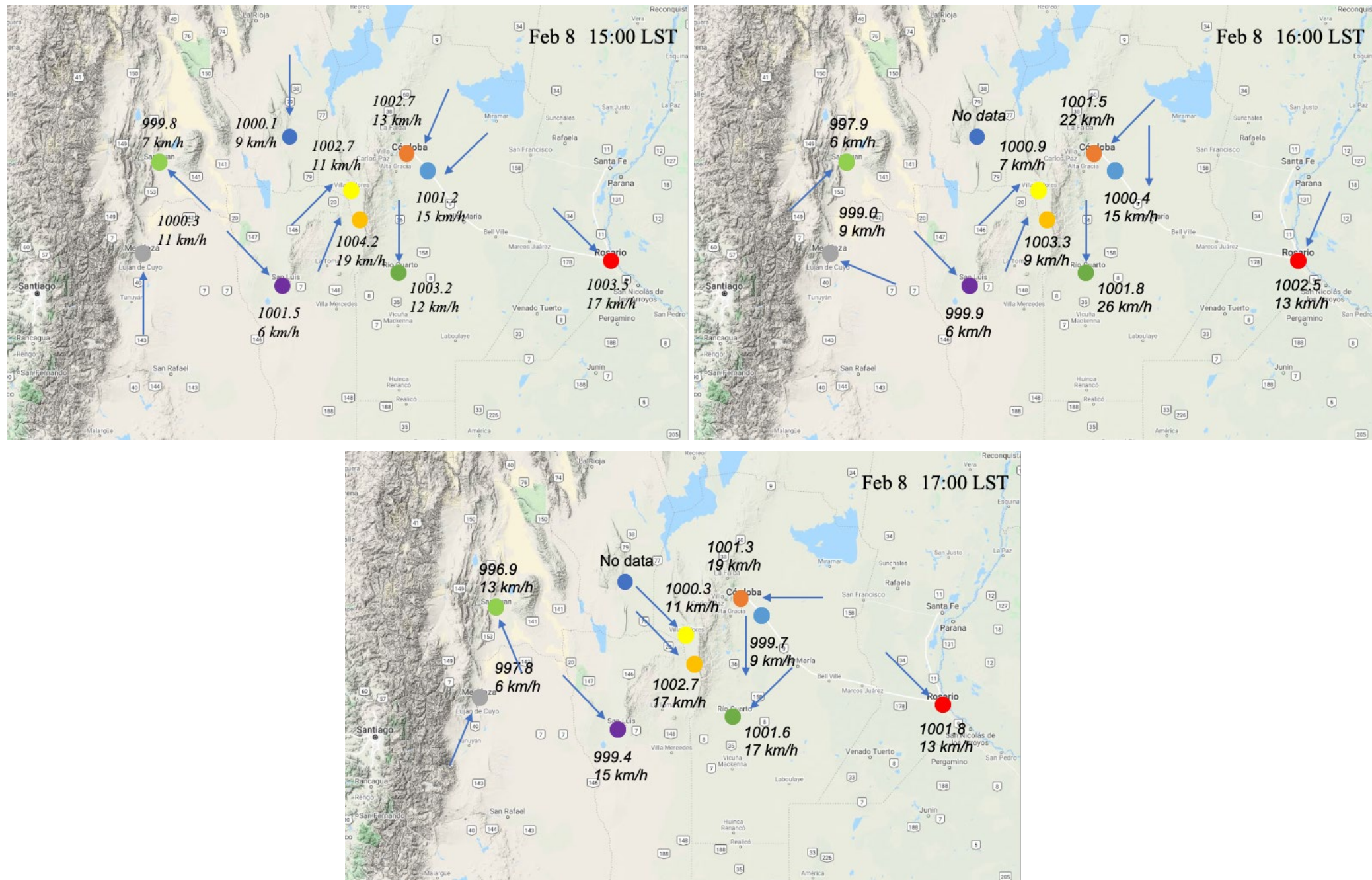


Figure 3.4.16: Pressure, wind speed and wind direction (arrow size not proportional to wind speed) observations measures in multiple weather station in the region studied for February 8<sup>th</sup>, 2018.

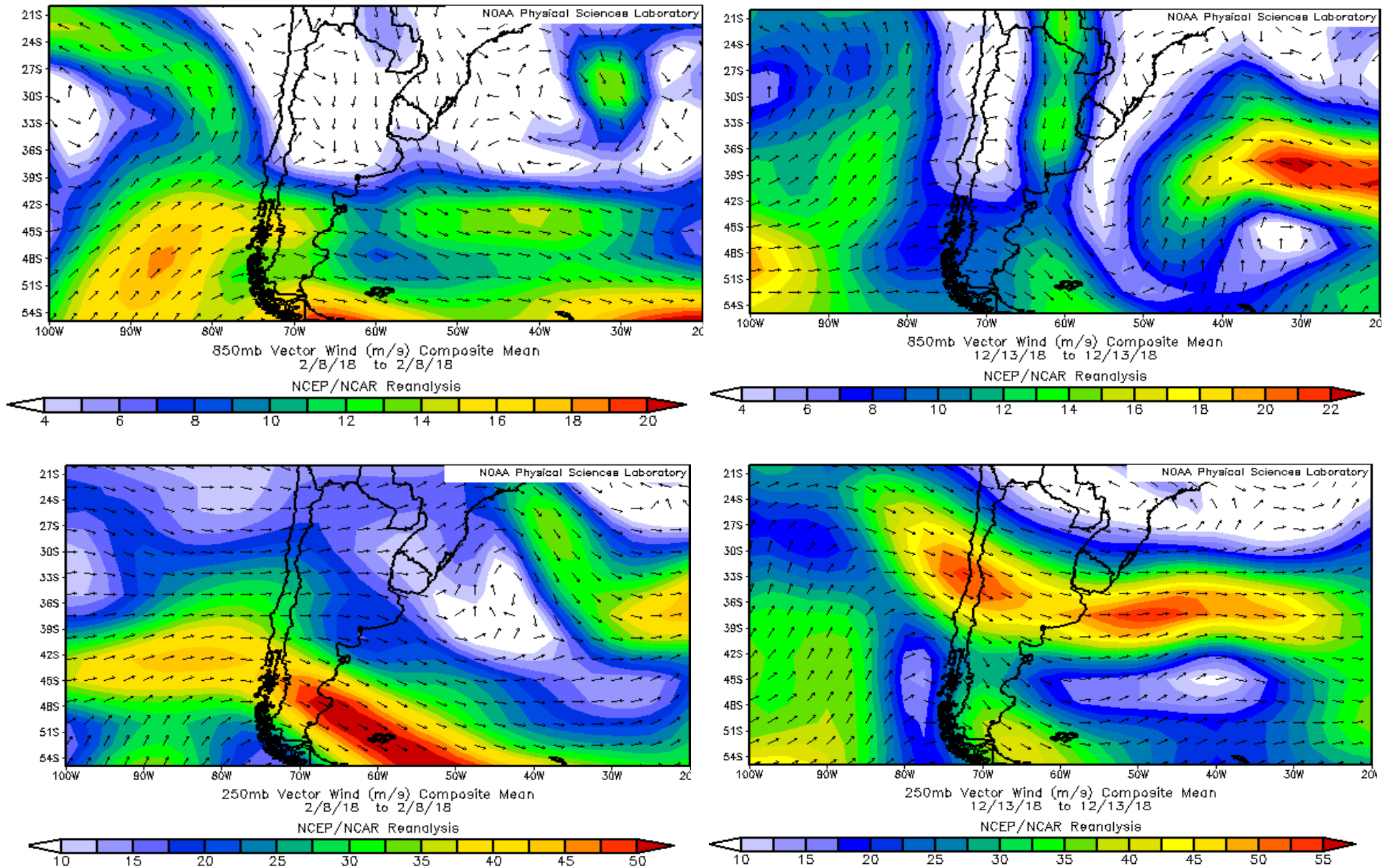


Figure 3.4.17: Images showing wind vector composite mean at 850 (top) and 250 (bottom) mb for February 8<sup>th</sup> (left column) and December 13<sup>th</sup> (right column).

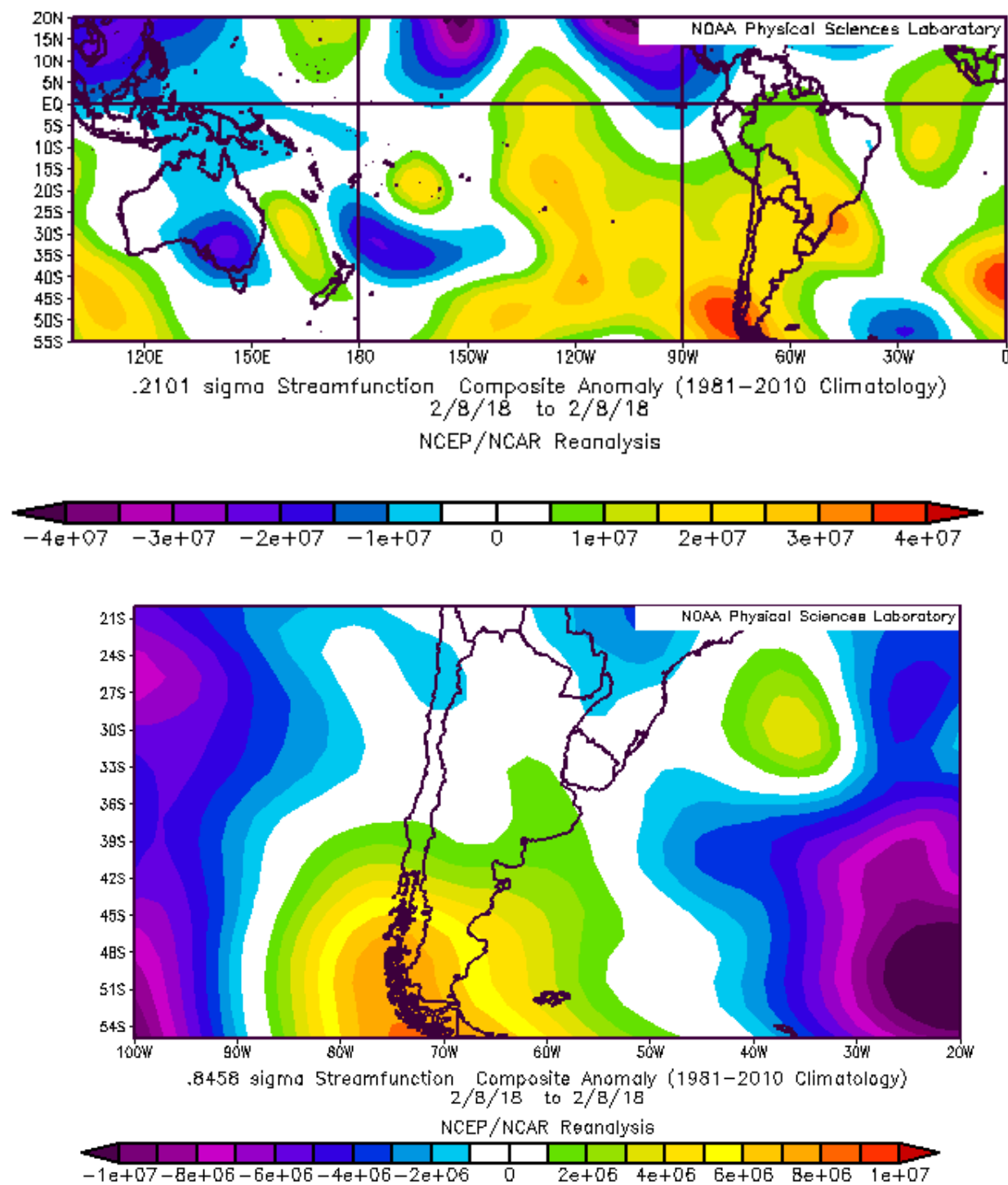


Figure 3.4.18: .21 sigma (top figure) and .84 sigma (bottom image) stream function composite anomalies for February 8<sup>th</sup>.

